

Berichte

zur Polar-
und Meeresforschung

672
2014

Reports
on Polar and Marine Research



The Expedition of the Research Vessel "Polarstern"
to the Antarctic in 2013 (ANT-XXIX/8)

Edited by
Vera Schindwein
with contributions of the participants



Alfred-Wegener-Institut
Helmholtz-Zentrum für Polar-
und Meeresforschung
D-27570 BREMERHAVEN
Bundesrepublik Deutschland

ISSN 1866-3192

Hinweis

Die Berichte zur Polar- und Meeresforschung werden vom Alfred-Wegener-Institut Helmholtz-Zentrum für Polar- und Meeresforschung in Bremerhaven* in unregelmäßiger Abfolge herausgegeben.

Sie enthalten Beschreibungen und Ergebnisse der vom Institut (AWI) oder mit seiner Unterstützung durchgeführten Forschungsarbeiten in den Polargebieten und in den Meeren.

Es werden veröffentlicht:

- Expeditionsberichte
(inkl. Stationslisten und Routenkarten)
- Expeditions- und Forschungsergebnisse
(inkl. Dissertationen)
- wissenschaftliche Berichte der
Forschungsstationen des AWI
- Berichte wissenschaftlicher Tagungen

Die Beiträge geben nicht notwendigerweise die Auffassung des Instituts wieder.

Notice

The Reports on Polar and Marine Research are issued by the Alfred-Wegener-Institut Helmholtz-Zentrum für Polar- und Meeresforschung in Bremerhaven*, Federal Republic of Germany. They are published in irregular intervals.

They contain descriptions and results of investigations in polar regions and in the seas either conducted by the Institute (AWI) or with its support.

The following items are published:

- expedition reports
(incl. station lists and route maps)
- expedition and research results
(incl. Ph.D. theses)
- scientific reports of research stations
operated by the AWI
- reports on scientific meetings

The papers contained in the Reports do not necessarily reflect the opinion of the Institute.

The „Berichte zur Polar- und Meeresforschung“
continue the former „Berichte zur Polarforschung“

* Anschrift / Address

Alfred-Wegener-Institut
Helmholtz-Zentrum für Polar-
und Meeresforschung
D-27570 Bremerhaven
Germany
www.awi.de

Editor:
Dr. Horst Bornemann

Assistant editor:
Birgit Chiaventone

Die "Berichte zur Polar- und Meeresforschung" (ISSN 1866-3192) werden ab 2008 als Open-Access-Publikation herausgegeben (URL: <http://epic.awi.de>).

Since 2008 the "Reports on Polar and Marine Research" (ISSN 1866-3192) are available as open-access publications (URL: <http://epic.awi.de>)

The Expedition of the Research Vessel "Polarstern" to the Antarctic in 2013 (ANT-XXIX/8)

**Edited by
Vera Schlindwein
with contributions of the participants**

**Please cite or link this publication using the identifier
hdl:10013/epic.????? or <http://hdl.handle.net/10013/epic.?????>**

ISSN 1866-3192

ANT-XXIX/8

09 November - 16 December 2013

Cape Town - Cape Town

**Chief scientist
Vera Schlindwein**

**Coordinator
Rainer Knust**

Contents

1.	Zusammenfassung und Fahrtverlauf	2
	1.1 Zusammenfassung	2
	1.2 Fahrtverlauf	4
	Summary and Itinerary	7
2.	Weather Conditions during ANT-XXIX/8	10
3.	Seismology	14
	3.1 Refraction seismics	16
	3.2 Passive seismology	18
4.	Heat flow Determinations	23
5.	Marine Geology	30
	5.1 Sediments	30
	5.2 Hard rocks	34
6.	Water Column Surveying and Sampling	39
7.	Biology and Biogeochemistry	54
	7.1 Geobiological observations	54
	7.2 Water column biogeochemistry	62
	7.3 Biological observations	66
	7.4 Biogeochemical and microbiological sampling	70
	7.5 Biological experiments	74
8.	Hydroacoustics	77
	8.1 Bathymetry	77
	8.2 Parasound	80
	8.3 Underwater positioning with Posidonia	82
 APPENDICES		
A.1	Teilnehmende Institute / Participating Institutions	85
A.2	Fahrtteilnehmer / Cruise Participants	87
A.3	Schiffsbesatzung / Ship's Crew	89
A.4	Stationsliste / Station List PS 81	91
A.5	Scientific Appendix	97
	A.5.1 Sample lists	97
	A.5.2 Summary of OFOS dives	100

1. ZUSAMMENFASSUNG UND FAHRTVERLAUF

Vera Schindwein
Alfred-Wegener-Institut Helmholtz-Zentrum für Polar- und Meeresforschung,
Bremerhaven

1.1 Zusammenfassung

Am 9. November 2013 verließ *Polarstern* gegen 20:00 Uhr Ortszeit Kapstadt, Südafrika, in südliche Richtung, um während Fahrtabschnitt ANT-XXIX/8 geologische Prozesse und biologische Lebensgemeinschaften am Südwestindischen Rücken bei ca. 52° 30' südlicher Breite und 12-15° östlicher Länge zu untersuchen (Fig. 1.1).

Der Südwestindische Rücken (SWIR) gehört mit Spreizungsraten von <15 mm/y zu den sich am langsamsten öffnenden mittelozeanischen Rücken der Welt, zu den sogenannten ultralangsamem Rücken. Die ultralangsamem Rücken, der SWIR und das arktische Rückensystem, sind wegen ihrer schlechten Erreichbarkeit bislang wenig erforscht. Alle bisherigen Erkenntnisse zeigen jedoch, dass diese Rücken nicht gängigen Modellen für Ozeanbodenspreizung entsprechen. So finden sich an den ultralangsamem Rücken trotz geringer Produktion von Schmelzen und einer sehr kalten Lithosphäre unerwartet viele hydrothermale Anomalien in der Wassersäule, die auf aktive Vents hindeuten könnten. Magma tritt an ultralangsamem Rücken fokussiert an einzelnen Vulkanzentren aus, während in den dazwischen liegenden Bereichen Mantelgestein am Meeresboden ansteht. Unsere Reise steuert einen solchen Magma-armen Rückenabschnitt an, das sogenannte Oblique Supersegment des SWIR, das von zwei großen Vulkanzentren begrenzt wird (Fig. 1.2).

Mit einem interdisziplinären Team von 33 Wissenschaftlern arbeiteten wir alle in demselben Messgebiet im gemeinsamen Projekt „SWEAP“ Southwestindian Ridge Earthquakes and Plumes. Unsere Reise war geprägt von einem ständigen Wechsel von Mess- und Beprobungsgeräten, die Hand in Hand greifend uns ein sehr differenziertes Bild des Südwestindischen Rückens als geologisch aktive Region und als Lebensraum geliefert haben.

Das geophysikalische Programm zielte darauf ab, die Struktur der Erdkruste zu erkunden und aktive tektonische Prozesse anhand der Erdbebenaktivität zu beobachten. Aus der maximalen Herdtiefe von Erdbeben sowie aus umfangreichen Messungen des Wärmestroms in Profilen senkrecht und parallel zum Rücken werden wir nach Auswertung der Messdaten einen Eindruck des thermischen Zustands der Lithosphäre gewinnen.

Die CTD Sonde lieferte in sogenannten tow-yo Einsätzen sofort ein Bild der physikalischen und chemischen Eigenschaften der Wassersäule wie Temperatur, Salzgehalt, Trübe und Redox Potential. Außerdem wurden Wasserproben genommen, um z.B. den Methangehalt des Wassers zu bestimmen. Ähnliche Sensoren waren auch an dem Ocean floor observing system OFOS angebracht.

Das OFOS diente dazu, den Meeresboden zu filmen und die am Meeresboden

siedelnden Organismen zu betrachten und deren Vorkommen quantitativ zu erfassen. Ebenso zum Einsatz kamen TV-Multicorer zur Beprobung der obersten Sedimentschicht, in der die Organismen leben. Das Schwerelot hingegen verschaffte uns Proben des Sediments bis 6 m Tiefe. Mit dem Agassiz Trawl gelang es an Lokationen mit dichter Besiedlung, einige der im OFOS beobachteten Lebewesen an Deck zu holen, um die Fauna bestimmen und analysieren zu können.

Wir kombinierten unsere Messungen gezielt an Orten, die entweder durch Anomalien in der Wassersäule auffällig waren, an geologischen Störungen lagen oder durch erhöhten Wärmestrom zeigten (Fig. 1.2). So konnten wir das geologisch-biologische System umfassend beschreiben und unser Wissen über die residente Tiefseefauna, mikrobielle Diversität und chemosynthetischer Produktivität dieser entlegenen Regionen erweitern.

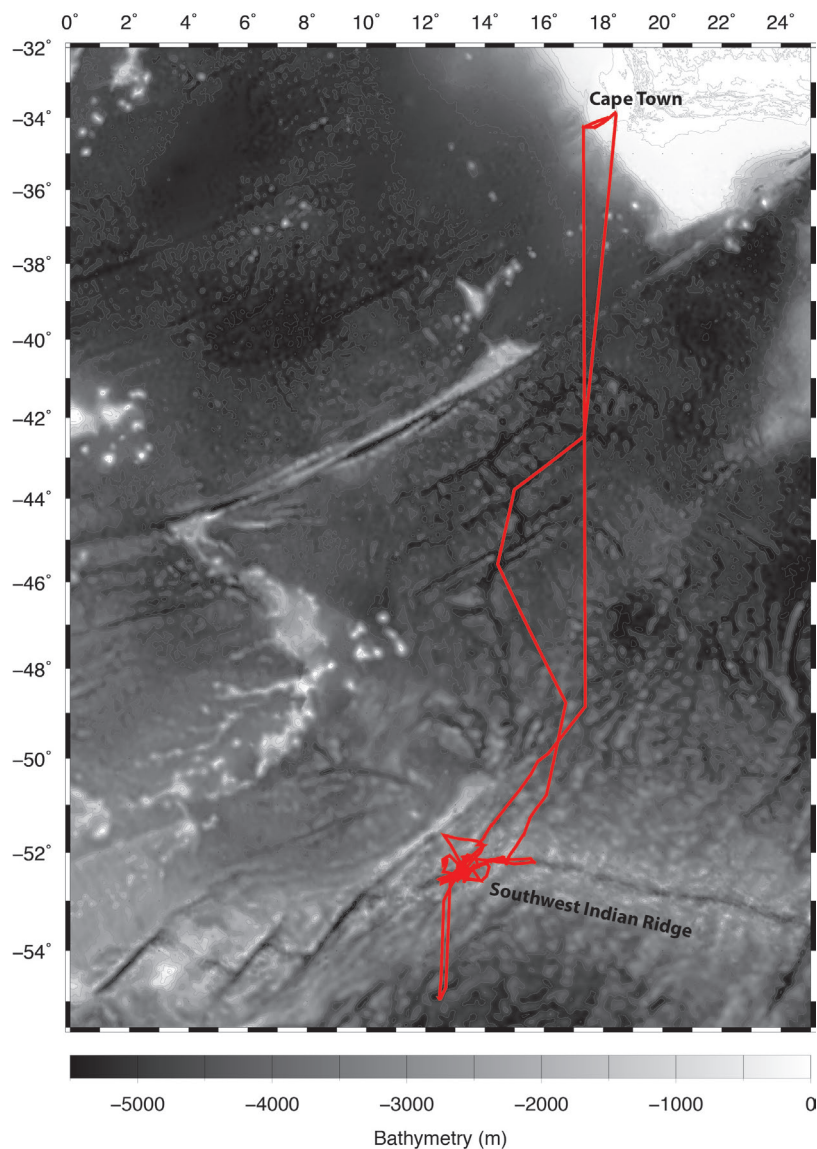


Fig. 1.1: Reiseroute von Polarstern während ANT-XXIX/8 zum Messgebiet am Südwestindischen Rücken

Cruise track of Polarstern during ANT-XXIX/8 to the research area at the Southwest Indian Ridge

1.2 Fahrtverlauf

Nachdem *Polarstern* Kapstadt verlassen hatte, wurden noch das DOLOG und das Posidonia System kalibriert. Die Arbeiten dauerten bis zum späten Abend des 10.11.2013. Am Morgen des 11. November wurden dann die für die Tests an Bord verbliebenen Techniker vom Hubschrauber abgeholt und *Polarstern* setzte ihren Kurs nach Süden fort.

Am 15.11.2013 führten wir eine Referenzwärmestrommessung in ca. 50 Millionen Jahre alter Erdkruste durch. Danach näherten wir uns dem Messgebiet entlang eines Profils mit weiteren Wärmestrommessungen, einer Referenz CTD und einem Test des TV Multicorers (TV MUC).

Vom 17.11. morgens bis zum 19.11. abends wurden 5 refraktionsseismische Profile über die im Dezember 2012 während ANT-XXIX/2 ausgebrachten Ozeanbodenseismometer geschossen. Danach begannen wir in unserem zentralen Messgebiet an einem von Störungen begrenzten Bergrücken südlich des Rifttals mit der CTD und dem OFOS nach Anzeichen hydrothermalen Aktivität zu suchen. An diesem Ort wurde von Bach *et al.* (2002) in einer früheren Expedition starke Trübe- und Temperatursignale in der Wassersäule gemessen. Am Morgen des 20.11. zeichneten sich ruhige Wetterverhältnisse ab, so dass wir - unterbrochen von einer Wärmestrommessung während der Dunkelheit - bis zum Abend des 21.11.13 insgesamt 8 OBS bergen konnten. Das 9. Gerät reagierte nicht auf die akustischen Auslösesignale. Wegen eines nahenden Schlechtwettergebiets mussten wir nach Süden ausweichen. Dort konnten wir bei ruhigeren Wetterverhältnissen mit dem TV MUC das Leben am Meeresboden weit außerhalb des Riftsystems beobachten und eine Sedimentprobe gewinnen. Nach Rückkehr ins Messgebiet am 23.11. setzten wir unsere CTD und OFOS Suche nach hydrothermalen Quellen fort, bevor wir am 24.11. morgens erneut zu 24 stündigem Abwettern diesmal weiter nördlich gezwungen waren. Bis zum 28.11. verblieben wir im zentralen Messgebiet und untersuchten die unterschiedlichen Lebensräume an beiden Riftflanken und im zentralen Rifttal, begleitet von Wärmestrommessungen und der Bergung eines weiteren OBS.

Nachdem wir bislang keine klassischen hydrothermalen Plumes finden konnten, sondern typischerweise inhomogene Wolken trüben Wassers nahe des Meeresbodens, wandten wir uns anderen Messorten weiter im Osten zu. Unterwegs zum sogenannten Narrowgate Vulkansegment stießen wir bei Wärmestrommessungen auf einen Punkt mit stark erhöhtem Wärmestrom. Zu diesem Punkt kehrten wir am 1.12.2013 zurück, nachdem wir uns davon überzeugt hatten, dass ein weiterer aus früheren Expeditionen bekannter Plume östlich von Narrowgate Vulkan wieder eine bodennahe Trübewolke darstellte. Wir beprobten diesen warmen Punkt ausführlich und konnten unter anderem feststellen, dass die mit der Wärmestromlanze gemessenen Temperaturen sich decken mit Messungen am Sediment, das wir mit dem Schwerelot gewannen. Nach einem erfolgreichen Agassiz Trawl kehrten wir am 3.12. in das zentrale Messgebiet zurück, um dort die *in-situ* Beprobung je eines Ortes an der nördlichen und südlichen Riftflanke und eines Punktes im tiefsten Teil des Rifttals durchzuführen. Unterwegs wollten wir das Wärmestromprofil entlang des Rückens verdichten, mussten bis zum Morgen des 4.12. aber unser Messprogramm wegen eines Defekts an der Wärmestromlanze und der CTD sowie ungünstiger Wetterverhältnisse unterbrechen. Am 5.12. suchten wir entlang eines langen CTD Transekts über eine junge Vulkanstruktur nach hydrothermalen Anomalien, aber auch hier konnten wir keine ausgeprägte Aktivität feststellen.

Am Abend warteten wir leider vergeblich auf das Auftauchen des letzten OBS. Nach einer CTD an einem Hang mit Sulfidablagerungen weiter westlich, und nun erfolgreichen Wärmestrommessungen im zentralen Rifttal wandten wir uns am 7.12. kraterähnlichen Strukturen nördlich des Rifttals zu, von deren Hängen uns der TV Greifer vulkanisches Material mitbrachte. Mit dem 8.12. verabschiedeten wir uns aus dem Hauptarbeitsgebiet und dampften unterbrochen von einem weiteren Agassiz Trawl zum Narrowgate Vulkansegment. Hier möchten wir die Unterschiede in Geologie und Biologie zu der amagmatischen Region feststellen. Zunächst wurden die Hänge der nördlichen Riftflanke mit dem OFOS untersucht und reiches Leben festgestellt. Beim Versuch, mit dem TV Greifer Bruchstücke von Laven, Sediment und Brachiopoden zu fassen, wurde das Glasfaserkabel beschädigt. Wir beendeten die Untersuchungen am Narrowgate Segment mit zwei CTD casts vorzeitig und dampften dann entlang des Wärmestromprofils ab dem 9.12. morgens gen Nordosten. Der 11.12. sah dann das Ende der Forschungsarbeiten mit einer OFOS und TVMUC Referenzstation bereits jenseits des 50. Breitengrades. Auf der Rückreise legten wir unsere Route so, dass wir noch von 2 ungewöhnlichen bathymetrischen Strukturen hochauflösende Daten gewinnen konnten. Am 16.12.2013 endete unsere Reise morgens in Kapstadt.

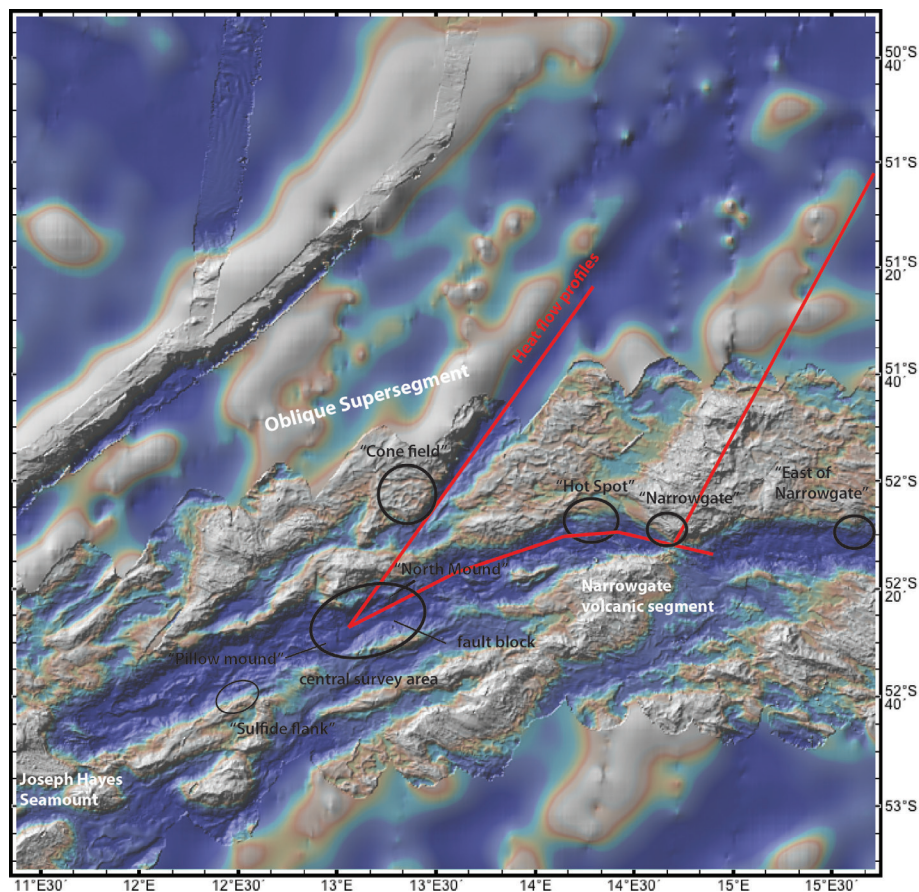


Fig. 1.2: Das Oblique Supersegment am Südwestindischen Rücken. Bathymetrie von Ryan et al. (2009). Schwarze Ellipsen markieren Orte und ihre Arbeitsnamen, an denen wir Messungen konzentrierten. Rote Linien sind Wärmestrom-Profile.

Map of the Oblique Supersegment of the Southwest Indian Ridge. Bathymetry is from Ryan et al. (2009). Black ellipses mark sites and their work names where we focussed our research. Red lines indicate sections along which heat flow measurements were made.

1.1 Zusammenfassung

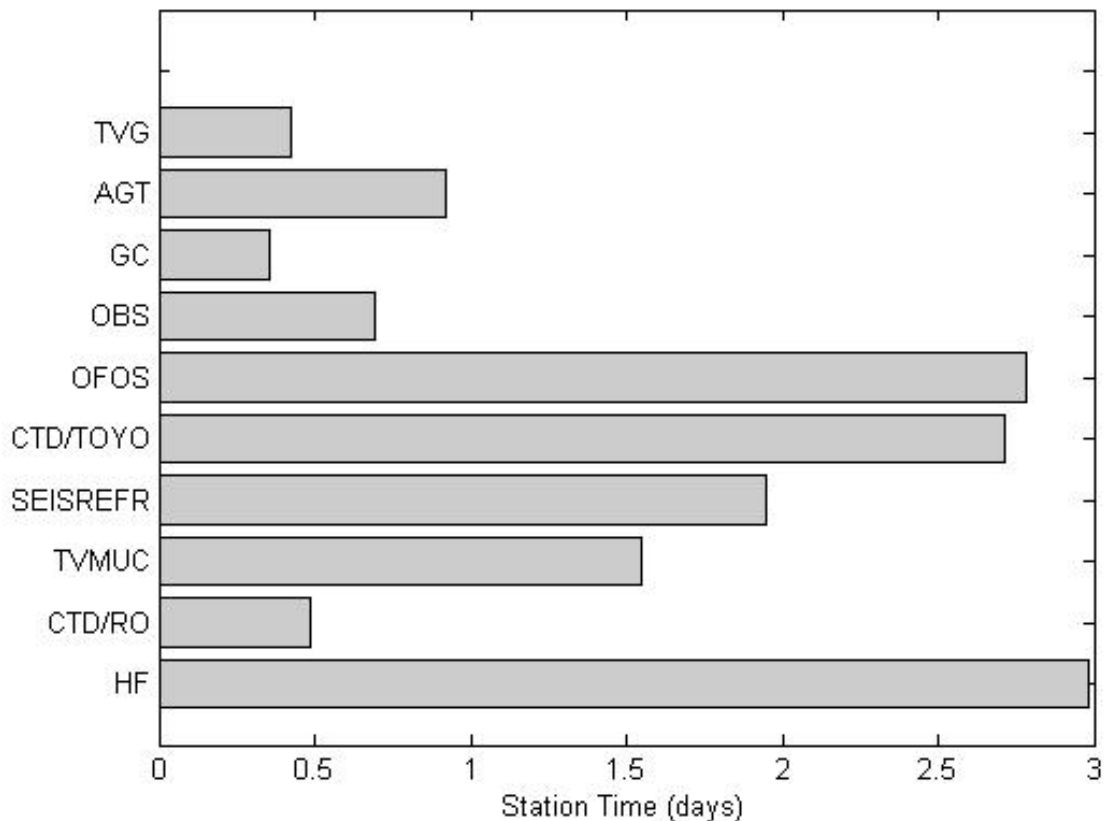


Fig. 1.3: Verteilung der Stationszeit auf die genutzten Geräte. TVG: TV-Greifer; AGT: Agassiz Trawl; GC: Schwerelot; OBS: Ozeanbodenseismometer; OFOS: Ocean Floor Observing System; CTD/TOYO: CTD im tow-yo mode; SEISREFR: Refraktionsseismik Profil; TVMUC: TV-Multicorer; CTD/RO: Einzel-CTD; HF: Wärmestromlanze

Fig 1.3: Distribution of station time on individual gear. TVG: TV-grab; AGT: Agassiz Trawl; GC: Gravity corer; OBS: ocean bottom seismometer; OFOS: ocean floor observing system; CTD/TOYO: CTD in tow-yo mode; SEISREFR: seismic refraction profiling; TVMUC: TV-Multicorer; CTD/RO: CTD single dip; HF: heat flow lance

Insgesamt absolvierten wir während des Fahrtabschnitts 80 wissenschaftliche Stationen, 79 davon im Messgebiet, die 80. Station galt der Erfassung der Schallgeschwindigkeit in der Wassersäule zur Kalibration der bathymetrischen Daten. Wir verbrachten 642 Stunden im Messgebiet und konnten 54 % davon rein für Stationszeit nutzen, gerechnet vom Eintauchen eines Geräts ins Wasser bis zur Rückholung an Deck. Weitere 36 % der Zeit vergingen mit Positionieren des Schiffs für die Messungen, bathymetrischen Messungen und mit Transitstrecken. Lediglich 10 % der Zeit fielen dem Wetter zum Opfer. Fig. 1.3 zeigt die Verteilung der Stationszeit auf die einzelnen Geräte.

SUMMARY AND ITINERARY

On November 9th, 2013, *Polarstern* left Cape Town, South Africa, around 8 p.m. heading southwards for the Southwest Indian Ridge near 52°30'S and 12-15°E. In this area, cruise ANT-XXIX/8 studied geological processes and biological communities of an active mid-ocean ridge (Fig. 1.1).

The Southwest Indian Ridge (SWIR) opens with less than 15 mm/y full spreading rate and therefore belongs to the slowest spreading mid-ocean ridges on Earth, the so-called ultraslow spreading ridges. Due to their remote location, ultraslow spreading ridges, namely the Arctic Ridge System and the SWIR, are only poorly explored. Our current knowledge of ultraslow spreading ridges indicates that spreading along these ridges differs greatly from established models of seafloor spreading. Despite a limited production of melts and an unusually cold lithosphere, ultraslow spreading ridges host surprisingly many hydrothermal anomalies in the water column above the central rift, which may hint to active hydrothermal venting. Magma at ultraslow spreading ridges is focussed to distinct volcanic centres whereas in the intermittent ridge sections, mantle rocks are exposed on the seafloor. Our cruise heads for such a magma-starved ridge section, the so-called Oblique Supersegment of the Southwest Indian Ridge that is flanked by two pronounced volcanic centres (Fig. 1.2).

With an interdisciplinary team of 33 scientists, we all worked in the same survey area on project "SWEAP", Southwest Indian Ridge Earthquakes and Plumes. Our cruise featured frequent changes of survey and sampling tools that hand in hand yielded a detailed picture of the Southwest Indian Ridge as geologically active region and as biological habitat.

The geophysics program studied the structure of the Earth's crust and observed the earthquakes activity related to active spreading processes. The maximum depths of earthquake hypocentres and comprehensive measurements of the heat flux in profiles parallel and perpendicular to the rift axis will allow us to conclude on the thermal state of the lithosphere once data are processed.

The CTD probe was used in tow-yo mode and yielded real-time data reflecting the physical and chemical properties of the water column, including temperature, salinity, turbidity and redox potential. In addition, water samples were taken to detect for example methane. Similar sensors were mounted to the Ocean floor observing system (OFOS).

OFOS was used to film the seafloor and observe organisms inhabiting the seafloor and to quantify their occurrence. We also employed a TV multicorer (TV MUC) to sample the uppermost part of the sedimentary layer where the organisms live. The gravity corer complemented these measurements penetrating up to 6 m into the sediment. In densely populated areas, the Agassiz Trawl was towed along the seafloor and brought some of the organisms observed with OFOS on board such that their species can be determined and further biological analysis is possible.

We combined and focussed our measurements at selected target sites, that either were characterized by anomalies in the water column, were situated at fault systems or showed increased heat flux. This approach allowed us to comprehensively describe the geo-biological system and improve our knowledge about the resident deep-sea fauna, microbial diversity and chemosynthetic productivity of this remote area.

Cruise narrative

After leaving Cape Town, *Polarstern's* onboard DOLOG and Posidonia systems had to be calibrated. The calibration procedure was terminated late on the evening of November 10th. The following morning, the technicians that had remained on board to conduct the tests were picked up by a helicopter and *Polarstern* could start her southward journey.

On November 15th, we measured the heat flow in 50 million year old crust to obtain a reference value. We then approached the survey area along a profile where we performed further heat flow measurements, got a CTD reference profile of the water column and tested the TV MUC.

From early on November 17th until the evening of November 19th, we shot altogether 5 refraction seismic profiles crossing the sites of 10 ocean bottom seismometers (OBS) that had been deployed in December 2012 during ANT-XXIX/2. After that, we started our CTD and OFOS-search for hydrothermal plumes in our central survey area at a fault bounded ridge forming the southern rift valley wall. At this location, Bach et al. (2002) had found significant turbidity and temperature anomalies during an earlier expedition. On November 20th, weather conditions were favourable such that we could recover 8 OBS, only interrupted by a heat flow station during the hours of darkness. The ninth OBS did not react to the release signals and we had to stop recovery heading south to avoid an approaching storm. At our shelter position, wind and sea conditions were calm enough to allow the use of the TV MUC. We could observe life at the seafloor away from the mid-ocean ridge and gain a sediment sample. After returning to the survey area on November 23rd, we continued our search for hydrothermal plumes but had to interrupt research for another 24 hours early on the morning of November 24th due to bad weather conditions. Until November 28th, we remained in the main survey area and studied the different habitats on both rift flanks and in the central rift valley and performed further heat flow measurements.

As we did not find hydrothermal plumes in the classical sense but typically detected inhomogeneous clouds of murky water close to the seafloor, we decided to investigate other sites further to the east. On our way to the Narrowgate volcanic segment, a heat flow station revealed a site of significantly increased heat flux and temperatures at the seafloor. We returned to this "hot spot" on December 1st, because the potential hydrothermal plume east of Narrowgate that had been described by a previous expedition turned out to be again a turbidity cloud close to the seafloor.

We focussed our activities at the "hot spot" and could for example confirm the increased temperature values measured *in-situ* with the heat flow probe with temperature measurements on sediment cores recovered with the gravity corer. After a successful Agassiz Trawl we headed back to the main survey area on December 3rd to complete the sampling of sites on the northern and southern rift flanks and in the central rift valley. Underway we intended to finish the heat

flow profile along the ridge, but were forced to interrupt measurements until the morning of December 4th due to a damaged heat flow probe, a technical problem of the CTD and strong winds. On December 5th, we searched a young volcanic mound for hydrothermal plumes but couldn't detect significant activity. Later in the evening, we waited in vain for the last OBS to surface. After a CTD along a ridge flank with sulfide deposits further to the west and now successful heat flow measurements in the central rift valley we headed on December 7th northwards to a field of crater-like structures north of the rift valley. With the TV-Grab we recovered volcanic material from the slopes of these craters. On December 8th we left the main survey area and steamed eastwards to the Narrowgate Segment, doing a final Agassiz Trawl underway. At Narrowgate, we wanted to determine the differences in geology and biology between a magmatic and an amagmatic region. We imaged the rocky slopes of the northern rift flank with OFOS discovering abundant life. When we tried to grab lava fragments, sediments and brachiopoda, the TV grab damaged the glass fibre cable. Therefore, we prematurely terminated our research programme at Narrowgate with two CTD casts and steamed from December 9th onwards towards the northeast along the planned heat flow profile which we prolonged with another two sites. December 11th saw the end of our research activities with an OFOS and TVMUC reference station already north of 50°S. On the way to Cape Town we gathered high resolution bathymetry data from two conspicuous structures at the seafloor. We reached Cape Town on the morning of December 16th, 2013.

Altogether, we completed a total of 80 scientific stations during this cruise, 79 in the survey area and the 80th station, a sound velocity profile to calibrate bathymetric data, on our way to Cape Town. We spent 642 hours in the survey area and could use 54 % solely for station work, calculated from the moment, an instrument enters the water until it is back on deck. An additional 36 % of the time was needed to position the ship for the measurements, conduct bathymetric surveys and transit between survey sites. Only during 10 % of the time, the weather prohibited any research activities. Fig. 1.3 shows the distribution of station time on the individual gear used.

References

- Bach W, Banerjee NR, Dick HJB, Baker ET (2002) Discovery of ancient and active hydrothermal deposits along the ultraslow spreading Southwest Indian Ridge 10-16°E. *Geochemistry, Geophysics, Geosystems* 3, 10.1029/2001GC000279, 1-14.
- Ryan WBF, Carbotte MS, Coplan JO, O'Hara S, Melkonian A, Arko R, Weissel RA, Ferrini V, Goodwillie A, Nitsche F, Bonczkowski J, Zemsky R (2009) Global multi-resolution topography synthesis. *Geochemistry, Geophysics, Geosystems*, 10, Q03014, doi:10.1029/2008GC002332.

2. WEATHER CONDITIONS DURING ANT-XXIX/8

Robert Hausen, Juliane Hempelt

DWD

We set sail from Cape Town in the evening hours of 9th November 2013 delayed by 4 hours. The weather situation was determined by an extensive high (1025hPa) east of Gough Island, with a ridge of 1,020 hPa being responsible for descending air with fair conditions so far. Combined with lower pressure (1,010 hPa) over the rural South Africa we hit the wind field of the so called „Cape-Doctor“ with Bft 7 from Southeast just after leaving the harbour. After short calibration measurements, some technicians from AWI were brought back to Cape Town by helicopter (flight weather conditions: Clouds And Visibility OK (CAVOK), hazard only due to moderate turbulence) and we proceeded to the survey area of the South West Indian Ridge (SWIR) in the evening of 10th November without a helicopter on board.

During this 4-days transit, we crossed a weak depression followed immediately by a ridge but without meteorological activities worth mentioning, except reduction of visibility. Approaching the research area, we were affected by the frontal system of a severe gale, but it was fortunately just in a weakening progress. As a consequence of the storm track south of us, a strong westerly flow set in with the permanent risk of shallow wave disturbances following from west. So from time to time we faced gale 7-8 Bft with gusts nearly 10 Bft from west to northwest including an about 6 metres significant wave height in the period from 16th to 19th November.

Afterwards the flow shifted intermittently to southwest leading to a widespread flood of polar air mass of Antarctic origin (T850hPa < -10°C). Within this air mass, a ridge developed at the surface but was superimposed by an upper-level trough inducing some snow showers as well. At this time, we registered the lowest temperature of the whole cruise with -2.0°C minimum in the night of 20th November.

In the mean time, the drift of westerly winds reproduced again. So a severe storm 960 hPa developed at 22.11. near 55°S 5°W moving eastwards very quickly. Due to the fact that the isobars in the centre of the storm did not show any significant gradient anymore, which was also calculated precisely from the models, master and chief scientist followed the recommendation of the meteorologist to go for shelter near 55°S 12.7°E in the vicinity of the core of the storm. There, we encountered conditions of cyclonic winds 3 to 5 Bft and hardly 3 m sea allowing even some research activities. On our return to the Southwest Indian Ridge, we had only 5 - 6 m outflowing swell from ahead, which was comfortable considering the avoidance of westerly winds 10 Bft and 10 m significant wave height. It did not take a long time until the next „disc“ developed west of us, but this time with a minimum pressure close to 940 hPa! Reaching its climax on western longitude, it moved more or less eastwards, pretending to take a south-easterly course at the beginning. So it became clear that a gale event of 10 Bft average wind speed with severe gale force gusts and 10 m cross sea would be very likely. In addition, the opportunities for shelter were reduced. An enhanced risk of drifting table icebergs existed in the south with an edge of sea ice near 58°S. Escaping to the north near

50°S would have meant an effective time loss of about three days. The Master and chief scientist decided for a compromise to go for shelter near 51°S, 14°E, to avoid at least the main storm field in the south. But the weather conditions worsened just in the noon hours of the 24th November to such an extent that we did not reach the originally planned shelter position, but leaned into the sea near 52°S, 14°E waiting until the wind died down during night time.

In fact, we registered averaged 10 minute winds of 10 Bft from northwest with maximum gusts of 64 knots (12 Bft) and a significant wave height at least of about 10 metres including some single peaks, which had probably almost twice the mean wave height, which is definitely not a contradiction to the classic wave spectrum. Estimates made by experienced crew members resulted in a maximum wave height approximately close to the ground level of the bridge corresponding to 17 metres height. Approaching the midnight hours, the wind slowly died down.

A couple of calmer days with wind speeds rarely above 7 Bft and sea heights around 5 m provided nearly undisturbed working conditions in the following time. Embedded in a moderate westerly flow between the subtropical high pressure zone near 40°S, depressions moved close to the edge of the sea ice along 60°S. As usual, fronts (warm fronts and cold fronts) crossed us periodically, leading to an at least partly snow-covered deck with a few degrees below zero in the morning hours of 26th and 27th November, respectively. But with increasing global radiance and starting daily "vessel's business", the snow melted instantaneously. In the morning hours of the 30th November, probably the biggest table ice mountain of the entire cruise appeared near the horizon in a distance of about 13 miles to southeast.

In the meantime the streaming shifted to northwest, so very warm air with subtropical origin (T850 hPa > 5°C) was advected into our survey area. In combination with water temperatures degrees at only a bit above zero widespread misty conditions with fog patches at times were not very surprising, concerning the high dew points spreading southwards. However, we hardly registered an air temperature above +3°C. Afterwards, we left already the last significant increase of wind speed and wave in the night to the 4th December behind us. It was caused by a powerful low (970 hPa), which moved towards east along the 58° S and so the pressure gradient on its northern flank became enhanced again. Considering the conditions of the days before, the sudden wind shift to southwest after the passage of the trough produced a rather rough, crossing sea with heights of 6 m in combination with the persistent swell of about 4 m from northwest. In the instant cold air advection in upper tropospheric layers, the unstable stratification lead to an enhanced activity of squalls in general, which forced up the 10 minute average wind speed to 9 Bft for a few hours without intense snow showers.

The next remarkable event was a break-down of the circumpolar circulation in a very unusual manner in these latitudes. The wave number of the circulation pattern in 500 hPa reduced from 5 to 4 in combination with an increase of amplitude stopping the further progressive movement of troughs and ridges almost instantaneously. At that moment, the survey area was located favourably inside a stable ridge axis of the powerful subtropical high near 40°S 10°E, so that we enjoyed almost ideal working conditions with wind speeds mostly below 6 Bft and wave heights around 3 m - especially for that marine region - during the period from 05th December until the date of our departure back to Cape Town in the morning hours of the 11th December. The only significant weather phenomenon had been the advection fog, which persisted a couple of days. But its vertical thickness was limited to only a few

hundred metres, so the sun appeared from time to time. A well-defined inversion developed with around 10°C in 950 hPa height compared to 0°C temperature of water and air at the surface. Above that inversion, descending fluxes caused a very dry troposphere.

On our return to Cape Town the visibility improved immediately with increasing water temperatures in combination with a wind shift towards south. Just before we reached the final destination a small low passed with an average wind speed of 7 Bft, but wave heights could not build up fully, so we safely entered the harbour in the morning hours of the 16th December.

Figures 2.1-2.4 summarize the weather and sea conditions.

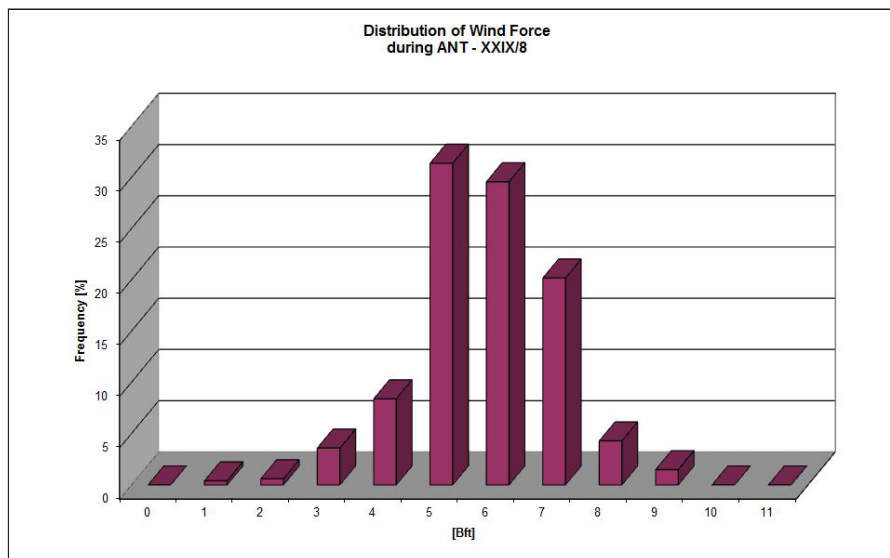


Fig. 2.1: Distribution of wind force

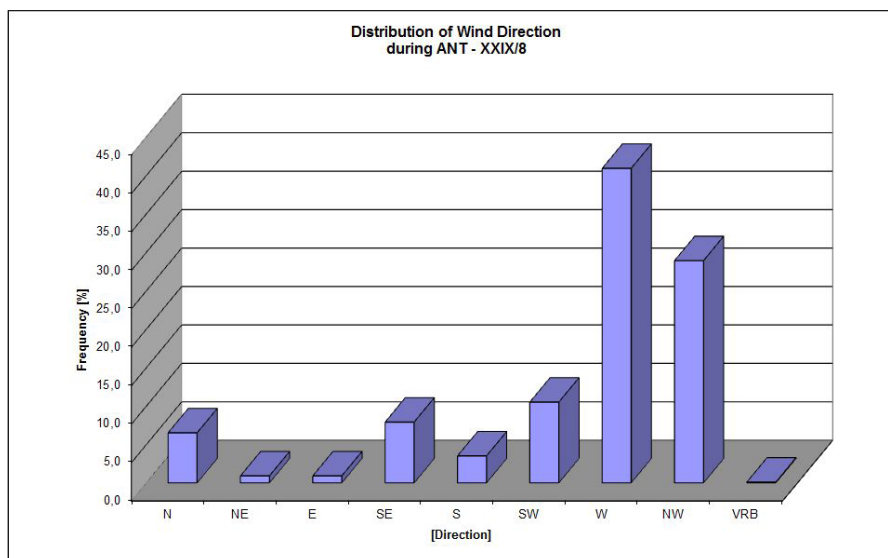


Fig. 2.2: Distribution of wind direction

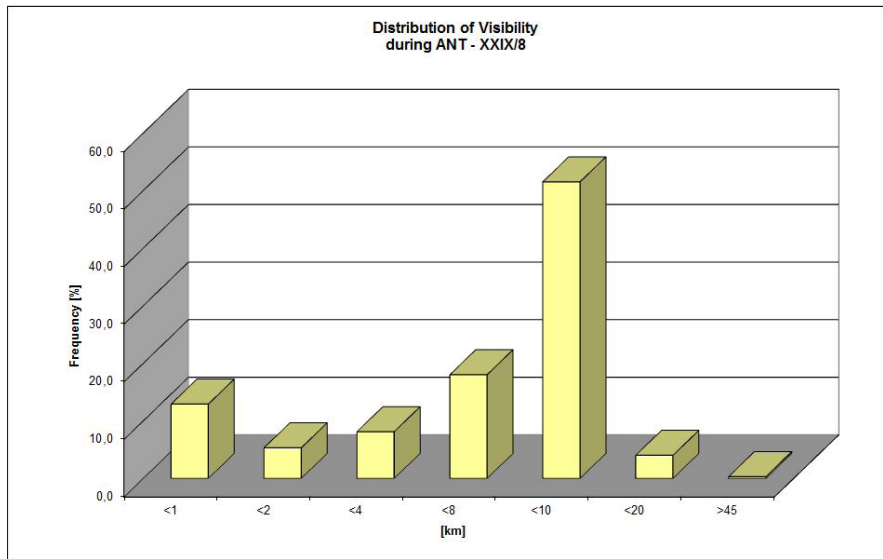


Fig. 2.3: Distribution of visibility

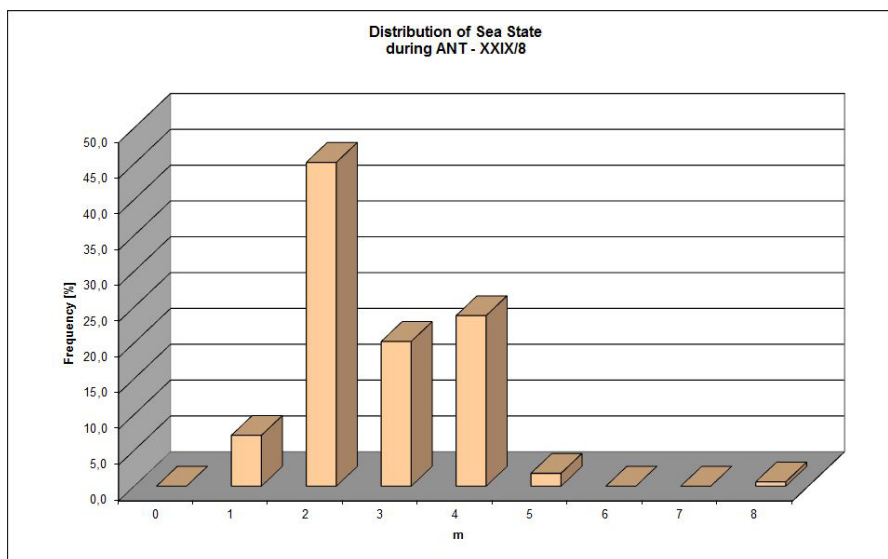


Fig. 2.4: Distribution of sea state

3. SEISMOLOGY

Vera Schlindwein, Susanne Coers, Katharina AWI
Hochmuth, Henning Kirk, Norbert Lensch,
Florian Schmid, John-Robert Scholz

Objectives

Ocean basins are formed by seafloor spreading at active mid-ocean ridges. Mantle material is upwelling under the ridges and melts to produce magma, which erupts onto the sea floor and crystallizes at depth to produce new oceanic crust. Crustal generation and plate separation rate keep pace over a wide range of spreading rates and produce oceanic crust with a uniform thickness of about 7 km. Yet, models predict that at spreading rates below about 20 mm/y, the mantle loses heat by conduction and only small amounts of melt are produced at large depths (Bown & White, 1994). Consequently, magmatism and crustal thickness should decrease with decreasing spreading rate. Volcanic eruptions should be unlikely at ultraslow-spreading ridges (< 20 mm/y). Until recently, very little data from ultraslow-spreading ridges were available to verify this theory because these ridges are located in remote ocean basins like the ice covered Arctic Ocean and the stormy Southern Ocean.

Contradicting the common theory, ultraslow-spreading ridges are divided into segments with pronounced volcanism and segments lacking any signs of mantle melting, their distribution being independent of the spreading rate (Michael *et al.*, 2003). New models are therefore necessary to describe the processes of crustal generation at ultraslow-spreading ridges.

Microearthquakes image the active tectonic and magmatic processes at mid-ocean ridges and therefore help to understand crustal generation. At ultraslow-spreading ridges the microseismicity is hardly explored. The junior research group "MOVE" at AWI studies the seismicity of ultraslow-spreading ridges in various projects (e.g. Läderach *et al.*, 2012; Schlindwein, 2012; Schlindwein *et al.*, 2013). Up to now, we have mainly studied the Arctic ridge system, which is tectonically less complicated than the Southwest-Indian ridge (SWIR). In the Arctic, we used land seismometers installed on drifting ice floes to record earthquakes as small as magnitude 1 or below (Läderach & Schlindwein, 2011). The drawback of this method is that we could only acquire data for time periods of 2-3 weeks, which is very little to record statistically representative numbers of earthquakes.

We therefore focus our current research activities at the SWIR, which is located halfway between Africa and Antarctica. The open waters allow using Ocean Bottom Seismometers (OBS), which are deployed on the seafloor and can remain there for a period of about one year and thus record sufficiently high numbers of small earthquakes. Up to now, no *in-situ* records of the seismicity of the SWIR exist, because the recovery of the OBS in stormy waters is risky. In addition, the SWIR is

not an ideal candidate for studying ridge processes as it is tectonically complicated, being oriented obliquely to the direction of plate motion. Especially at the eastern part of the SWIR, magmatic and amagmatic crustal production are unstable in time and space such that a complicated structure results.

In our current project, we want to compare the seismicity and structure of a site of magmatic crustal production and a site of amagmatic crustal production. For the magmatic site, we chose a recently active submarine volcano at the eastern SWIR. It has been instrumented during a cruise with Marion Dufresne in September and October 2012 with 8 OBS. Recovery took place parallel to our cruise during Meteor cruise M101/2. Our current *Polarstern* expedition is dedicated to the exploration of spreading processes of an amagmatic ridge section, the so-called Oblique Supersegment. We aim to record several thousands of small earthquakes, the location of which can tell us for example about the maximal depth of faulting and thus the thermal structure of the lithosphere. In addition, we obtain information about the crustal structure of the survey area from refraction seismic profiling. We instrumented the survey site during ANT-XXIX/2 one year ago (Fig. 3.1) with 10 OBS, which needed to be recovered during ANT-XXIX/8.

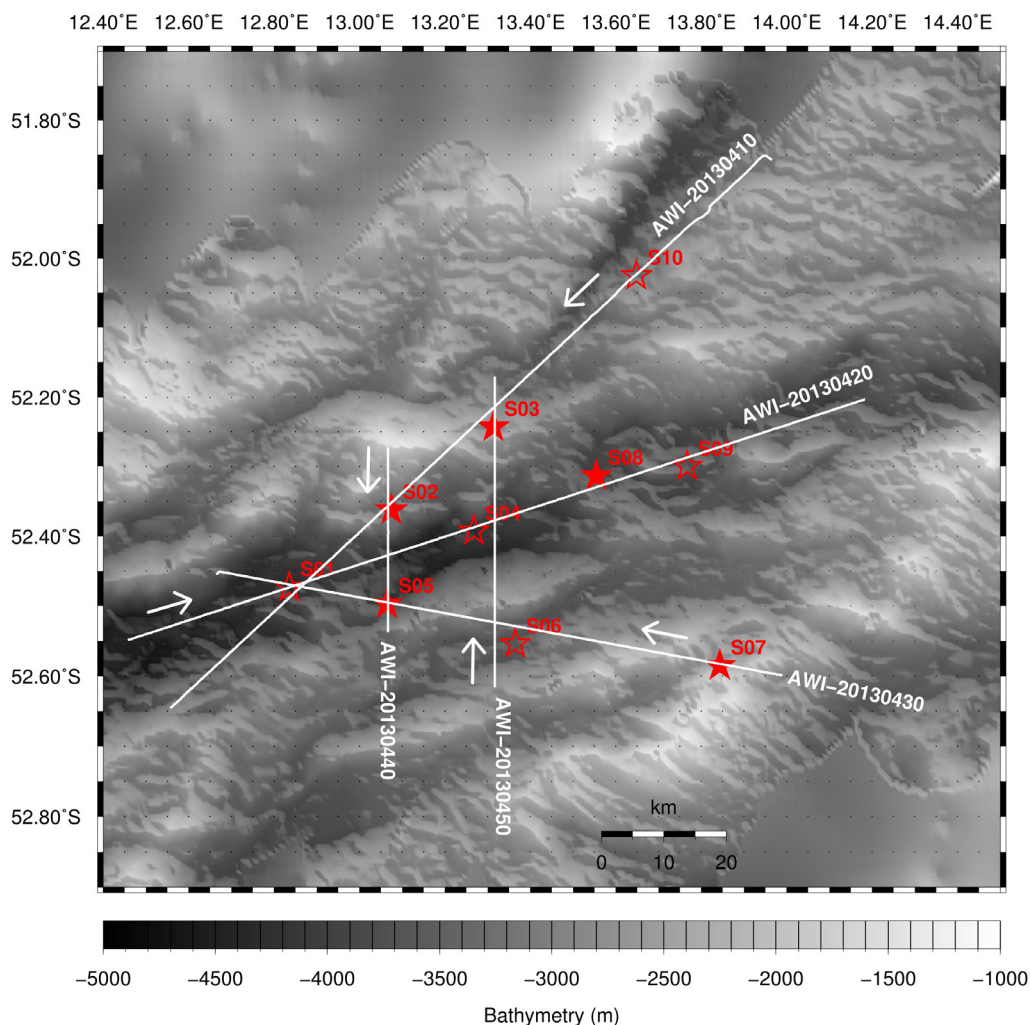


Fig. 3.1: OBS positions and refraction seismic profiles of the SWEAP seismic experiment at the Oblique Supersegment of the Southwest Indian ridge. Filled stars indicate OBS stations that have recorded airgun signals. Empty stars indicate OBS stations that have not recorded the airgun signals. White arrows indicate the profile direction.

3.1 Refraction seismics

Work at sea

For the SWEAP refraction seismic experiment, four G-gun type airguns were used as seismic sources, each having a volume of 520 cubical inch (approx. 8.5 liters). The guns were arranged in two clusters and were towed at a depth of 12 m behind the vessel (Fig. 3.2).



Fig. 3.2: Impression of the airgun operations at sea. From left to right: the triggerbox unit, providing the electric pulse to fire the G-guns; G-gun cluster, hanging in the deployment frame on the aft deck; flotation buoys to maintain a fixed depth of the airguns in the water.

The positions of the two clusters relative to *Polarstern's* Trimble 1 GPS antenna are displayed in 33.

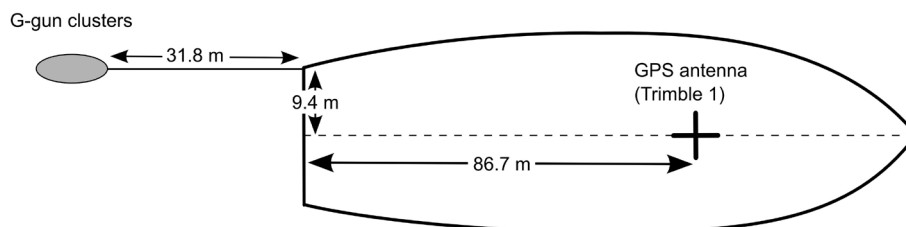


Fig. 3.3: Relative positions of the airgun clusters to *Polarstern's* Trimble 1 GPS antenna. Figure not to scale.

The G-guns were operated at a pressure of 200 bars and were synchronously fired every full minute. The trigger signal was provided by the triggerbox (Fig. 3.2)

which received the time stamp from a high precision Meinberg clock. Shot point coordinates were retrieved via Davis-ship scientific data management system and afterwards corrected for the offset between the GPS antenna (Trimble 1) and the G-gun clusters.

Prior to the start of airgun operations for individual refraction seismic profiles, a soft start was performed switching on the airguns one after another, within a period of 20 min. Airguns were shut off for transit between individual profiles. In order to prevent any marine mammals from potentially harmful seismic noise produced by our airguns, two marine mammal observers took position on *Polarstern's* bridge. Marine mammal observation was started 40 minutes prior to each soft start and continued throughout the period of airgun operations, except for hours of darkness. In case of marine mammals entering the 300 m exclusion zone around the vessel, airgun operations would have been abandoned immediately. However, no marine mammals were observed throughout the period of airgun operations, neither in the mitigation zone of 1,000 m radius around the vessel nor in the exclusion zone.

Table 3.1 gives an overview over the airgun operations. Throughout the airgun operations, the vessel maintained a speed of 5 kn. At 2013/11/18 20:25 (on profile AWI-20130430) the Meinberg clock falsely went off and was quickly replaced by a spare clock. Apart from this 20 minute lasting interruption, no further incident occurred during the airgun operations.

Tab. 3.1: Airgun profiles

Profile number	Start		End		Length
	Date Time (UTC)	Position: Latitude Longitude	Date Time (UTC)	Position: Latitude Longitude	Distance [km]
AWI-20130410	17.11.2013 09:05:00	51° 51.446' S 13° 57.935' E	17.11.2013 23:36:00	52° 38.756' S 12° 33.451' E	130.2
AWI-20130420	18.11.2013 01:06:00	52° 32.908' S 12° 27.459' E	18.11.2013 13:54:00	52° 12.204' S 14° 11.048' E	123.7
AWI-20130430	18.11.2013 18:15:00	52° 35.938' S 13° 59.426' E	19.11.2013 04:10:00	52° 27.319' S 12° 39.991' E	91.3
AWI-20130440	19.11.2013 07:33:00	52° 32.243' S 13° 03.998' E	19.11.2013 10:46:00	52° 16.336' S 13° 04.010' E	29.5
AWI-20130450	19.11.2013 13:01:00	52° 10.245' S 13° 19.014' E	19.11.2013 18:25:00	52° 36.956' S 13° 19.017' E	49.5

After the recovery of the OBS stations, the data recording was stopped, wherever still in progress and the drift (skew) of the recorder clock was measured by comparison with the GPS time signal, using the *sendcom2* software. The compressed raw data were downloaded to a local hard drive, extracted, demultiplexed and *.seggy files were produced. The *.seggy files were plotted as time versus offset seismograms, wherever data was available, for purposes of data quality control.

3.2 Passive seismology

Preliminary results

The airgun signals were recorded only by five OBS instruments (S02, S03, S05, S06, S08), due to the recording of some instruments had stopped beforehand (S06, S09, S10), one recorder was malfunctioning (S04) and one OBS could not be recovered (S01). All in all, data from 8 stations on five refraction seismic profiles was acquired. The recovered seismic data is of good quality, showing clear onsets of seismic phases refracted in the subsurface. An example seismogram for the hydrophone channel of Station S02 on profile AWI-20130410 is shown in Fig. 3.4. Further processing, modelling and interpretation of the refraction seismic data will be done at AWI within the scope of a PhD project.

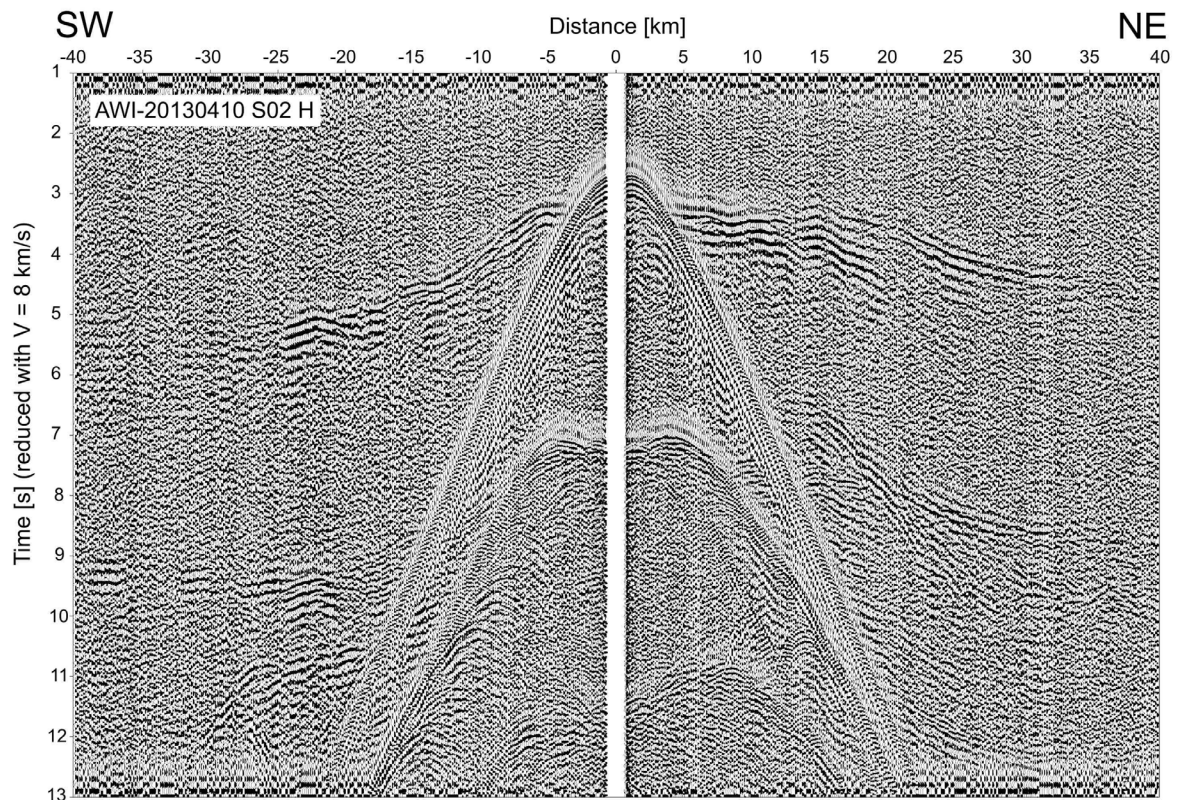


Fig. 3.2: Example of a refraction seismic OBS record (hydrophone channel), plotted as traveltimes (reduction velocity 8 km/s) versus offset for Station S02 on profile AWI-20130410.

3.2 Passive seismology

Work at sea

Seismological work at sea during ANT-XXIX/8 consisted of the recovery of 10 OBS that had been deployed during ANT-XXIX/2. After completion of the airgun operations, we started with the recovery of OBS S10. *Polarstern* approached the deployment position stopping at a distance of about 100-300 m such that the

starboard-side of the ship faced the OBS position. The OBS was then released acoustically, detached itself from its anchor weight and travelled with 1.2 m/s to the sea surface. The ship waited at a distance of 300 - 500 m downwind. Ranging of the OBS produced in all but one recovery no answer from the releaser such that we had no feed-back if the release command has been executed. The OBS surfaced within one minute of the estimated time and could in most cases visually detected before the radio direction finder received a signal of the OBS. The fastest recovery took as little as 10 minutes after surfacing of the OBS until the OBS was on board. On two of the OBSs, the antenna of the radio beacon was missing due to complete corrosion. In addition, the flash light on OBS S09 did not work. This was the first OBS, which we attempted to recover during the hours of darkness. Luckily, the radio beacon still sent weak signals despite the lacking antenna. This finally allowed us to track the OBS and find it with *Polarstern's* search light. As heavy snow fall further complicated the situation, we discontinued OBS recovery at night. OBS S01 did not react to two attempts of release commands executed from various positions. We returned to the OBS at its auto release time and again waited in vain for its appearance. Weather conditions were favourable and we gave up the OBS after two hours of waiting as we were convinced that it would not surface.

Once on board, the OBS were inspected by biologists for any form of life. The biological colonization experiment and the temperature loggers installed on some of the instruments were taken off. Afterwards, we synchronized the OBS clocks and terminated the recording where possible. OBS 06, 09 and 10 suffered from a mechanical problem of the seismometers (Güralp Serial Numbers T4L95, T4K92, T4M50) that drained the battery prematurely. The seismometer failure occurred in the same form on several OBS deployed in the partner experiment and recovered at the same time from *Meteor*. The hydrophone channel of these instruments yielded usable data (Table 3.2). The recorder of OBS S04 failed, data are not readable (Serial Number 120203).

Data of the OBS recorders were downloaded in raw format and then converted to seed day files that we organized in a Seiscomp archive. We inspected day plots (Fig. 3.5) of several stations for quality control. We then selected two representative days, one with plenty of earthquakes, the other one with little activity and phases of high noise amplitudes. These records were used to determine the optimal parameter settings for a STA/LTA trigger by testing several combinations of parameters and visually assessing the results. With a band-pass filter of 3 - 15 Hz, an STA and LTA window length of 5 s and 100 s, respectively, a trigger threshold STA/LTA of 3.6 and a minimum trigger duration of 6.5 s we obtained 1,649 seismic events that triggered at least 3 stations of our network. These events were extracted from the continuous data set with 60 s pre-event time and a file length of 300 s.

3.2 Passive seismology

Tab. 3.2: Summary of OBS recovery

Station name	Deployment			Recovery		Data	
	Date Time (UTC)	Position: Latitude Longitude	Depth [m]	Date Time (UTC)	Position: Latitude Longitude	Amount [GB]	Recorded days
S01	06.12.2012 02:42	52° 28.37'S 12° 50.13'E	4426	-	-	-	-
S02	06.12.2012 00:10	52° 21.81'S 13° 04.22'E	3310	26.11.2013 11:03	52° 21.90'S 13° 04.83'E	23.34	356
S03	05.12.2012 22:27	52° 14.60'S 13° 18.67'E	2977	20.11.2013 13:25	52° 14.60'S 13° 18.81'E	22.19	350
S04	05.12.2012 21:00	52° 23.62'S 13° 15.77'E	4395	20.11.2013 11:00	52° 23.87'S 13° 16.30'E	No data	No data
S05	06.12.2012 01:20	52° 29.89'S 13° 03.76'E	4227	21.11.2013 14:21	52° 29.77'S 13° 04.09'E	23.30	351
S06	05.12.2012 19:30	52° 33.05'S 13° 21.71'E	3695	21.11.2013 11:29	52° 33.15'S 13° 21.94'E	18.60	314
S07	05.12.2012 16:55	52° 34.84'S 13° 50.40'E	2708	21.11.2013 07:52	52° 35.08'S 13° 50.64'E	23.00	351
S08	05.12.2012 14:54	52° 18.66'S 13° 33.33'E	3974	21.11.2013 04:52	52° 18.82'S 13° 33.30'E	23.50	351
S09	05.12.2012 13:20	52° 17.70'S 13° 45.82'E	3818	20.11.2013 20:22	52° 18.31'S 13° 46.51'E	7.56	177
S10	05.12.2012 09:58	52° 01.14'S 13° 38.94'E	3422	20.11.2013 16:55	52° 01.95'S 13° 38.98'E	17.50	296

Preliminary results

The data quality of the seismic records is reasonable, although only about 70 events out of the 1,649 extracted earthquakes were recorded across the entire network. This implies that the majority of the recorded events is of weak and local nature, being detected only by a subset of the network whose dimensions are roughly 70 km. Records contain clearly local events with multiple water reflections (Fig. 3.6) that occur only for records in the vicinity of the source and extend to more regional events where a clearly developed T-phase is discernible. The waveforms are thus comparable to seismic records on the ultraslow spreading Gakkel Ridge obtained by seismometers on drifting ice floes (Schlindwein *et al.* 2007, Läderach & Schlindwein 2011). The event rate with 4.7 locatable seismic events per day in this experiment is lower than at a magmatic site on Gakkel Ridge, although station set-up is not comparable. Nevertheless, the seismicity rate is certainly lower than we expected.

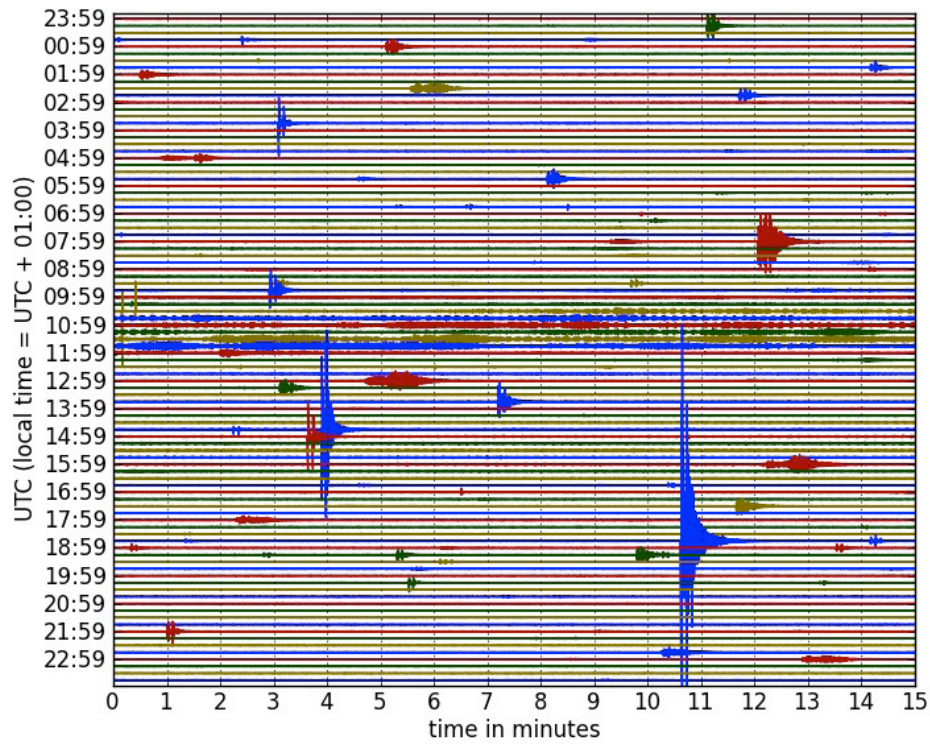


Fig. 3.5: Continuous seismic data of February 7th, 2013, recorded by the vertical component of Station OBS S08. A high-pass filter of 3 Hz is applied. Numerous local seismic events can be seen and a period of increased harmonic noise around 11 am UTC.

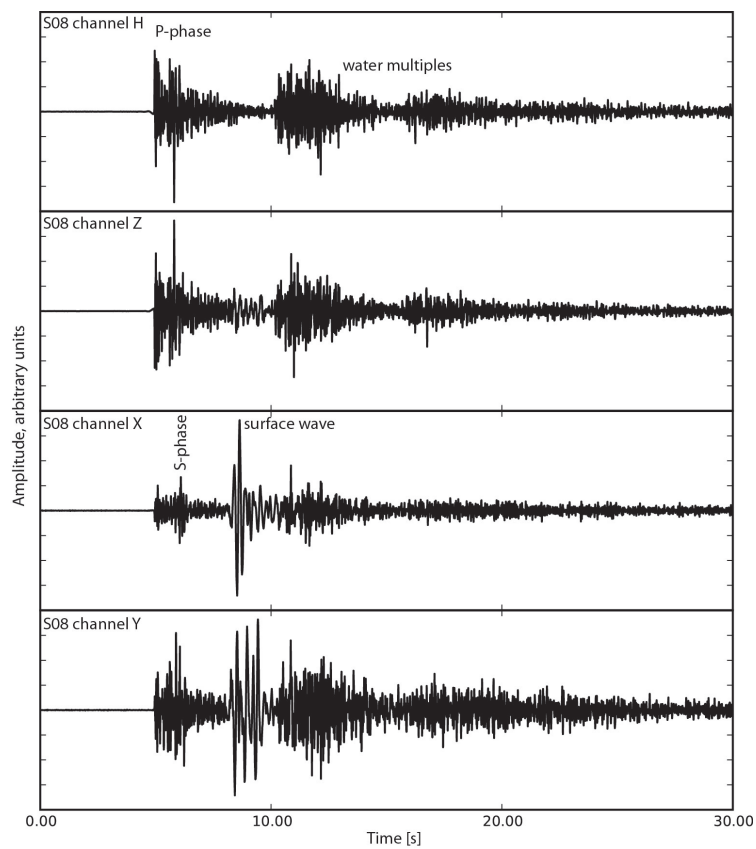


Fig. 3.6: Example of a local seismic event recorded by the 4 components of OBS 08. Note the clearly identifiable phases. Seismogram is highpass filtered with a corner frequency of 3 Hz.

3.2 Passive seismology

Further processing of the data could not be performed on board *Polarstern*. The next processing steps require the correction of the clock drift and the exact determination of the OBS position on the sea floor using the water wave arrivals of the airgun shots, discernible as hyperbolae in the seismic sections (Fig. 3.4). After that, picking of phase arrival times and subsequent earthquake localisation can start. Only then we will be able to relate the seismicity to spreading processes.

Data management

Our seismic data will be archived in a common data repository for all data acquired with the OBSs of the DEPAS instrument pool. This archive is currently being developed and implemented at AWI. After 3 years of restricted access, the data will be made publicly available through the GEOFON seismic data request system.

References

- Bown JW, White RS (1994) Variation with spreading rate of oceanic crustal thickness and geochemistry. *Earth Planet. Sci. Lett.*, 121, 435-449.
- Dick, HJB, Lin J, Schouten H (2003) An ultraslow-spreading class of ocean ridge. *Nature* 426, 405-412.
- Läderach C, Schlindwein V (2011) Seismic Arrays on Drifting Ice Floes: Experiences from Four Deployments in the Arctic Ocean. *Seismol. Res. Lett.*, 82(4), pp. 494-503, doi:10.1785/Gssrl.82.4.494.
- Läderach C, Korger EIM, Schlindwein V, Müller C, Eckstaller A (2012) Characteristics of tectonomagmatic earthquake swarms at the Southwest Indian Ridge between 16°E and 25°E. *Geophys. J. Int.*, 190, p. 429-441, doi: 10.1111/j.1365-246X.2012.05480.x.
- Michael PJ et al. (2003) Magmatic and amagmatic seafloor generation at the ultraslow-spreading Gakkel ridge, Arctic Ocean. *Nature*, 423, 956-961.
- Schlindwein V, Müller C, Jokat W (2007) Microseismicity of the ultraslow-spreading Gakkel ridge, Arctic Ocean: a pilot study. *Geophys. J. Int.*, 169, pp. 100-112, doi:10.1111/j.1365-246X.2006.03308.x
- Schlindwein V (2012) Teleseismic earthquake swarms at ultraslow spreading ridges: indicator for dyke intrusions? *Geophys. J. Int.*, 190, pp. 442-456, doi: 10.1111/j.1365-246X.2012.05502.x.
- Schlindwein V, Demuth A, Geissler WH, Jokat W (2013) Seismic gap beneath Logachev Seamount: Indicator for melt focusing at an ultraslow mid-ocean ridge? *Geophys. Res. Lett.*, 40, pp. 1703-1707, doi:10.1002/grl.50329.

4. HEAT FLOW DETERMINATIONS

Norbert Kaul, Bernd Heesemann,
Daniel Thiel

FB5, Uni Bremen

Objectives

The Southwest-Indian Ridge (SWIR) is an ultraslow spreading mid ocean ridge (< 20 mm/a full rate). Petrological investigations revealed that centers of magmatic activity and magmatic quiet zones interchange. The poor amount of locally generated melt requires a lateral transport from greater depths and a concentration of magma at the active centers. This led to the hypothesis that the lithosphere-



Fig. 4.1: The 6 m Bremen heat flow probe immediately before deployment on Polarstern.

asthenosphere boundary (LAB) varies significantly along the ridge axis. Seismological observations at the ultraslow spreading Knipovich Ridge (Arctic) showed a distinct distribution of earthquake hypocenters (Schlindwein *et al.*, 2013). The depth of the deeper earthquakes draw a sinusoidal contour between 8 and 25 km. Shallower hypocenter depths correlate with active centers, greater depths with an amagmatic section of the ridge. The maximum hypocenter depths follow most likely the LAB which in turn can be regarded as isotherm ($\sim 800^{\circ}\text{C}$). A significant depth change of LAB should therefore be reflected in the measured seafloor heat flow.

Heat flow measurements in conjunction with new seismological observations of AWI will provide important constraints of the concept of a strongly varying LAB potentially also observable at this section of the SWIR.

Work at sea

The 6 m long Bremen heat probe (Fig. 4.1) was used during the cruise to carry out a survey on different segments of the Southwest Indian Ridge. Two heat flow profiles were designed in SSW-NNE direction to sample values on hypothesized "cold" and "warm" off-axis segments on the ridge flank (for location, see Fig. 4.2). They are positioned north of the ridge on the African plate, one along a bathymetric low and one on a bathymetric high supposedly representing a former active center. A connecting W-E profile along the rift axis is intended to observe the transition between both areas. A reference site is situated some 500 km northward of the rift axis on approximately 50 Ma old crust. On each site several penetrations were carried out in a local spread. One station consists of two to three single penetrations, positioned 500 – 1,000 m apart. The transit is done in pogo style with the instrument approximately 200 m above ground. One station takes about 4 – 5 hours altogether.

Furthermore, miniaturized temperature loggers (MTLs, Pfender & Villinger , 2002) were used for monitoring variations in bottom water temperature in time and space (Fig. 4.3). Five were mounted onto OBSs and deployed for one year. Four of them worked reliable and produced one year time series of 0.001°C temperature resolution and 10 minutes time resolution. After retrieving the OBSs with the attached MTLs, data could be saved and evaluated.

On this cruise those loggers were mounted onto the frame of the Ocean Bottom Observatory System (OFOS) during surveys to monitor the temperature at the flight height of the OFOS, nominally 4 m above ground.

Preliminary results

A number of 48 heat flow sites were attempted on 18 different stations. 42 or 87.5 % of them yielded temperature gradients of good or very good quality. The list of stations is summarized in Table 4.1. In those cases where the penetration failed, hard ground was the reason. Data reduction and processing of measured time series was done using the program MHFRED according to an algorithm of Villinger and Davis (Villinger & Davis., 1987). *In-situ* thermal conductivity could be measured on 21 sites resulting in very good and representative regional estimates. Values between 0.70 and 0.75 W/m*K are fairly low, reflecting the water rich and soft sediments, mainly consisting of diatomaceous ooze, found in two gravity corers (PS 81/652 and PS 81/656).

Almost all measured thermal gradients are of good quality. Nevertheless the scatter spreads from values below 0.009 K/m up to 1.200 K/m. A vigorous hydrothermal circulation is supposed to be one reason for that. Rough terrain with significant topography might be a second one due to thermal refraction. This needs further investigation.

Flow rates of upward and downward moving pore water can be calculated in many cases from the deviation of the linear geothermal gradient. A data example of station PS 81/640_1 (HF11) near the point with the maximum encountered gradient is given in Fig. 4.4.

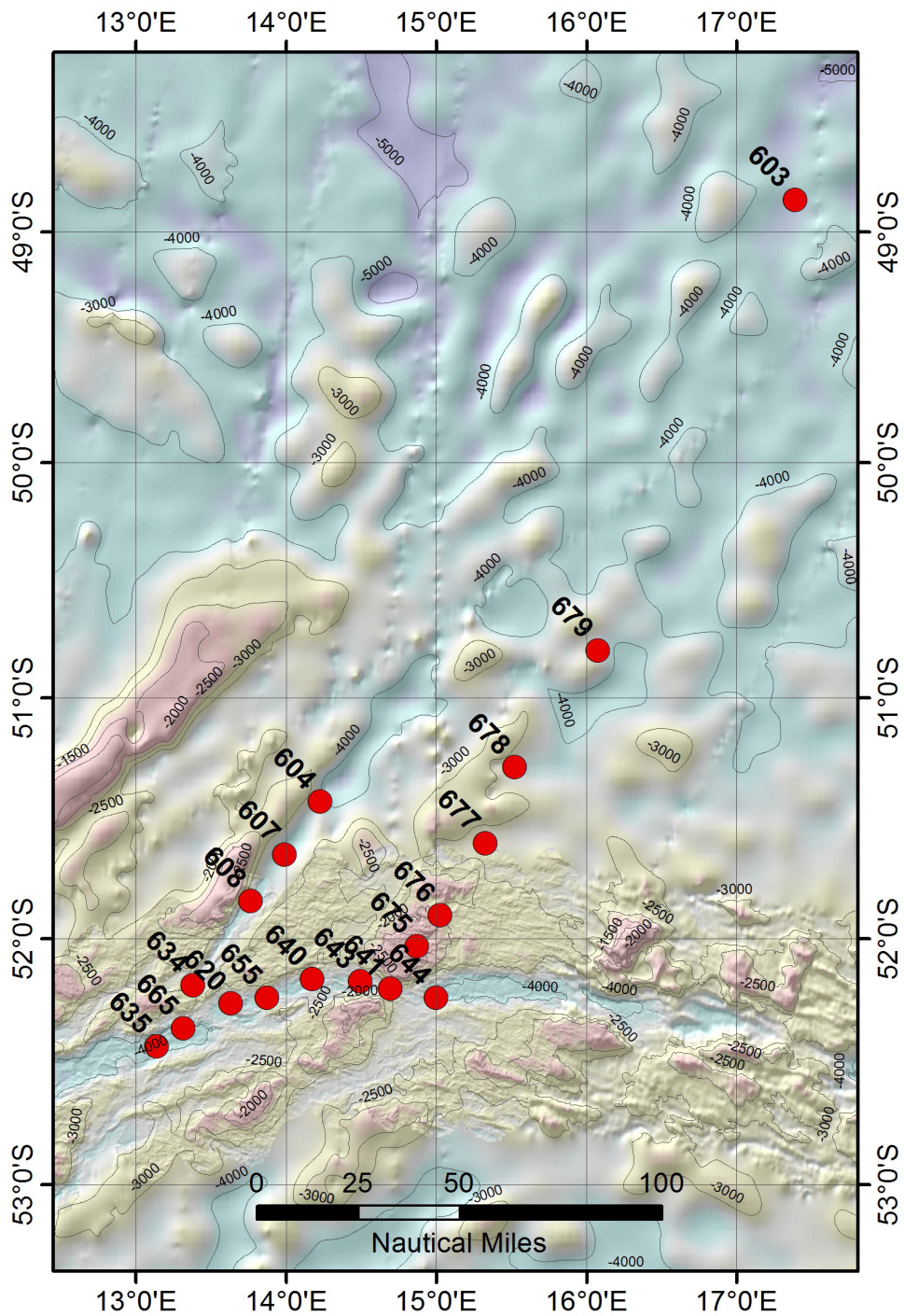


Fig. 4.2: Overview map of heat flow sites during the SWEAP cruise, ANT-XXIX/8. Numbers are abbreviations for the Polarstern labeling PS 81/XXX. The layout of the heat flow survey follows the spreading direction on a "cold" flowline and a parallel "hot" flowline. A connecting profile follows the ridge axis.



Fig. 4.3: Miniaturized Temperature Logger (MTL), produced by Antares, Stuhr. They operated reliable on long term and short term deployments. They are rated at 6,000 m water depth, 1 second time resolution max. and 64,000 samples max.

Evaluating the temperature data of the MTL's long term deployment brought additional information, regarding the stability of bottom water masses. On two positions temperature data show a stable situation with only statistical variations. The second two recorded bottom water variation of up to +/- 0.015 K in a non-statistical manner.

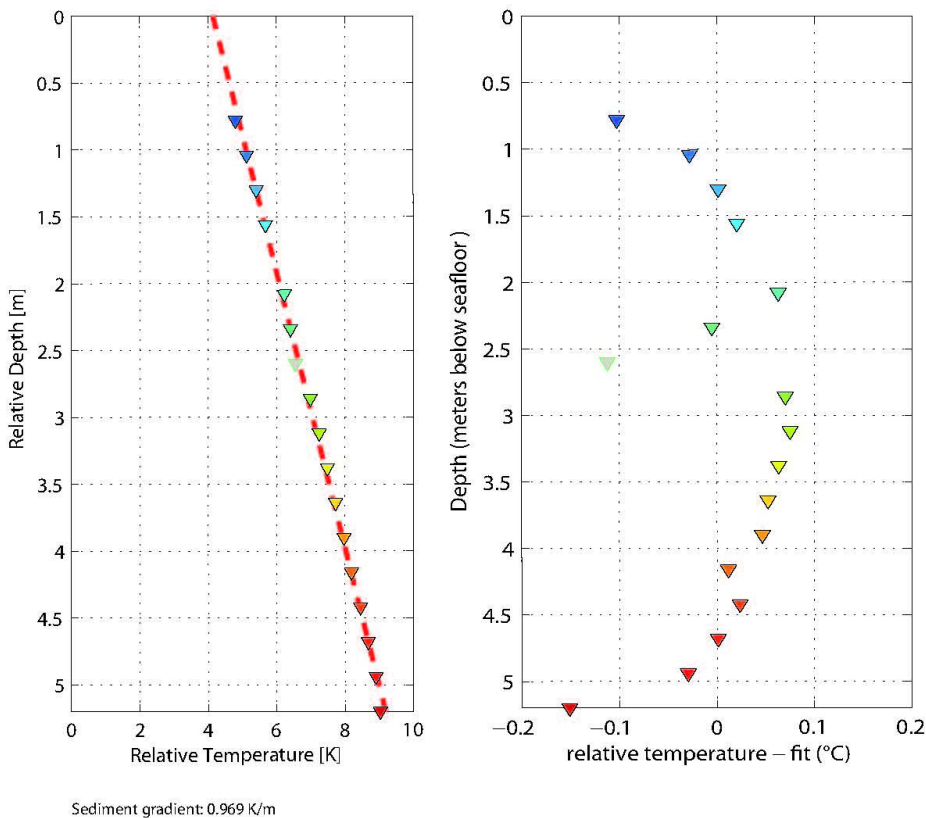


Fig. 4.4: Temperature gradient of position PS 81/640_1. The gradient of 969 mK/m is one of the highest gradients observed during the survey. The horizontal axis is relative temperature, the vertical axis depth relative to the instrument. The panel on the right side shows the temperature data as residuals to the linear trend. A convex curvature indicates a significant upward flow of pore water.

Temperature data of the MTLs, mounted onto the OFOS, deliver *in-situ* temperatures with 1 mK resolution. They support the search for seeps and were extensively used by biologists. To compare these data with other data, i.e. from the CTD, they had to be recalculated into potential temperatures. At water depth beyond 3,000 m the adiabatic temperature increase due pressure effects can not be neglected. A data example of raw data from OFOS dive PS 81/650_2, containing a remarkable peak of 0.016 K over a short distance, is shown in Fig. 4.5.

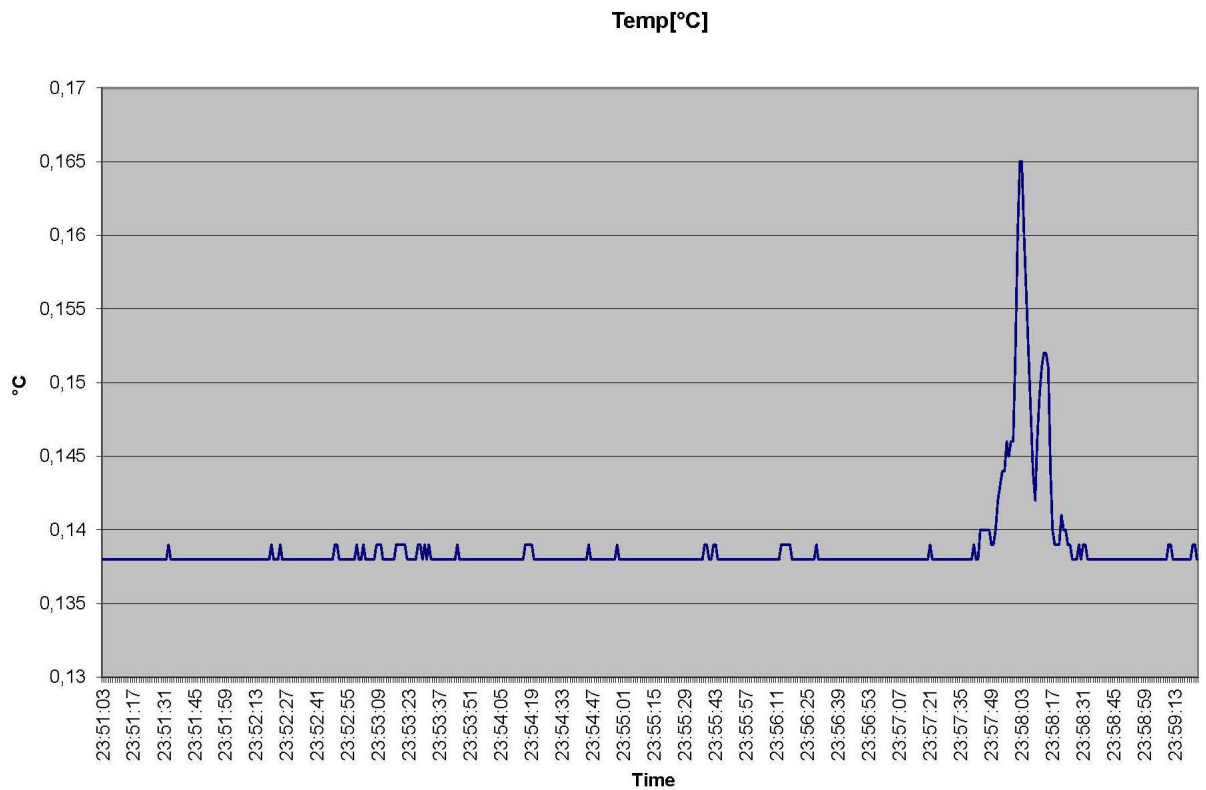


Fig. 4.5: In-situ temperature on OFOS dive on December, 2nd 2013 measured with one MTL. Flight height of the OFOS above ground is 4 m. There is a peak-like temperature increase of 16 mK over a short time span around 23:58 representing app. 12 m in distance.

Data management

All data produced by the heat flow probe and by MTL deployments on OFOS and OBSs will be submitted to the PANGAEA Data Publisher for Earth & Environmental Science.

Tab. 4.1: List of heat flow stations on ANT-XXIX/8

Name	HF	PS_Name	Latitude	Longitude	Heat flow	Comment
H1311P01	HF01	PS 81/603_1	-48°51.500'	17°23.400	low	
H1311P02		PS 81/603_2	-48°51.700'	17°23.155	low	
H1312P01	HF02	PS 81/604_1	-51°26.000'	14°13.640	high	
H1312P02		PS 81/604_2	-51°26.190'	14°13.425	high	
H1312P03		PS 81/604_3	-51°26.365'	14°13.197	high	
H1313P01	HF03	PS 81/607_1	-51°39.200'	13°59.280	low	
H1313P02		PS 81/607_2	-51°39.415'	13°59.033	NAN	No data
H1314P01	HF04	PS 81/608_1	-51°50.674'	13°45.714	low	
H1315P01	HF12	PS 81/620_1	-52°15.974'	13°37.959	low	
H1315P02		PS 81/620_2	-52°16.080	13°37.570	low	
H1315P03		PS 81/620_3	-52°16.210'	13°37.190'	low	
H1316P01	HF05	PS 81/634_1	-52°11.450'	13°22.700'	high	
H1316P02		PS 81/634_2	-52°11.700'	13°22.480'	high	
H1316P03		PS 81/634_3	-52°11.900'	13°22.200'	high	
H1317P01	HF07	PS 81/635_1	-52°26.451'	13°8.164'	low	
H1317P02		PS 81/635_2	-52°26.595'	13°7.730'	low	
H1318P01	HF11	PS 81/640_1	-52°9.828'	14°10.540'	very high	
H1318P02		PS 81/640_2	-52°10.145'	14°10.530'	very high	
H1318P03		PS 81/640_3	-52°10.311'	14°10.815'	high	
H1319P01	HF07	PS 81/641_1	-52°12.372'	14°41.770'	NAN	No pen.
H1319P02		PS 81/641_2	-52°12.440	14°41.240	NAN	No pen.
H1319P03		PS 81/641_3	-52°12.520	14°40.793	NAN	No pen.
H1320P01	HF13	PS 81/643_1	-52°10.543'	14°29.203'	low	
H1320P02		PS 81/643_2	-52°10.746'	14°30.113'	low	
H1320P03		PS 81/643_3	-52°10.912'	14°30.540'	low	
H1321P01	HF14	PS 81/644_1	-52°14.544'	14°59.803'	low	
H1321P02		PS 81/644_2	-52°14.463'	15°00.078'	low	
H1321P03		PS 81/644_3	-52°14.422'	15°00.659'	low	

4. Heat Flow Determinations

Name	HF	PS_Name	Latitude	Longitude	Heat flow	Comment
H1322P01	HF15	PS 81/655_1	-52°14.470'	13°52.460'	intermediate	
H1323P01	HF16	PS 81/665_1	-52°21.458'	13°19.011'	high	
H1323P02		PS 81/665_2	-52°21.95'	13°19.810'	Intermediate	
H1323P03		PS 81/665_3	-52°21.967'	13°20.755'	high	
H1323P04		PS 81/655_4	-52°22.000'	13°21.700'	intermediate	
H1323P05		PS 81/655_5	-52°22.020'	13°22.490'	intermediate	
H1324P01	HF08	PS 81/675_1	-52°1.876'	14°52.326'	intermediate	Partial pen.
H1324P02		PS 81/675_2	-52°2.238'	14°51.965'	intermediate	Partial pen.
H1324P03		PS 81/675_3	-52°2.610'	14°51.333'	NAN	No pen.
H1325P01	HF09	PS 81/676_1	-51°54.196'	15°1.435'	high	
H1325P02		PS 81/676_2	-51°54.350'	15°1.231'	high	
H1326P01	HF10	PS 81/677_1	-51°36.469'	15°19.419'	intermediate	
H1326P02		PS 81/677_2	-51°36.640'	15°19.690'	intermediate	
H1326P03		PS 81/677_3	-51°36.790'	15°19.875'	low	
H1327P01	HF17	PS 81/678_1	-51°17.385'	15°31.278'	low	
H1327P02		PS 81/678_1	-51°17.298'	15°30.822'	low	
H1327P03		PS 81/678_1	-51°17.283'	15°30.350'	low	
H1328P01	HF18	PS 81/679_1	-50°47.495'	16°4.511'	NAN	No pen.
H1328P02		PS 81/679_2	-50°47.933'	16°4.557'	intermediate	
H1328P03		PS 81/679_3	-50°48.185'	16°4.552'	intermediate	

References

- Pfender M, Villinger H (2002) Miniaturized data loggers for deep sea sediment temperature gradient measurements. *Marine Geology*, 186, 557 – 570.
- Schindwein V, Demuth A, Geissler WH, Jokat W (2013) Seismic gap beneath Logachev Seamount: Indicator for melt focusing at an ultraslow mid-ocean ridge? *Geophys. Res. Lett.*, 40, pp. 1703-1707 doi:10.1002/grl.50329.
- Villinger H, Davis EE (1987) A new reduction algorithm for marine heat flow measurements. *Journal of Geophysical Research*, 92 (B12), 846-856.

5. MARINE GEOLOGY

5.1 Sediments

Wolfgang Bach¹, Niels Jöns¹, Christian Hansen¹, Norbert Lensch², Katharina Hochmuth², Susanne Coers¹, Wiebke Stiens³, Rafael Stiens³

¹University of Bremen

²AWI

³MPI-MM

Objectives

Sediment sampling by gravity corer in the work area was conducted to determine the type and lithostratigraphy of sediments in the rift valley. One goal was to look for ash layers and layers of metalliferous sediments, which would indicate distinct volcanic or hydrothermal events. Another objective was to learn about diagenetic processes and sedimentary biogeochemical cycling of elements such as sulfur and carbon. Lastly, gravity core sampling in an area of high heat flow was carried out to test for the presence of hydrothermal precipitates in the uppermost sediments.

Work at sea

A 5.75-m long gravity corer with a 1,500-kg weight stack was lowered into the seabed at a speed of 0.8 m/s. After hoisting on board, the plastic liner holding the core material was retrieved from the corer and cut into 1-m long sections. The tops of each section were sampled for biogeochemical analyses, and temperatures were measured before the section ends were capped. The sections were then brought into the reefer for rhizone-extraction of pore waters. Six to twelve hours after sampling, the cores were split lengthwise into an archive half and a working half. The working half was sampled for microbiological and biogeochemical analyses immediately after opening of the core sections (*cf.* Chapter 7). The archive halves were photographed and described, before both working and archive halves were placed into D-tubes and stored in racks in *Polarstern's* geolab, where they were kept for the remainder of the cruise.

Preliminary (expected) results

Cores were retrieved from four sites, of which two represent an area of elevated heat flow. At each site, the core liner was completely filled, and mud was pushed up into the weight stack, which is indicative of overshooting during coring. The sediments are very soft and porous throughout the entire length of the cores. All sediments are diatomaceous ooze; however, there are distinct differences between the sediments from three of the four sites. Stations PS81/0652-01GC (at 52°10.14'S and 14°10.54'E in 3,703 m water depth) and PS81/0653-01GC (at 52°10.17'S and 14°10.83'E in 3,709 m water depth) coincide with Station PS81/0640-01HF, where heat flow densities between 320 and 1,000 mW/m² were measured. The sediments are uniform (see Figures 5.1 and 5.2), light greenishgray, soft diatomaceous ooze, lacking any sign of hydrothermal precipitate or diagenetic induration. A

slight rotten-egg smell came off the core, which suggests the presence of small quantities of H₂S in the sediment pore water.

GeoB 18201-01

0-561cm

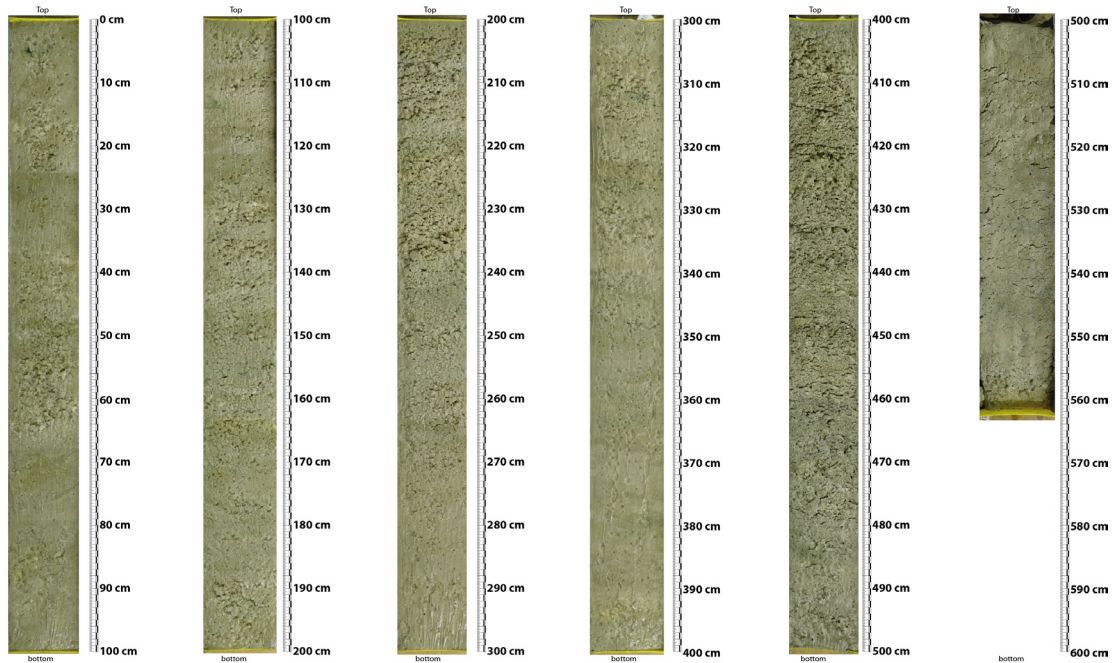


Fig. 5.1: Overview of core GeoB 18201-01 from Station PS81/0652-01GC

GeoB 18202-01

0-565cm

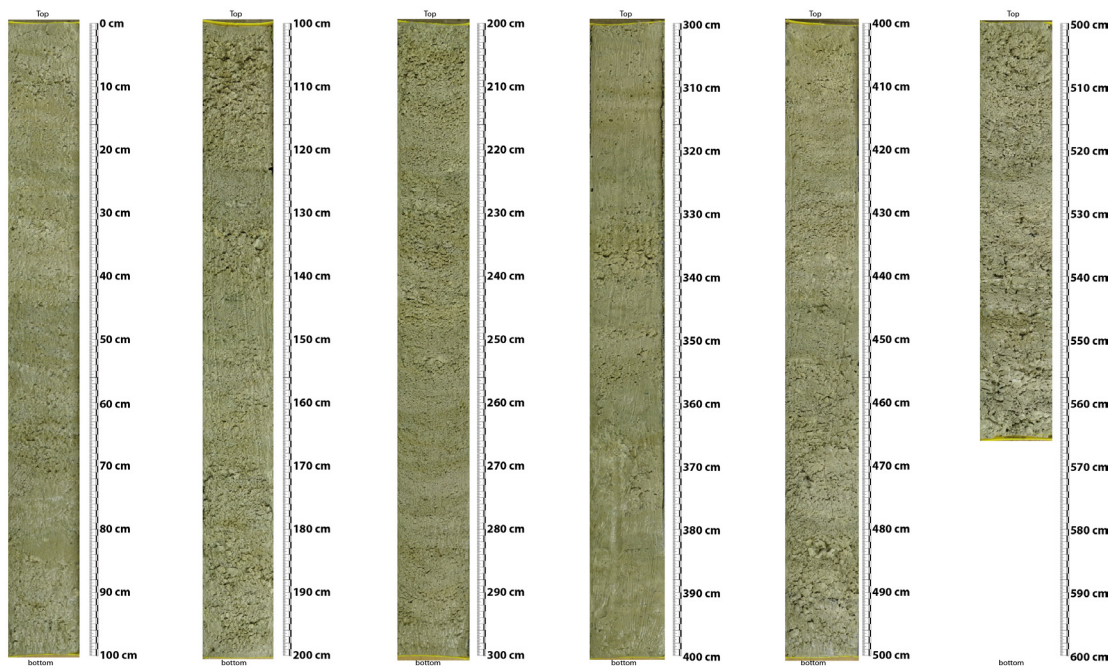


Fig. 5.2: Overview of core GeoB 18202-01 from Station PS81/0653-01GC

5.1 Sediments

Station PS81/0656-01GC (at 52°21.97'S and 13°19.04'E in 3,968 m water depth) on the northern valley wall revealed similar soft diatomaceous ooze with colours ranging from light greenishgray to grayishgreen (Fig. 5.3). The patchy distribution of the differently coloured domains and the complete lack of any layering indicate massive bioturbation.

Station PS81/0657-01GC (at 52°26.45'S and 13°08.11'E in 4,448 m water depth) from the valley floor near a site of low heat flow shows a pronounced banding with colours ranging from light grayishgreen to dark green to black (Fig. 5.4). The banding is developed at scales of centimetres (as much as to 3 to 5 cm in some intervals) but can be on the order of several millimetres in other sections. Intermittent are intervals, up to 20 cm thick, in which dark bands are missing. There is a general tendency of increasing layer thickness down section. The core reeked intensely of hydrogen sulfide, giving rise to the suspicion that the black layers are stained by finely dispersed Fe-sulfides. It cannot be ruled out, however, that some of the dark layers are of different origin (e.g., containing small amounts of volcanic ash). X-ray fluorescence scanning will be conducted on shore to look for enrichments for Al, Ti, and Mn that would point to a volcanic or hydrothermal provenance of some of these layers.

GeoB 18203-01 0-569cm

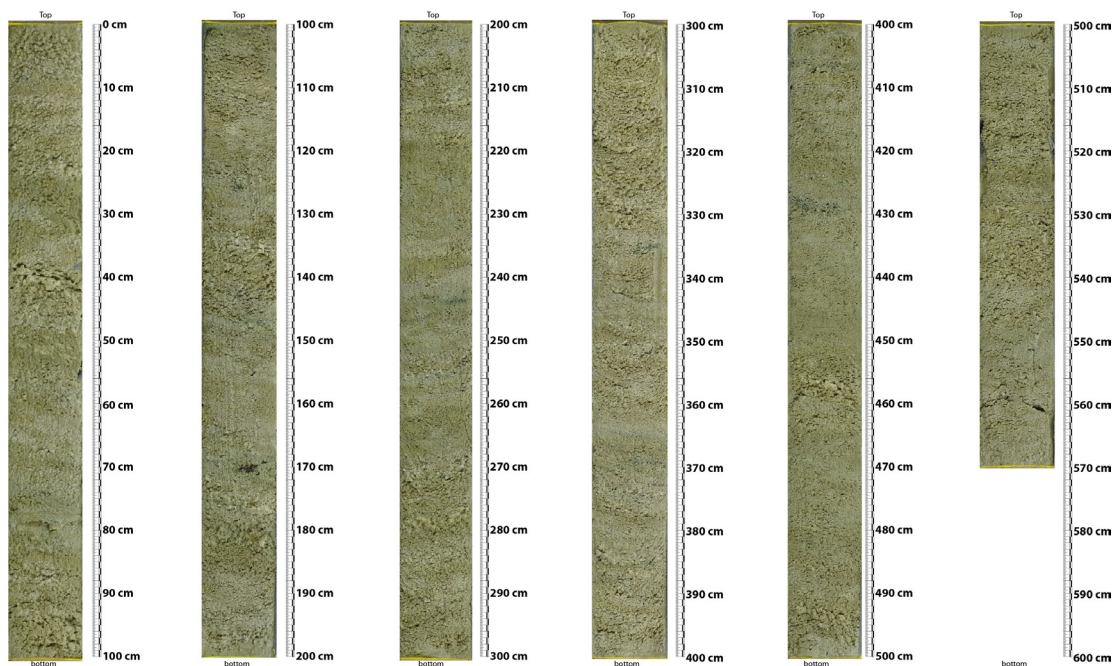


Fig. 5.3: Overview of core GeoB 18201-01 from Station PS81/0656-01GC

GeoB 18204-01
0-568cm

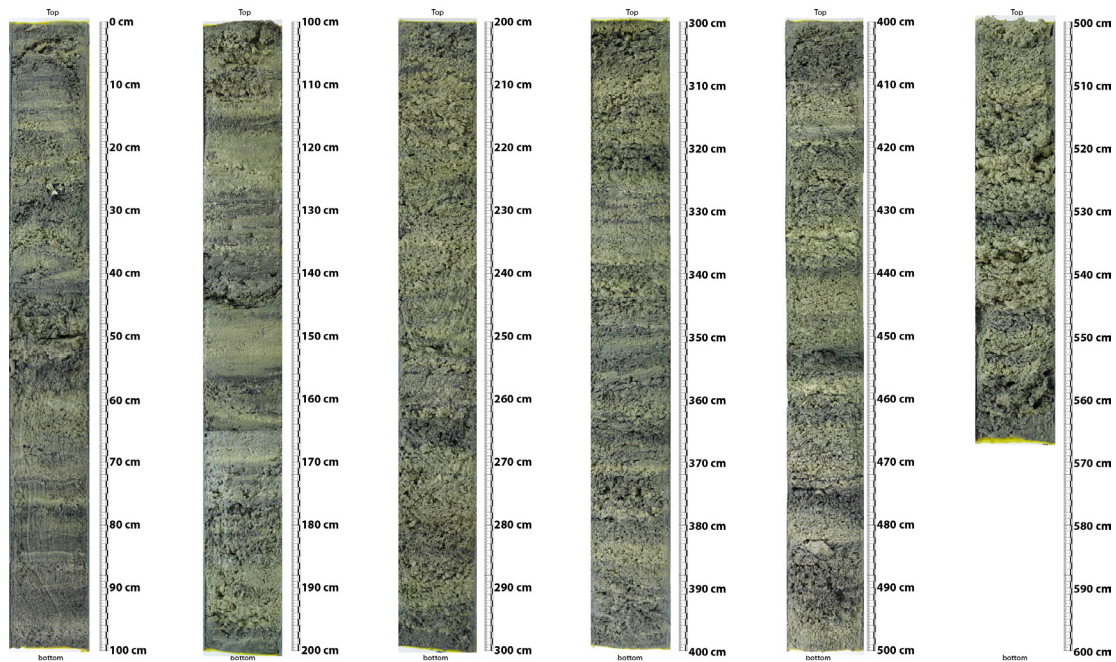


Fig. 5.4: Overview of core GeoB 18201-01 from Station PS81/0657-01GC

The temperatures measured upon sectioning of the core liner are listed in Table 5.1. The temperature increases down section are consistent with heat flow measurements at nearby sites, suggesting elevated heat flow at sites 652 and 653 and low heat flow at sites 656 and 657.

Tab. 5.1: Results of temperature measurements on the ends of 1-m sections of gravity core

Station	depth bsf [cm]	Temp [°C]	Station	depth bsf [cm]	Temp [°C]
PS81/652	90	5.4	PS81/656	10	1.0
PS81/652	190	7.2	PS81/656	110	1.0
PS81/652	290	9.2	PS81/656	210	1.1
PS81/652	390	11.8	PS81/656	310	1.3
PS81/652	410	12.8	PS81/656	410	1.5
PS81/652	510	12.1	PS81/656	510	1.6
PS81/653	10	1.4	PS81/657	10	0.6
PS81/653	110	2.3	PS81/657	110	0.5
PS81/653	210	3.2	PS81/657	210	0.5
PS81/653	310	4.5	PS81/657	310	0.7
PS81/653	410	5.8	PS81/657	410	0.8
PS81/653	510	6.0	PS81/657	510	0.9

Data management

All data produced by the XRF scanner will be submitted to the PANGAEA Data Publisher for Earth & Environmental Science.

5.2 Hard rocks

Wolfgang Bach, Niels Jöns, Christian
Hansen

University of Bremen

Objectives

The oblique orientation of the ridge axis relative to the spreading direction makes the SW Indian Ridge 10-16°E segment an area of minimal effective mantle upwelling rates. Extensive geophysical surveying and rock dredging in the area took place in 2001 and 2003. The basement was found to be mainly peridotitic with only scattered vesicular, alkaline basalt. Consequently, the lithosphere in the area is believed to be thick, resulting in reduced magma production rates and heat flux (Dick *et al.*, 2003). However, two volcanic centers (Joseph Mayes Seamount at 11°E, and Narrowgate at 15°E) feature sparsely vesicular tholeiitic lavas indicative of more extensive melting, perhaps in places where the lithosphere is thinner (Standish *et al.*, 2008). Age dating of the volcanic rocks indicated common off-axis volcanism, suggesting that the zone of magmatic accretion is unusually wide (Standish & Sims 2010). Another result of the previous surveys was the discovery of mineral deposits (sulfide breccia, opal/sepiolite, nontronite/birnessite) indicating hydrothermal activity, in particular along the magma-starved portion of the segment (Bach *et al.*, 2002).

One of the main cruise objectives of Expedition ANT-XXIX/8 was the discovery and sampling of these hydrothermal vent fields.

Work at sea

Hydrothermal vents were looked for using CTD tow-yo and OFOS surveys (see chapters 6 and 7). Since we were unsuccessful in locating these vents, rock sampling was minimal. A dedicated basement rock-sampling program was never intended. Yet, unintentional rock sampling was made use of. Rock fragments were retrieved coincidentally during occasional deployments of the Multicorer and the Agassiz-Trawl. The TV-guided grab was operated twice to collect volcanoclastic samples from sedimented areas. A TV-grab deployment aimed at recovering volcanic rock from the Narrowgate summit area failed. An overview of the sample material from these stations is given in Table 5.2.

Preliminary (expected) results

A multicorer test dive at Station PS81/0606-01MUC (51°26.60'S, 14°13.55'E in 4,196 m water depth) recovered several <2-cm long fragments of rounded buff-coloured pumice and three <5-mm long pieces of angular, black scoriaceous rock.

The dive video revealed black sediments underlying a fluffy layer of siliceous ooze. These black sediments were not recovered, but we tentatively identified them as ash layers. The site with these pyroclastic deposits is 45 m north of the spreading axis in an area of elevated heat flow (*PS81/0604-01HF*).







Agassiz Trawl Station *PS81/0664AGT* started at 52°29.81'S and 13°03.77'E in 4,181 m water depth and ended at 52°29.79'S, 13°02.80'E in 4,128 m water depth. The trawl yielded a range of rock types, ranging from buff-coloured and black pumice to scoriaceous lapilli to sparsely vesicular lava. The black scoriaceous rock is likely alkali basalt or basanite, based on the occurrence of euhedral phenocrysts, tentatively identified as nepheline and Ti-augite. Glacial erratics and mantle peridotite were also retrieved. The peridotites are orthopyroxene-rich harzburgites with orthopyroxene veins. They are partially serpentinized and show thick (up to 5-6 mm) Mn-oxide coatings. Orthopyroxene is fully serpentinized. Olivine-rich domains are reddish in colour, indicating that olivine relic to the serpentinization process was later iddingitized during low-temperature oxidative seawater alteration.


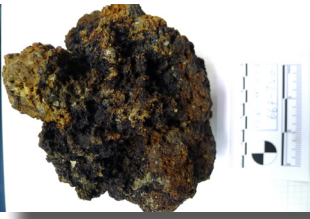




Two deployments of the TV-guided grab were conducted in an area of shallow seafloor roughly 20 m north of the spreading axis. The area has a number of peculiar circular to ellipsoidal features surrounded by 100-m high walls. *PS81/0667TVG* (52°03.88'S, 13°24.93'E in 2,748 m water depth) recovered grayishgreen to white diatomaceous ooze with rock fragments from the northern wall of one of these features. The ooze carries an assortment of buff-coloured to black scoriaceous to pumaceous lapilli. These rocks are aphyric to sparsely plagioclase-phyric. The Mn-oxide coating ranges from very thin to mm-thick, and the thicker coatings display botryoidal surfaces. Two samples have bomb-size; one is a moderately plagioclase-phyric scoriaceous rock with vesicles ranging from sub-mm to 3 mm in size. The other bomb is aphyric and has a smooth, ropey surface on one side and a highly irregular, frothy surface on the other. It is highly vesicular, with a rather uniform vesicle size of around 1 mm. Both bombs have very minor, if any, Mn-oxide coatings and appear very fresh. The fraction of glacial erratics is <10 % of all pieces.

The second TV-grab (*PS81/0668-01TVG* at 52°06.75'S, 13°17.03'E in 3,074 m water depth) targeted the northern wall of a bean-shaped crater-like structure 4.8 m WSW of the previous sampling site. Again, grayishgreen to light brown to white diatomaceous ooze is the main lithology, followed by black volcanic ash. The ash forms pockets and swirls in the ooze, which are likely due to biological irrigation of formerly layered ooze-ash sequences. Lapilli of scoriaceous dark gray to black rock and buff pumice as well as cm-sized fragments of vesicular, aphyric lava are rare and occur at the same frequency as glacial erratics of varied lithology (granite, chert, etc.).




5.2 Hard rocks

Tab. 5.2: Overview of rock samples taken during ANT-XXIX/8

Sample ID	Description	Sample Photograph
<p>PS81_664-AGT-01</p> <p>(between 52°29.81'S, 13°03.77'E and 52°29.79'S, 13°02.80'E)</p>	<p>cm-sized and slightly rounded pieces of greyish to light-yellowish pumice; elongate vesicles are up to 4mm long; only few idiomorphic to hypidiomorphic phenocrysts are identifiable (Cpx, Pl)</p>	
<p>PS81_664-AGT-02</p> <p>(between 52°29.81'S, 13°03.77'E and 52°29.79'S, 13°02.80'E)</p>	<p>irregularly shaped pieces of dark-brownish scoriaceous lapilli; round vesicles; euhedral phenocrysts (Ti-Aug, Neph) point to alkali basaltic or basanitic whole-rock composition</p>	
<p>PS81_664-AGT-03</p> <p>(between 52°29.81'S, 13°03.77'E and 52°29.79'S, 13°02.80'E)</p>	<p>well-rounded, cm-sized pieces of volcanic rock; light-yellow rock matrix containing brownish patches, which are strongly altered portions occurring around vesicles; no phenocrysts observable</p>	
<p>PS81_664-AGT-04</p> <p>(between 52°29.81'S, 13°03.77'E and 52°29.79'S, 13°02.80'E)</p>	<p>slightly vesicular pieces of cm-sized volcanic rocks; dark brown to black in colour; fine grained and aphyric; vesicles are filled with white-coloured minerals</p>	
<p>PS81_664-AGT-05</p> <p>(between 52°29.81'S, 13°03.77'E and 52°29.79'S, 13°02.80'E)</p>	<p>serpentinized harzburgite; Opx is completely serpentinized; former Ol is iddingitized and therefore of reddish to orange colour; rock is magnetic; some pieces are crosscut by orthopyroxenite veins, in which also massive serpentine layers occur; pieces are coated with a Mn-Fe oxide layer (up to 5 mm thick)</p>	
<p>PS81_664-AGT-06</p> <p>(between 52°29.81'S, 13°03.77'E and 52°29.79'S, 13°02.80'E)</p>	<p>a variety of different rocks and minerals, which likely are glacial erratics; this group includes e.g. quartz grains and pieces of granitic gneiss.</p>	

Sample ID	Description	Sample Photograph
<p>PS81_667-TVG-01 (52°03.88'S, 13°24.93'E)</p>	<p>plagioclase-phyric scoriaceous lapilli; mm-sized euhedral Pl crystals in dark-brown to black fine-grained matrix; strongly vesicular</p>	
<p>PS81_667-TVG-02 (52°03.88'S, 13°24.93'E)</p>	<p>bomb-sized dark-brownish volcanic rock; highly vesicular and aphyric; coated with a thin crust of Mn-Fe oxide</p>	
<p>PS81_667-TVG-03 (52°03.88'S, 13°24.93'E)</p>	<p>bomb-sized dark-brownish to black volcanic rock; vesicular (1-3 mm); ropey surface on one side; contains plagioclase phenocrysts</p>	
<p>PS81_667-TVG-04 (52°03.88'S, 13°24.93'E)</p>	<p>several rounded, buff-colored pieces of pumice; strongly vesicular with elongate vesicles; very fine-grained rock matrix with few plagioclase phenocrysts are observable on weathered surfaces</p>	
<p>PS81_667-TVG-05 (52°03.88'S, 13°24.93'E)</p>	<p>group of different rock types, which are interpreted as glacial erratics; contains e.g. pieces of shale as well as a Mag-rich dioritic gneiss</p>	
<p>PS81_668-TVG-01 (52°06.75'S, 13°17.03'E)</p>	<p>black volcanic ash; occurred enriched in layers within diatomaceous ooze</p>	
<p>PS81_668-TVG-02 (52°06.75'S, 13°17.03'E)</p>	<p>darkish-gray to black scoriaceous lapilli of irregular shape; Pl phyric; strongly vesicular</p>	<p>no photograph</p>

5.2 Hard rocks

Sample ID	Description	Sample Photograph
PS81_668-TVG-03 (52°06.75'S, 13°17.03'E)	slightly rounded, pieces of buff-coloured pumice; strongly vesicular with elongate vesicles; very fine-grained rock matrix; few mm-sized Pl phenocrysts	
PS81_668-TVG-04 (52°06.75'S, 13°17.03'E)	cm-sized fragments of aphyric lava; slightly variable vesicularity; dark gray to black colour; some pieces contain a thin coating of Mn-Fe oxides	
PS81_668-TVG-05 (52°06.75'S, 13°17.03'E)	glacial erratics of variable size and lithology (e.g., granitic gneiss, chert,...)	

Data management

The apparent volcanic tephra will be analyzed for major and trace element composition at the University of Bremen. All geochemical data generated will be submitted to the PANGAEA Data Publisher for Earth & Environmental Science.

References

- Bach W, Banerjee NR, Dick HJB, Baker ET (2002) Discovery of ancient and active hydrothermal deposits along the ultraslow spreading Southwest Indian Ridge 10-16°E. *Geochemistry, Geophysics, Geosystems*, 3(7), pp 1-14, doi:10.1029/2001GC000279.
- Dick HJB, Lin J, Schouten H (2003) An ultraslow-spreading class of ocean ridge. *Nature*, 426, 405-412.
- Standish JJ, Dick HJB, Michael PJ, Melson WG, O'Hearn T (2008) MORB generation beneath the ultraslow spreading Southwest Indian Ridge (9–25°E): Major element chemistry and the importance of process versus source. *Geochemistry, Geophysics, Geosystems*, 9(5), doi:05010.01029/02008GC001959.
- Standish JJ, Sims KWW (2010) Young off-axis volcanism along the ultraslow-spreading Southwest Indian Ridge. *Nature Geoscience* 3, 286-292.

6. WATER COLUMN SURVEYING AND SAMPLING

Martin Vogt^{1,3}, Tim Hannemann³, Kerstin
Hans³, Niels Jöns², Christian Hansen²,
Wolfgang Bach²

¹MPI
²MARUM/Uni Bremen
³UHB-IUP

Objectives

Our aim was to find indications of hydrothermal activity in the research area by sampling the water column and surveying for traces of hydrothermal plumes. The survey took place along a segment of the Southwest Indian Ridge that features a minimal magma budget (Dick *et al.*, 2003), yet appears hydrothermally very active (Bach *et al.*, 2002). *Polarstern* cruise ANT-XXIX/8 provided an excellent opportunity for conducting comprehensive and systematic water column work in the ultramafic 13–14°E segment. Targeted exploration of hydrothermal plumes in this area were intended to contribute to solving a long-standing conundrum in hydrothermal vent research: Magmatic and hydrothermal activities are correlated across much of the range of global spreading rates, but ultraslow-spreading segments appear to be anomalously active in terms of venting (Baker *et al.*, 2004). These vents are in great water depths and hosted in mantle rock, making them interesting prospects for unusually large point sources of heat and metabolic energy. We intended to (1) locate these vents, (2) determine the heat and chemical fluxes, and (3) establish the regional extent and global contribution of these poorly studied vents. The latter objective was to be met by measuring He concentrations and ³He/⁴He isotope ratios.

Noble gases are good tracers for hydrothermal activity, for different reasons. Firstly, they are chemically inert, so are not produced or used up by biological processes. Secondly, the sources of noble gases are well known. For neon, the only source is the atmosphere, the neon content then remains unchanged in the water. Helium, especially the ³He isotope, has another source in hydrothermal vents. This additional source then changes the isotope ratios, which makes the hydrothermal plumes traceable. The sampling objective was to take samples from in- and outside the plume to find out more about their local distribution.

Work at sea

Fourteen stations (see Fig. 6.1) between 12.53°E and 15.74°E were dedicated to hydrographic surveying in conductivity-temperature-depth (CTD) casts. The instrument used was a Sea-Bird Electronics, Inc. SBE9plus system equipped with a custom-built Seapoint Turbidity Meter (5x normal gain). The underwater unit was attached to a SBE 32 carousel water sampler with 22 Niskin bottles. The two remaining slots for bottles were taken up by the lowered acoustic Doppler current profiler system (LADCP). The complete system worked properly for the first 9 stations, after which the CTD-system had a serious failure and needed to be replaced. All sensors (except the pressure sensor, that is built into the CTD) remained the same. We used a pair of sensors for temperature und conductivity,

one uncalibrated sensor for oxygen, a fluorometer, a transmissiometer and the forementioned turbidity sensor. All sensors worked well, with the exception of a malfunctioning of the transmissiometer during the cast immediately after the replacement of the CTD.

For the calibration of the conductivity sensor 51 water samples have been taken and analysed on board. The concentrations of dissolved oxygen were determined on board by iodometric titration (*cf.* Chapter 7). These data allowed us to calibrate the oxygen sensor of the CTD.

Station work consisted of 5 standard CTD-casts, and 9 tow-yo stations. Tow-yo stands for a special sampling strategy, where the CTD is continuously lowered and hoisted in a certain depth layer, while the ship is slowly (0.5 to 1.5 knots) moving in a constant direction for about 6 to 8 hours. In our case the depth range were the lowermost 700 to 1,000 meters. The idea behind this strategy is to get a high spatial resolution without having to pass through the upper 3,000 m of the water column. To record the exact position of the instrument during the tow-yos a Posidonia pinger was attached to the frame of the CTD.

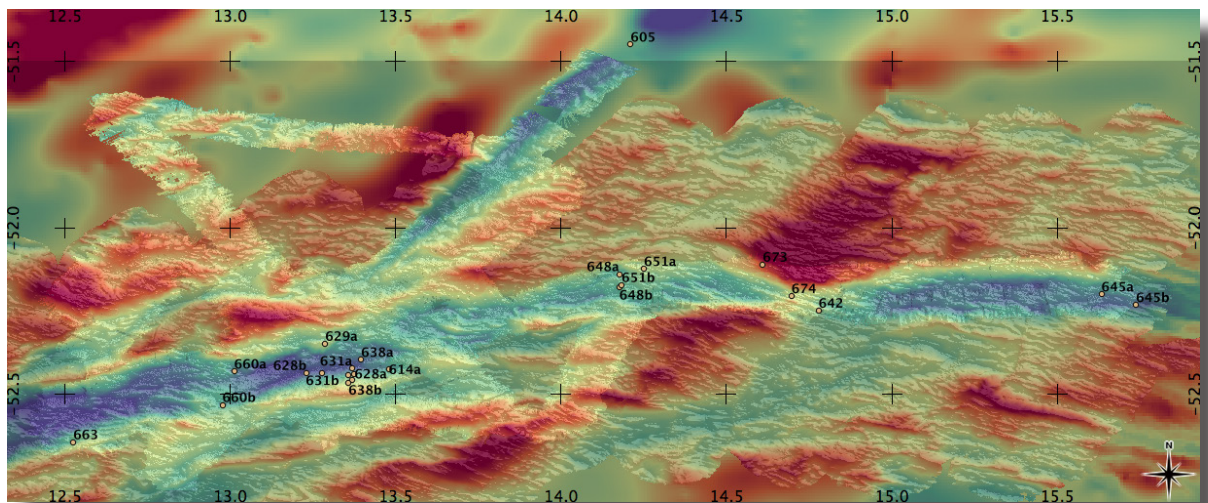


Fig. 6.1: Bathymetric map of the survey area depicting the locations of the CTD stations. Letter a and b denominate the start and end coordinates, respectively, of tow-yo casts.

IADCP

Attached to the CTD frame were also 2 RDI Workhorse 150 KHz LADCPs. These instruments measure the relative currents between two units by sampling the Doppler shift of an emitted acoustic signal. The LADCPs are owned by the oceanography group of the University of Bremen. The frame and battery case of the instruments were rented from AWI. After having some trouble with the data on the first stations using a different battery case, the system could be set up with the AWI battery case and performed well.

He/Ne

A total of 136 water and blank samples for noble gas analysis were taken. The method used is that of Roether *et al.* (2013), where previously evacuated glass ampoules are filled half with the sample. The ampoules are then transported back and measured in the Bremen Helium Isotope Lab. Only two ampoules broke during the closing and another two were not filled, because they had leaks. This shows that, if conducted properly, this method has a very low loss rate of samples compared to the standard copper-tube method.

Since most of the Niskin Bottles were closed to map and detect the plume, the aim of a detailed vertical resolution could not be fulfilled. But since the sampled region was fairly small, there are enough samples for a detailed background distribution of the noble gases.

Methane

Elevated methane concentrations in the water column are indicative of venting from ultramafic-hosted hydrothermal system. Methane measurements of water samples, collected during CTD casts have been successfully used in the past to find vents in ultraslow spreading environments (German *et al.*, 2010). We collected seawater samples from Niskin bottles immediately after recovery. For CH₄ analysis, 20 ml seawater were drawn into 60 ml plastic syringes. After headspace extraction in nitrogen, CH₄ concentrations were determined using an Agilent 7820A Gas Chromatography System equipped with a flame ionisation detector. Columns used were either a 6 foot 5 Å molecular sieve or a 6 foot HAYESEP Q column.

MAPR

Four Miniature Autonomous Plume Recorders (MAPRs) were rented from the National Oceanographic and Atmospheric Association (NOAA; MAPR serial numbers: 65, 66, 67, 68). These standard devices for plume searching carry sensors for temperature, pressure, optical backscatter (LBSS), and oxidation-reduction potential (Eh). Especially anomalies in optical backscatter and oxidation-reduction potential are good indicators for hydrothermal sources.

MAPRs were deployed with several instruments, e.g. OFOS, MUC, CTD and CTD-tow-yo, on 29 stations. MAPRs were attached to OFOS dives starting with Station 615 and to MUC starting with Station 639. Single MAPR measurements were carried out fixed to the frame of the main instrument. Additionally, up to three MAPRs were attached for CTD-tow-yos to the cable of the CTD (for details, see table 6.2). Data were recorded in 5-second intervals.

Preliminary (expected) results

Oceanographic work on this cruise concentrated on the detection of hydrographic irregularities, e.g. regional temperature anomalies, and variations in turbidity. CTD tow-yo stations were planned to detect anomalies in turbidity and temperature, then sample the plume waters, and measure methane concentrations on board to verify a hydrothermal source of the turbidity. Additional water samples were collected for onshore analyses of metal concentrations and He isotope work.

The hydrographic data recorded show the expected mixing of water masses in the polar front, where the cold Antarctic circumpolar waters mix with the surface

waters south of Africa. This is also the region where the cold and low-salinity Antarctic Intermediate Water is formed. In depths below 3,000 m, cold Antarctic Bottom Water (AABW) seems to overflow the ridges and fill the basins. Since detailed hydrographic sections (i.e., CTD casts every 10 to 20 nautical miles) had not been the aim of the cruise, we cannot infer about the intensity and regional variation of these waters.

The hydrographic data do not show any sign of local temperature variations that would be an indicator of strong hydrothermal activity. But at several locations high turbidity and low transmissivity signals outlined cloudlike features in the water column. These turbidity clouds were occasionally found near the bottom, but also 500 to 700 meters above the seafloor. The values and methane concentrations were unremarkable in water samples taken from the turbid water masses. It is hence uncertain if the source of the turbidity is hydrothermal. The nature of the turbidity clouds could hence not be determined, and we have to await the results of onshore analyses (e.g. noble gas measurements).

The primary target of plume search was an area where a previous cursory plume survey (Bach *et al.*, 2002) had detected a pronounced turbidity signal. The plume seemed to be sourced in the 13.1 – 13.6°E area on the northern wall of a shallow dipping (16°), lenticular fault block, 35 km long and 14 km wide. The footwall of this fault block rises 1,200 m up a smooth continuous slope from the rift valley floor to the crest of the rift valley wall. Extensive surveying took place in this area (Fig. 6.2).

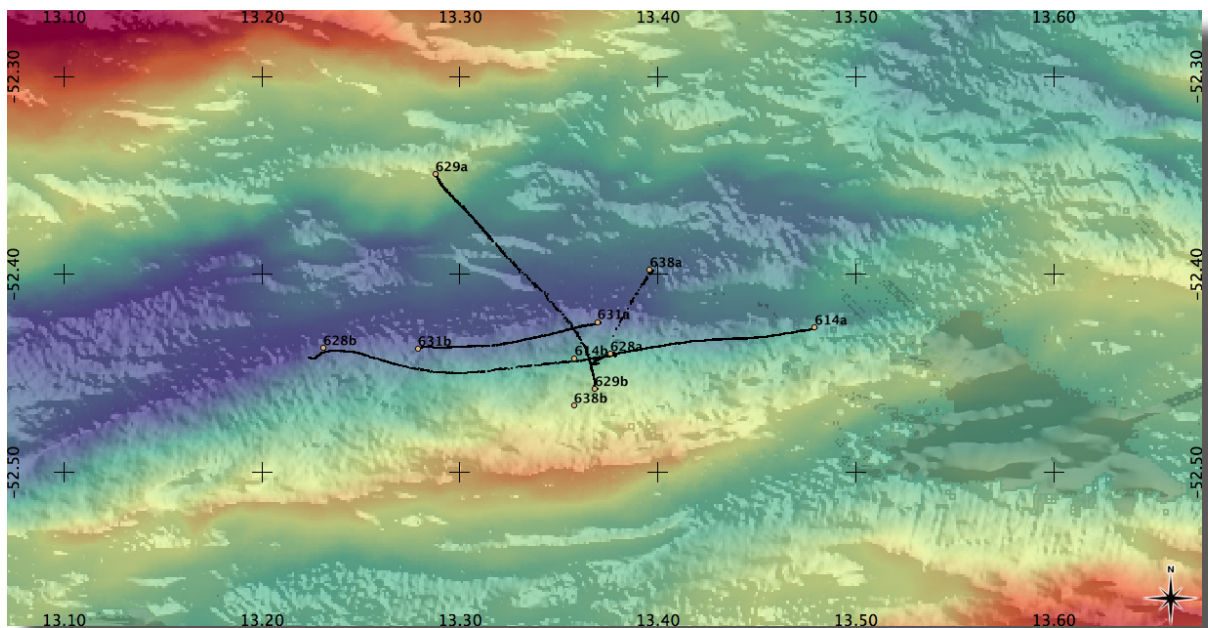


Fig. 6.2: CTD tow-yo track lines in the most intensely studied area between 13.2 and 13.5°E

Fig. 6.3 shows the potential temperature recorded during CTD-tow-yo Station 629, which started at the northern valley wall, crossed the valley and continued up on the aforementioned fault block in the south. Density variations (white lines) are very small, since inside the basin-like trough formed by the rift mountains, salinity is nearly constant. On the left hand side, south of 52.42°, one of the turbidity clouds described above is clearly recognizable (Fig. 6.4). This cloud is neutrally buoyant, so it follows the isopycnals (white lines) very closely. The figure also

6. Water Column Surveying and Sampling

depicts clouds near the bottom and at lower depths. These features have been recorded in other CTD casts in the area as well, so they appear to be a regional phenomenon.

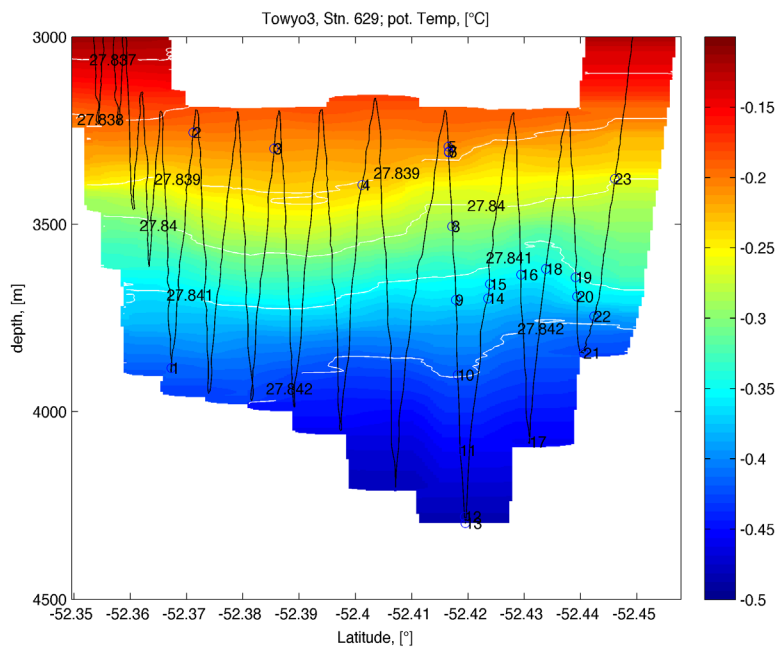


Fig. 6.3: Potential temperature (in °C) during TowYo Station 629. Blank line indicate the path of the CTD, white lines are isopycnals. Circles mark water bottles (bottle number).

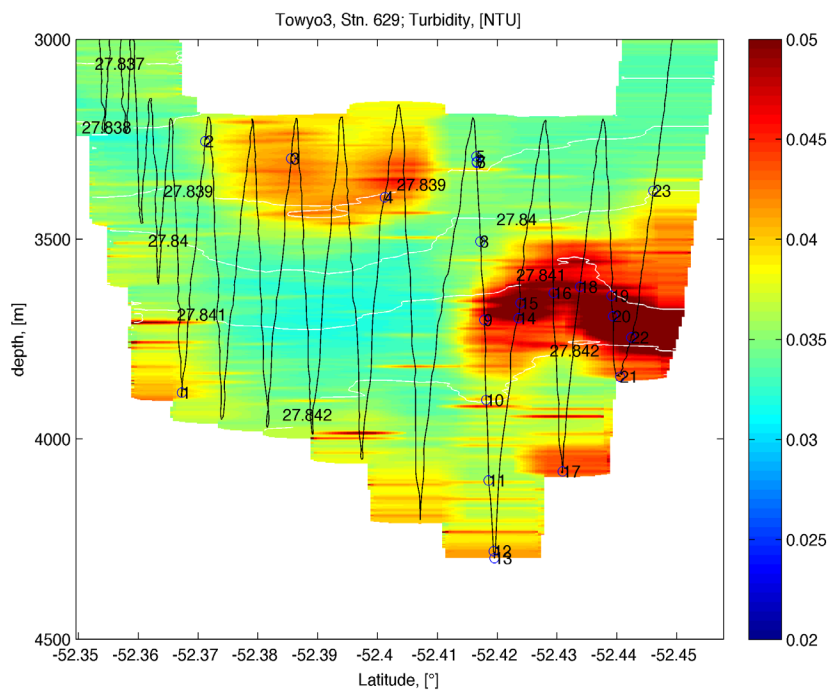


Fig. 6.4: Same as Fig. 6.3 but contoured for turbidity

Since the LADCP only measure currents relative to the instrument, the data processing needs to be done very carefully and is time consuming, so it could not be done on board.

We also surveyed areas where heat flow and OFOS observations indicated the potential presence of hydrothermal or volcanic anomalies. Additional surveying took place in areas where seafloor bathymetry indicated terminations of long-lived faults that may provide pathways for hydrothermal fluids. Clear hydrothermal plumes were not recorded in any of these CTD stations. Turbidity anomalies were occasionally detected, in particular near the seafloor at CTD-tow-yo Station 645 in the easternmost survey area, but these anomalies were not matched by low Eh values or elevated methane concentrations.

Methane concentrations:

The results of on board analyses of methane concentrations are reported in Table 6.1. The data range between <1 nmol/L (i.e., background concentrations in the deep sea) to values as high as 13.8 nmol/L. Elevated methane concentrations were detected in some bottom water samples. Samples taken around 2,500 m water depth during all casts had uniformly low background concentrations of <1.5 nmol/L. In contrast, deep (>3,000 m) water masses revealed varying methane levels in different areas. Methane concentrations were highest (3.3–8.4 nmol/L) in the easternmost trough (Station 645), followed by the area of high heat flow around Station 648 (2.8–5.0 nmol/L). Deep-sea water at the background sites had uniformly low methane concentrations.

Tab. 6.1: Methane concentrations determined on board *Polarstern* by gas chromatography

Exp.	Station	Bottle No.	Latitude [°]	Longitude [°]	Depth [mbsl]	CH ₄ [nmol/l]
PS81	605-1 CTD	1	-51,44867	14,21050	4290	0,3
PS81	605-1 CTD	2	-51,44867	14,21050	4286	0,7
PS81	605-1 CTD	5	-51,44867	14,21050	4279	0,3
PS81	605-1 CTD	10	-51,44867	14,21050	4250	0,5
PS81	605-1 CTD	13	-51,44867	14,21050	4200	---
PS81	605-1 CTD	16	-51,44867	14,21050	3801	0,5
PS81	605-1 CTD	19	-51,44867	14,21050	2500	0,8
PS81	605-1 CTD	21	-51,44867	14,21050	1494	0,3
PS81	605-1 CTD	22	-51,44867	14,21050	998	0,9
PS81	605-1 CTD	23	-51,44867	14,21050	494	0,9
PS81	614 CTD-TOWYO	1	-52,44166	13,36284	3780	4,5
PS81	614 CTD-TOWYO	2	-52,44200	13,36000	3393	1,1
PS81	614 CTD-TOWYO	3	-52,44234	13,35800	3862	0,6
PS81	614 CTD-TOWYO	4	-52,44234	13,35800	3862	0,9
PS81	614 CTD-TOWYO	5	-52,44234	13,35800	3862	0,6
PS81	614 CTD-TOWYO	10	-52,44250	13,35816	3866	1,1

6. Water Column Surveying and Sampling

Exp.	Station	Bottle No.	Latitude [°]	Longitude [°]	Depth [mbsl]	CH ₄ [nmol/l]
PS81	614 CTD-TOWYO	11	-52,44266	13,35834	3832	0,9
PS81	614 CTD-TOWYO	13	-52,44266	13,35834	3830	0,6
PS81	614 CTD-TOWYO	14	-52,44284	13,35916	3760	1,7
PS81	614 CTD-TOWYO	16	-52,44350	13,36084	3364	1,0
PS81	614 CTD-TOWYO	17	-52,44350	13,36084	3362	1,4
PS81	614 CTD-TOWYO	18	-52,44516	13,36484	2493	0,9
PS81	614 CTD-TOWYO	19	-52,44516	13,36484	2498	0,8
PS81	614 CTD-TOWYO	20	-52,44500	13,36984	1002	0,9
PS81	614 CTD-TOWYO	21	-52,44500	13,37000	1002	0,6
PS81	614 CTD-TOWYO	22	-52,44484	13,37134	500	0,7
PS81	614 CTD-TOWYO	23	-52,44484	13,37134	500	0,6
PS81	614 CTD-TOWYO	24	-52,44450	13,37300	11	2,0
PS81	628 CTD-TOWYO	1	-52,44784	13,26984	3245	13,8
PS81	628 CTD-TOWYO	2	-52,44616	13,26427	3786	2,4
PS81	628 CTD-TOWYO	3	-52,44416	13,25750	3201	1,0
PS81	628 CTD-TOWYO	4	-52,44250	13,25234	4001	1,6
PS81	628 CTD-TOWYO	5	-52,44016	13,24784	3388	1,2
PS81	628 CTD-TOWYO	8	-52,44016	13,24734	3305	1,2
PS81	628 CTD-TOWYO	9	-52,44000	13,24666	3197	0,9
PS81	628 CTD-TOWYO	10	-52,43900	13,24434	2999	1,0
PS81	628 CTD-TOWYO	11	-52,43566	13,23350	3362	0,7
PS81	628 CTD-TOWYO	12	-52,43516	13,23200	3150	0,6
PS81	628 CTD-TOWYO	13	-52,43484	13,23094	3363	1,2
PS81	628 CTD-TOWYO	14	-52,43550	13,23134	3553	1,1
PS81	628 CTD-TOWYO	15	-52,43716	13,23100	4260	5,1
PS81	629 CTD-TOWYO	1	-52,38100	13,31284	3889	---
PS81	629 CTD-TOWYO	3	-52,39984	13,32816	3300	---
PS81	629 CTD-TOWYO	4	-52,42100	13,34700	3395	---
PS81	629 CTD-TOWYO	21	-52,45716	13,36797	3840	1,4
PS81	629 CTD-TOWYO	22	-52,45784	13,36816	3742	---
PS81	629 CTD-TOWYO	5	-52,43450	13,35834	3291	1,0
PS81	629 CTD-TOWYO	8	-52,43534	13,35916	3501	2,0
PS81	629 CTD-TOWYO	9	-52,43634	13,36000	3700	1,1
PS81	629 CTD-TOWYO	10	-52,43734	13,36100	3900	1,1
PS81	629 CTD-TOWYO	11	-52,43834	13,36134	4102	0,8
PS81	629 CTD-TOWYO	12	-52,43916	13,36184	4281	0,6
PS81	629 CTD-TOWYO	13	-52,43934	13,36200	4296	0,6
PS81	629 CTD-TOWYO	14	-52,44250	13,36416	3696	2,2
PS81	629 CTD-TOWYO	15	-52,44266	13,36450	3699	2,2
PS81	629 CTD-TOWYO	16	-52,44684	13,36700	3633	1,5

Exp.	Station	Bottle No.	Latitude [°]	Longitude [°]	Depth [mbsl]	CH ₄ [nmol/l]
PS81	629 CTD-TOWYO	17	-52,44934	13,36666	4080	1,2
PS81	629 CTD-TOWYO	18	-52,45166	13,36700	3620	2,1
PS81	629 CTD-TOWYO	19	-52,45634	13,36716	3639	4,4
PS81	629 CTD-TOWYO	20	-52,45650	13,36716	3690	3,7
PS81	629 CTD-TOWYO	23	-52,45800	13,36766	3379	3,4
PS81	629 CTD-TOWYO	24	-52,45766	13,36934	10	2,1
PS81	631 CTD	1	-52,42734	13,35434	2948	0,9
PS81	631 CTD	2	-52,42884	13,34916	3665	2,0
PS81	631 CTD	3	-52,43116	13,34134	3677	2,3
PS81	631 CTD	4	-52,43366	13,33200	3635	3,1
PS81	631 CTD	5	-52,43534	13,32200	3718	2,4
PS81	631 CTD	8	-52,43566	13,32066	3528	2,4
PS81	631 CTD	9	-52,43816	13,30484	4134	0,7
PS81	631 CTD	10	-52,43900	13,30200	3530	2,5
PS81	631 CTD	11	-52,43866	13,30184	3310	1,1
PS81	631 CTD	12	-52,43700	13,29176	4140	0,6
PS81	631 CTD	13	-52,43634	13,28534	3448	1,1
PS81	631 CTD	14	-52,43634	13,28350	3250	1,1
PS81	631 CTD	15	-52,43666	13,28150	4310	0,7
PS81	631 CTD	16	-52,43650	13,28150	4315	0,6
PS81	631 CTD	17	-52,43650	13,28150	4317	0,9
PS81	631 CTD	18	-52,43650	13,28134	4320	1,0
PS81	631 CTD	19	-52,43650	13,28134	4320	0,9
PS81	631 CTD	20	-52,43700	13,28116	3492	1,6
PS81	631 CTD	21	-52,43616	13,28116	2501	3,8
PS81	631 CTD	22	-52,43634	13,28034	998	1,3
PS81	631 CTD	23	-52,43684	13,27966	461	3,0
PS81	631 CTD	24	-52,43750	13,27884	10	2,1
PS81	638 CTD	1	-52,40716	13,38966	4180	---
PS81	638 CTD	2	-52,41200	13,38516	3200	---
PS81	638 CTD	3	-52,41566	13,38334	4281	0,4
PS81	638 CTD	4	-52,42116	13,37950	3200	1,1
PS81	638 CTD	5	-52,42534	13,37634	4319	1,2
PS81	638 CTD	8	-52,43500	13,37034	4201	---
PS81	638 CTD	9	-52,44016	13,37566	3217	1,1
PS81	638 CTD	10	-52,44134	13,37566	2999	1,3
PS81	638 CTD	11	-52,44616	13,37050	3950	1,0
PS81	638 CTD	12	-52,44684	13,36950	3800	1,0
PS81	638 CTD	13	-52,44816	13,36734	3500	1,4
PS81	638 CTD	14	-52,44900	13,36516	3445	1,8

6. Water Column Surveying and Sampling

Exp.	Station	Bottle No.	Latitude [°]	Longitude [°]	Depth [mbsl]	CH ₄ [nmol/l]
PS81	638 CTD	15	-52,45034	13,36166	3235	1,1
PS81	638 CTD	16	-52,45134	13,36084	3479	1,3
PS81	638 CTD	17	-52,45250	13,35950	3735	1,0
PS81	638 CTD	18	-52,45366	13,35800	3475	1,6
PS81	638 CTD	19	-52,45466	13,35750	3225	1,6
PS81	638 CTD	20	-52,45566	13,35750	2955	1,3
PS81	638 CTD	21	-52,45800	13,35584	2350	1,2
PS81	638 CTD	22	-52,46184	13,35784	1300	1,4
PS81	638 CTD	23	-52,46466	13,35784	372	1,5
PS81	638 CTD	24	-52,46466	13,35784	334	1,7
PS81	642 CTD	1	-52,24967	14,77867	3251	1,0
PS81	642 CTD	2	-52,24967	14,77867	3252	1,2
PS81	642 CTD	3	-52,24967	14,77867	3253	1,3
PS81	642 CTD	4	-52,24967	14,77867	3000	0,8
PS81	642 CTD	5	-52,24967	14,77867	2844	0,9
PS81	642 CTD	9	-52,24967	14,77867	2750	0,9
PS81	642 CTD	10	-52,24967	14,77867	2659	0,7
PS81	642 CTD	11	-52,24967	14,77867	2500	0,6
PS81	642 CTD	12	-52,24967	14,77867	2500	0,5
PS81	642 CTD	13	-52,24967	14,77867	1999	1,0
PS81	642 CTD	14	-52,24967	14,77867	1499	0,7
PS81	642 CTD	15	-52,24967	14,77867	997	0,7
PS81	642 CTD	16	-52,24967	14,77867	501	0,9
PS81	642 CTD	17	-52,24967	14,77867	356	1,1
PS81	642 CTD	18	-52,24967	14,77867	9,8	2,5
PS81	645 CTD	1	-52,20050	15,63450	3448	3,6
PS81	645 CTD	2	-52,20100	15,63700	3889	3,5
PS81	645 CTD	3	-52,20150	15,63916	4154	7,4
PS81	645 CTD	4	-52,20650	15,66016	4119	4,5
PS81	645 CTD	5	-52,20966	15,67884	3801	5,7
PS81	645 CTD	8	-52,21000	15,68134	4035	3,3
PS81	645 CTD	9	-52,21034	15,68350	4169	4,5
PS81	645 CTD	10	-52,21516	15,70566	4057	4,4
PS81	645 CTD	11	-52,21616	15,71050	3960	4,4
PS81	645 CTD	12	-52,21650	15,71216	3790	8,4
PS81	645 CTD	13	-52,21900	15,72400	3580	4,3
PS81	645 CTD	14	-52,22100	15,72650	4100	6,9
PS81	645 CTD	15	-52,22150	15,72666	4000	7,7
PS81	645 CTD	16	-52,22184	15,72684	3897	5,8
PS81	645 CTD	17	-52,22216	15,72716	3800	4,6

Exp.	Station	Bottle No.	Latitude [°]	Longitude [°]	Depth [mbsl]	CH ₄ [nmol/l]
PS81	645 CTD	18	-52,22250	15,72784	3699	4,6
PS81	645 CTD	19	-52,22300	15,72834	3600	4,2
PS81	645 CTD	20	-52,22334	15,72900	3501	3,8
PS81	645 CTD	21	-52,22616	15,73166	2501	1,1
PS81	645 CTD	22	-52,23116	15,73584	373	1,5
PS81	645 CTD	23	-52,23251	15,73834	9,4	2,9
PS81	645 CTD	24	-52,23266	15,73821	9,6	3,0
PS81	648 CTD	1	-52,14391	14,17469	3276	5,1
PS81	648 CTD	2	-52,14466	14,17487	3701	5,3
PS81	648 CTD	3	-52,14797	14,17607	3101	2,2
PS81	648 CTD	4	-52,14924	14,17632	3606	4,0
PS81	648 CTD	5	-52,15461	14,17699	3452	5,1
PS81	648 CTD	8	-52,16143	14,17726	3555	4,0
PS81	648 CTD	9	-52,16210	14,17728	3630	4,0
PS81	648 CTD	10	-52,16291	14,17728	3476	5,3
PS81	648 CTD	11	-52,16886	14,17698	3540	4,4
PS81	648 CTD	12	-52,17066	14,17699	3697	3,4
PS81	648 CTD	13	-52,17067	14,17699	3696	2,8
PS81	648 CTD	14	-52,17643	14,17663	3741	3,0
PS81	648 CTD	15	-52,17681	14,17649	3701	3,3
PS81	648 CTD	16	-52,17690	14,17647	3659	3,9
PS81	648 CTD	17	-52,17698	14,17647	3621	3,8
PS81	648 CTD	18	-52,17705	14,17647	3579	4,0
PS81	648 CTD	19	-52,17710	14,17647	3539	4,8
PS81	648 CTD	20	-52,17717	14,17648	3499	4,9
PS81	648 CTD	21	-52,17723	14,17647	3462	4,1
PS81	648 CTD	22	-52,17779	14,17612	2501,5	1,3
PS81	648 CTD	23	-52,17804	14,17594	348	1,3
PS81	648 CTD	24	-52,17804	14,17594	9,2	2,8
PS81	651 CTD	1	-52,13000	14,24266	3092	2,7
PS81	651 CTD	2	-52,13900	14,23050	3083	1,9
PS81	651 CTD	3	-52,14334	14,22400	3106	2,2
PS81	651 CTD	4	-52,15634	14,20516	3475	2,5
PS81	651 CTD	5	-52,16050	14,19950	3526	3,0
PS81	651 CTD	8	-52,16384	14,19416	3401	2,7
PS81	651 CTD	9	-52,16484	14,19316	3657	2,3
PS81	651 CTD	10	-52,16966	14,18916	3700	2,8
PS81	651 CTD	11	-52,17050	14,18184	3673	2,3
PS81	651 CTD	15	-52,17000	14,18150	3683	2,9
PS81	651 CTD	21	-52,16984	14,18116	2501	0,9

6. Water Column Surveying and Sampling

Exp.	Station	Bottle No.	Latitude [°]	Longitude [°]	Depth [mbsl]	CH ₄ [nmol/l]
PS81	651 CTD	22	-52,16984	14,18116	2501	0,8
PS81	651 CTD	23	-52,17116	14,18466	372	1,0
PS81	651 CTD	24	-52,17250	14,18400	12	2,5
PS81	660 CTD	1	-52,44550	13,00866	3350	1,4
PS81	660 CTD	3	-52,50766	12,98566	3700	0,7
PS81	660 CTD	4	-52,50850	12,98550	3549	0,8
PS81	660 CTD	5	-52,51316	12,98450	3687	0,7
PS81	660 CTD	8	-52,51384	12,98416	3566	1,1
PS81	660 CTD	9	-52,51384	12,98400	3538	1,0
PS81	660 CTD	10	-52,51884	12,98150	3690	1,0
PS81	660 CTD	11	-52,51966	12,98100	3538	1,0
PS81	660 CTD	12	-52,52234	12,98034	3332	1,3
PS81	660 CTD	13	-52,52484	12,97916	3680	0,9
PS81	660 CTD	14	-52,52566	12,97900	3541	0,8
PS81	660 CTD	15	-52,53050	12,97850	3699	1,4
PS81	660 CTD	16	-52,53150	12,97766	3551	0,9
PS81	660 CTD	17	-52,53200	12,97834	2475	0,9
PS81	660 CTD	18	-52,53316	12,97666	335	1,5
PS81	660 CTD	19	-52,53328	12,97666	12	2,7
PS81	660 CTD	20	-52,53334	12,97666	11	2,7
PS81	663 CTD	1	-52,64550	12,52617	3651	0,7
PS81	663 CTD	2	-52,64550	12,52617	3652	0,9
PS81	663 CTD	3	-52,64550	12,52617	3581	1,4
PS81	663 CTD	4	-52,64550	12,52617	2999	1,3
PS81	663 CTD	5	-52,64550	12,52617	2502	0,8
PS81	663 CTD	8	-52,64550	12,52617	2242	0,5
PS81	663 CTD	9	-52,64550	12,52617	2000	0,9
PS81	663 CTD	10	-52,64550	12,52617	1499	0,7
PS81	663 CTD	11	-52,64550	12,52617	999	0,7
PS81	663 CTD	12	-52,64550	12,52617	501	0,7
PS81	663 CTD	13	-52,64550	12,52617	9	2,0
PS81	673 CTD	1	-52,11100	14,61000	2208	0,2
PS81	673 CTD	2	-52,11100	14,61000	2001	0,5
PS81	673 CTD	3	-52,11100	14,61000	1800	0,5
PS81	673 CTD	4	-52,11100	14,61000	1502	0,6
PS81	673 CTD	5	-52,11100	14,61000	1000	0,6
PS81	673 CTD	8	-52,11100	14,61000	500	0,7
PS81	673 CTD	9	-52,11100	14,61000	363	1,1
PS81	673 CTD	10	-52,11100	14,61000	8	2,8
PS81	674 CTD	1	-52,20583	14,69667	3102	0,6

Exp.	Station	Bottle No.	Latitude [°]	Longitude [°]	Depth [mbsl]	CH ₄ [nmol/l]
PS81	674 CTD	2	-52,20583	14,69667	3000	0,6
PS81	674 CTD	3	-52,20583	14,69667	2679	0,7
PS81	674 CTD	4	-52,20583	14,69667	2500	0,5
PS81	674 CTD	5	-52,20583	14,69667	2000	0,6
PS81	674 CTD	8	-52,20583	14,69667	1500	0,9
PS81	674 CTD	9	-52,20583	14,69667	1000	0,6
PS81	674 CTD	10	-52,20583	14,69667	500	0,6
PS81	674 CTD	11	-52,20583	14,69667	376	0,9
PS81	674 CTD	12	-52,20583	14,69667	9	2,0

MAPR

After the subtraction of the background signal of each MAPR, a Savitzky-Golay filter was applied to the recovered backscatter data. A typical plot is shown in Fig. 6.5, displaying increased backscatter signals close to the sea floor and around 3,200 m. Similar changes in the backscatter signals were recorded at all CTD-tow-yo stations. No significant Eh signal was found in any of the MAPR deployments. The relevance of turbidity variations is subject to further investigation (e.g. He/Ne analysis).

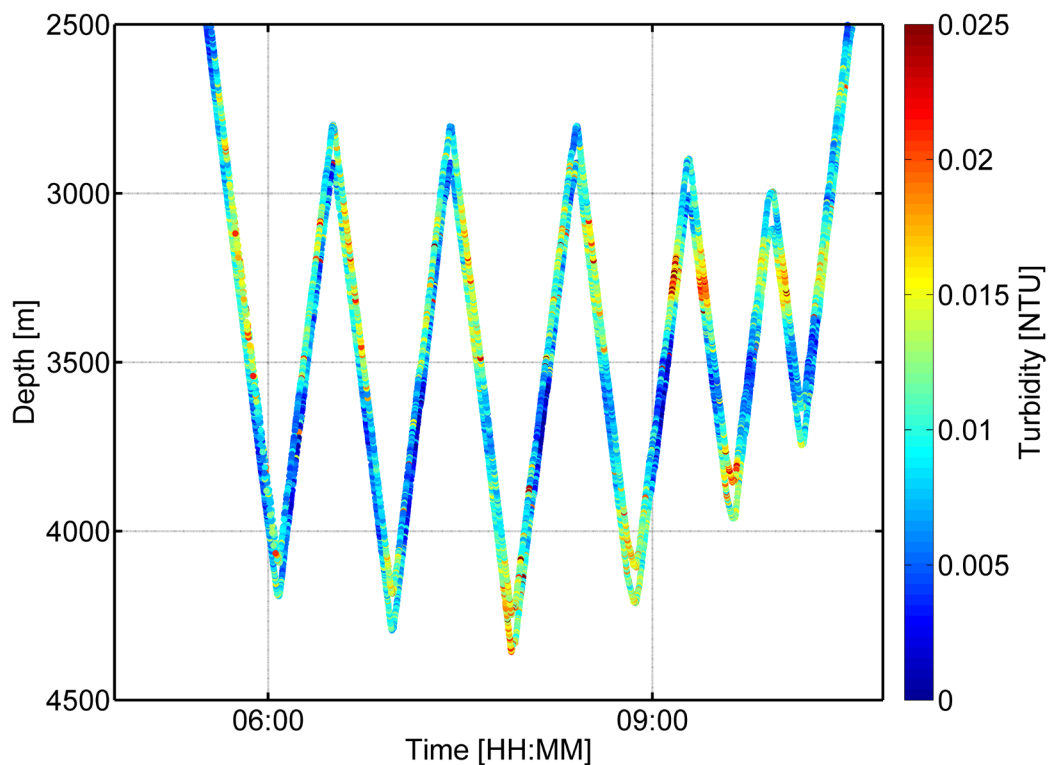


Fig. 6.5: MAPR data from CTD-tow-yo Station 638. The optical backscatter signal is plotted vs depth and time. (MAPR 65, 66). Higher backscatter signals are recorded close to the sea floor and around 3,200 m.

6. Water Column Surveying and Sampling

A full account of all MAPR deployments is provided in the following Table 6.2.

Tab. 6.2: Overview of MAPR deployments

Station ID	Survey	Date and time	Water depth [m]	MAPR No	Distance to CTD [m]	Comments
605	CTD	16.11.13 11:24 - 15:00	4285	66	0 m	
614	tow-yo	19.11.13 21:35 - 04:58	3905	65	50 m	
				66	0 m	
				67	150 m	
				68	100 m	Backscatter sensor malfunctioning
615	OFOS	20.11.13 05:18 - 08:20	3975	67	-	
627	OFOS	23.11.13 10:54 - 17:49	4278	65	-	
628	tow-yo	23.11.13 19:26 - 04:06	4275	65	0 m	
				66	100 m	
				67	50 m	
				68	150 m	Backscatter sensor malfunctioning
629	tow-yo	25.11.13 08:43 - 17:29	4308	65	0 m	
				66	50 m	
				68	100 m	
630	OFOS	25.11.13 17:54 - 02:30	3916	67	-	
631	tow-yo	26.11.13 02:57 - 08:30	4329	65	0 m	
				66	100 m	
				68	50 m	Backscatter sensor malfunctioning
633	OFOS	26.11.13 12:25 - 20:10	4127	67	-	
637	OFOS	27.11.13 19:38 - 03:45	4395	67	-	
638	tow-yo	28.11.13 04:33 - 11:30	4357	65	0 m	
				66	100 m	
				68	50 m	Backscatter sensor malfunctioning

Station ID	Survey	Date and time	Water depth [m]	MAPR No	Distance to CTD [m]	Comments
639	MUC	28.11.13 12:22 - 16:30	4402	67	-	
642	CTD	29.11.13 08:15 - 10:34	3369	65	0m	
645	tow-yo	30.11.13 04:24 - 10:18	4202	65	0 m	
				66	50 m	
				67	0 m	
				68	100 m	Backscatter sensor malfunctioning
646	MUC	30.11.13 11:40 - 15:45	4063	67	-	
648	tow-yo	01.12.13 09:33 - 15:25	3754	65	0 m	
				66	75 m	
				68	150 m	Backscatter sensor malfunctioning
649	MUC	01.12.13 16:35 - 19:45	3681	67	-	
650	OFOS	01.12.13 20:29 - 04:30	3681	67	-	
651	tow-yo	02.12.13 05:24 - 13:00	3717	65	0 m	
				66	75 m	
				68	150 m	Backscatter sensor malfunctioning
656	tow-yo	03.12.13 15:02 - 16:30	263	65	0 m	tow-yo cancelled
		03.12.13 15:02 - 16:30		66	75 m	
		03.12.13 15:02 - 16:30		68	150 m	
659	MUC	04.12.13 02:53 - 06:08	3952	67	-	
660	tow-yo	05.12.13 08:20 - 16:26	4013	65	0 m	
				66	75 m	
				68	150 m	Backscatter sensor malfunctioning
661	MUC	05.12.13 17:35 - 21:20	4441	67	-	

6. Water Column Surveying and Sampling

Station ID	Survey	Date and time	Water depth [m]	MAPR No	Distance to CTD [m]	Comments
663	CTD	06.12.13 05:10 - 08:00	3669	65	0 m	
666	OFOS	07.12.13 09:42 - 14:25	2763	67	-	
670	OFOS	08.12.13 13:28 - 17:43	1977	67	-	
671	OFOS	08.12.13 18:18 - 21:34	912	67	-	
673	CTD	09.12.13 01:04 - 02:45	2282	65	0 m	
674	CTD	09.12.13 03:43 - 05:48	3204	65	0 m	
680	OFOS	11.12.13 09:05 - 14:36	4233	67	-	

Data management

Data from uncalibrated CTD-sensors was available for all cruise participants on board. Calibration and post-processing of the data will be done as soon as possible after the cruise and made public on PANGAEA Data Publisher for Earth & Environmental Science data base.

All geochemical, noble gas, and MAPR data will be made public in the PANGAEA Data Publisher for Earth & Environmental Science as soon as we have them available (approx. one year after the cruise), carefully quality controlled, and published in a peer reviewed journal.

References

- Bach W, Banerjee NR, Dick HJB, Baker ET (2002) Discovery of ancient and active hydrothermal deposits along the ultraslow spreading Southwest Indian Ridge 10-16°E. *Geochemistry, Geophysics, Geosystems*, 3(7), pp 1-14, doi:10.1029/2001GC000279.
- Baker ET, Edmonds HN, Michael PJ, Bach W, Dick HJB, Snow JE, Walker SL, Banerjee NR, Langmuir CH (2004) Hydrothermal venting in a magma desert: The ultraslow-spreading Gakkel and Southwest Indian Ridges. *Geochemistry Geophysics Geosystems* 5(8), doi: 10.1029/2004GC000712.
- Dick HJB, Lin J, Schouten H (2003) An ultraslow-spreading class of ocean ridge. *Nature*, 426, 405-412.
- German CR, Bowen A, Coleman ML, Honig DL, Huber JA, Jakuba MV, Kinsey JC, Kurz MD, Leroy S, McDermott JM, Mercier de Lépinay B, Nakamura K, Seewald JS, Smith J, Sylva SP, Van Dover CL, Whitcomb LL & Yoerger DR Diverse styles of submarine venting on the ultra-slow spreading Mid-Cayman Rise. *PNAS* 107, 14020-14025, 2010.
- Roether W, Vogt M, Vogel S, Sültenfuß J (2013) Combined sample collection and gas extraction for the measurement of helium isotopes and neon in natural waters. *Deep-Sea Research I*, 76(6), 27-34.

7. BIOLOGY AND BIOGEOCHEMISTRY

Outline

A main objective was to investigate community composition and function of the SWIR in relation to the oceanography and geology of this area. The SWIR may provide a gateway for dispersal of deep-sea life including vent species between Antarctica, the Atlantic and the Indian Ocean. The exploration of the SWIR will thus provide crucial data for understanding dispersal and colonization pathways for chemosynthetic organisms and associated fauna between ocean basins. The former Census of Marine Life program ChEss had identified this ridge segment as a priority area to elucidate global biogeographic patterns and processes in chemosynthetic ecosystems. We have combined video-guided and sensor-equipped towed instruments with seafloor and water column sampling to explore benthic communities, microbiology and biogeochemistry of valleys and ridge flanks between 13-16°E (Fig. 7.1.1).

Main overarching goals of the mission included

- Localization and characterization of the SWIR landscape including hydrothermal vents, and mapping to determine structural controls on community distribution
- Sampling of porewater and hydrothermal fluids to determine high-temperature water-rock interactions in the deep root zone of the systems, fluid mixing and cooling processes in the sub-seafloor and potential linkages to microbial activity
- Analyses of background and vent communities, to determine dispersal and colonization pathways along spreading ridges

7.1 Geobiological observations

Yann Marcon¹, Sebastian Albrecht²,
Norbert Rieper³, Antje Boetius⁴

¹MARUM
²FIELAX,
³ISITEC
⁴AWI

Objectives

Bottom observations from previous work on the Southwest Indian Ridge (SWIR) are scarce and visual information about geostructures, habitat landscapes, benthic faunal communities and their distribution in this area have so far been missing. Previous expeditions to the SWIR discovered hydrothermal deposits as well as turbidity anomalies (plume) in several locations along the ridge (Bach *et al.*, 2002).

However, due to the lack of seafloor observations in this segment of the SWIR, the presence of active hydrothermal venting has never been confirmed. One main objective of ANT-XXIX/8 was to palliate this lack by deploying the OFOS and the TV-MUC systems at various locations along the ridge. The initial locations were chosen based on their identification as potential hydrothermal targets from the previous works in the area.

With the OFOS observations we planned to (1) to document the benthic macro- and megafauna that populates the SWIR, (2) to analyse the faunal density, distribution pattern and habitats, (3) to search for signs of hydrothermal activity (presence of chemosynthetic organisms, hydrothermal precipitates, fluid venting), and (4) to find targets for the sediment, biological, and rock sampling devices, such as the TV-guided multicorer (TV-MUC), the TV-Grab, and the Agassiz Trawl.

Work at sea

The OFOS is a towed underwater camera system equipped with both a high-resolution photo-camera (iSiTEC, CANON EOS 1Ds Mark III) and a high-definition video-camera (iSiTEC, Sony FCB-H11). The cameras are mounted on a steel frame (140L x 92W x 135H cm), together with two strobe lights (iSiTEC UW-Blitz 250, TTL driven), three lasers, four LED lights, a Trittech Altimeter, and a USBL positioning system (Posidonia) to track the position of the OFOS during deployments. The TV-MUC is a video-guided multi-corer system, which is able to sample up to eight 1 m-long cores. It is equipped with a high-definition video-camera, two strobes, and a USBL positioning system (Posidonia) in order to visualize the sampling area and to record its precise location. The OFOS and the TV-MUC were deployed from the side of *Polarstern* and towed at speeds of 0.5 to 2 knots at distances between 0 and 10 m above the seafloor, depending on the sea state.

In total, 11 OFOS and 9 TV-MUC deployments were carried out during the cruise (Table 7.1.1). Deployments were conducted in various locations both along the ridge, and off axis (Fig. 7.1.1). On-axis OFOS and TV-MUC deployment targets were chosen during the cruise based on existing and new water column data, geological and biological samples, heat flow measurements, seafloor visual observations, as well as on multi-beam and PARASOUND echosounder surveys. The most intensively investigated areas are referred to as Plume Area (Fig. 7.1.2), Clam Area (Fig. 7.1.3), Heat Flow Area (Fig. 7.1.4), Crater Area (Fig. 7.1.5), and Narrowgate Mound Area (Fig. 7.1.6). In addition, a few deployments were conducted off-axis at latitudes both south and north of the ridge in order to get reference sediment samples and seafloor observations from both the Antarctic and the African plates.

7.1 Geobiological observations

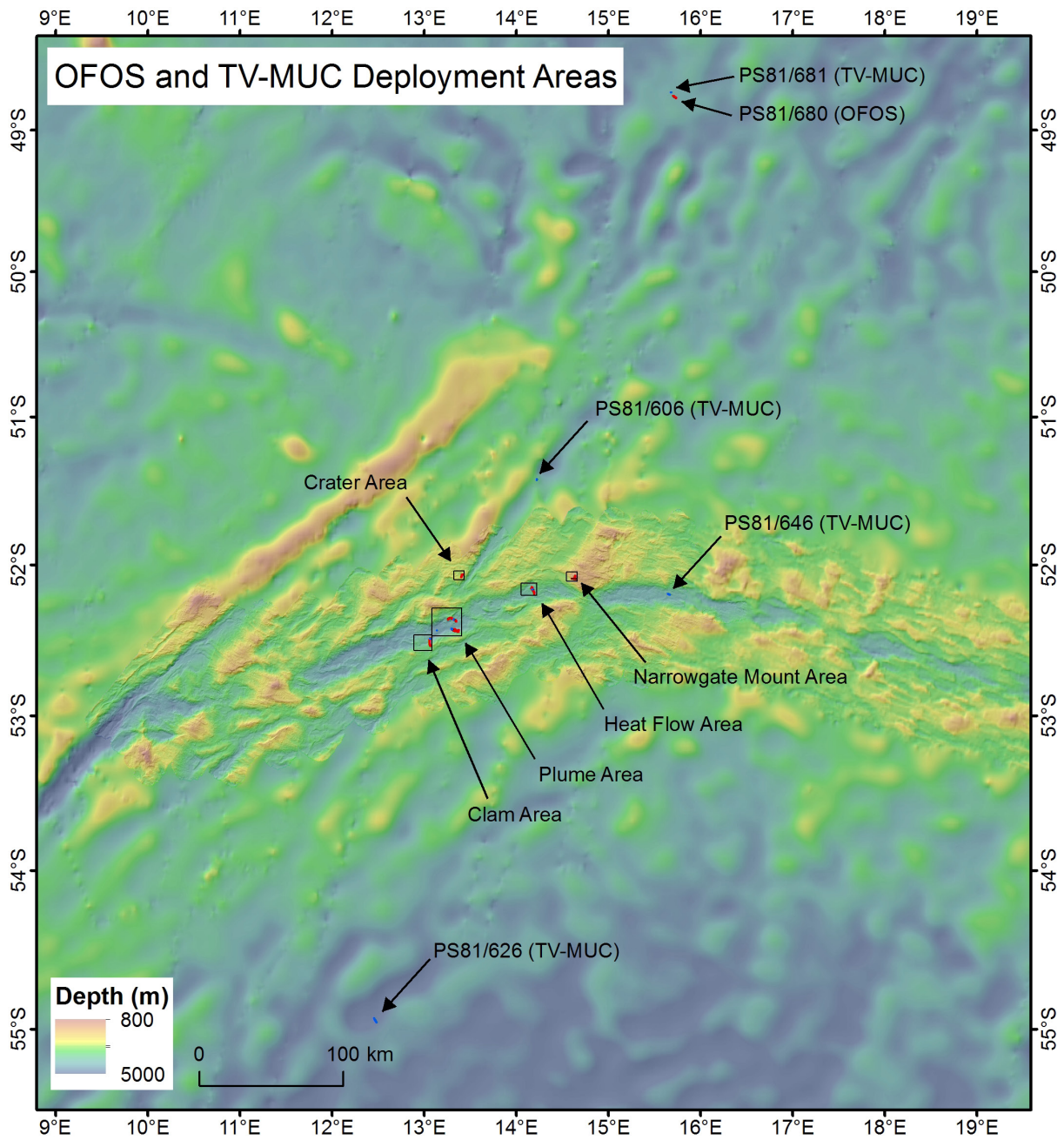


Fig. 7.1.1: Locations of the areas of OFOS and TV-MUC deployments

Tab. 7.2.1: Summary of OFOS and TV-MUC deployments during ANT-XXIX/8

Device	Area	Station No	Date	Start				End				Mounted sensors	Comments		
				Off deck	At bottom	Latitude	Longitude	Depth	From bottom	On deck	Latitude			Longitude	Depth
TV-MUC	Off-axis (North side)	PS81/606	16.11.2013	16:02:00	18:00:00	-51°25.498'	14°13.303'	4416	18:51:00	20:03:00	-51°25.984'	14°13.418'	4456	None	1 core taken
OFOS	Plume Area (South Mount)	PS81/615	20.11.2013	05:18:00	06:27:20	-52°26.52'	13°21.576'	3892	07:29:54	08:27:59	-52°26.915'	13°22.352'	3590	Microsensors MAPR 67	
TV-MUC	Off-axis (South side)	PS81/626	22.11.2013	11:28:07	13:07:25	-54°55.977'	12°27.275'	4862	16:01:43	17:45:59	-54°57.551'	12°28.776'	4864	None	4 cores taken
OFOS	Clam Area	PS81/627	23.11.2013	10:56:48	12:26:03	-52°29.525'	13°4.267'	4272	16:22:16	17:37:59	-52°32.655'	13°4.42'	3335	Microsensors MTL MAPR 65	
OFOS	Plume Area (South Mount)	PS81/630	25.11.2013	17:54:00	19:08:39	-52°26.204'	13°22.596'	3932	00:50:54	02:12:59	-52°25.864'	13°17.883'	4363	Microsensors MTL MAPR 67	
OFOS	Plume Area (North Mount)	PS81/633	26.11.2013	12:24:00	13:43:45	-52°22.879'	13°21.003'	4128	19:43:00	21:06:59	-52°22.046'	13°15.441'	3719	Microsensors MTL MAPR 67	
TV-MUC	Clam Area	PS81/636	27.11.2013	13:29:00	14:48:00	-52°29.776'	13°3.917'	4190	14:50:00	16:16:59	-52°29.783'	13°3.905'	4194	None	6 cores taken
OFOS	Plume Area (South Mount)	PS81/637	27.11.2013	19:36:00	21:02:30	-52°25.985'	13°18.457'	4385	02:17:41	03:41:59	-52°26.999'	13°21.863'	3586	Microsensors MTL MAPR 67	
TV-MUC	Plume Area (South Mount)	PS81/639	28.11.2013	12:25:11	13:49:55	-52°25.67'	13°17.663'	4379	14:56:19	16:19:59	-52°26.083'	13°18.255'	4360	MAPR 67	All corers empty
TV-MUC	Axis Centre (East of Narrogate)	PS81/646	30.11.2013	11:41:11	13:02:21	-52°11.837'	15°38.705'	4076	14:07:22	15:34:59	-52°12.176'	15°39.843'	4149	MAPR 67	
OFOS	Heat Flow Area	PS81/647	01.12.2013	01:53:00	03:00:57	-52°9.031'	14°10.06'	3647	06:50:00	08:33:59	-52°11.812'	14°11.649'	3741	Microsensors MTL	
TV-MUC	Heat Flow Area	PS81/649	01.12.2013	16:35:00	17:45:00	-52°10.05'	14°10.575'	3649	18:15:57	19:34:59	-52°10.099'	14°10.605'	3635	MAPR 67	4 cores taken
OFOS	Heat Flow Area	PS81/650	01.12.2013	20:29:41	21:44:08	-52°9.591'	14°10.122'	3648	02:46:23	04:12:59	-52°9.964'	14°10.269'	3667	Microsensors MTL MAPR 67	
TV-MUC	Plume Area (North Mount)	PS81/659	05.12.2013	02:53:32	04:26:27	-52°22.063'	13°19.19'	3933	04:37:00	06:08:59	-52°22.048'	13°19.22'	3921	MAPR 67	6 cores taken
TV-MUC	Axis Centre	PS81/661	05.12.2013	17:34:00	19:12:03	-52°26.474'	13°8.198'	4416	19:31:42	21:06:59	-52°26.464'	13°8.205'	4397	MAPR 67	6 cores taken
OFOS	Crater Area	PS81/666	07.12.2013	09:42:00	10:38:44	-52°3.98'	13°25.688'	2753	13:11:55	14:14:59	-52°5.22'	13°24.127'	2596	Microsensors MTL MAPR 67	
OFOS	Narrogate Mount	PS81/670	08.12.2013	13:29:26	14:13:42	-52°5.859'	14°36.292'	2012	17:14:39	17:43:59	-52°5.872'	14°38.786'	1368	Microsensors MAPR 67	No USBL data
OFOS	Narrogate Mount	PS81/671	08.12.2013	18:33:32	18:42:10	-52°4.717'	14°38.245'	963	21:05:13	21:34:59	-52°5.873'	14°37.662'	1400	Microsensors MAPR 67	
OFOS	Off-axis (North side)	PS81/680	11.12.2013	09:06:55	10:31:36	-48°46.236'	15°44.134'	4236	13:00:23	14:36:59	-48°45.317'	15°42.212'	4337	MAPR 67	
TV-MUC	Off-axis (North side)	PS81/681	11.12.2013	15:00:00	16:41:00	-48°43.838'	15°40.717'	4351	16:42:00	18:24:59	-48°43.837'	15°40.718'	4354	None	No video signal 8 cores taken

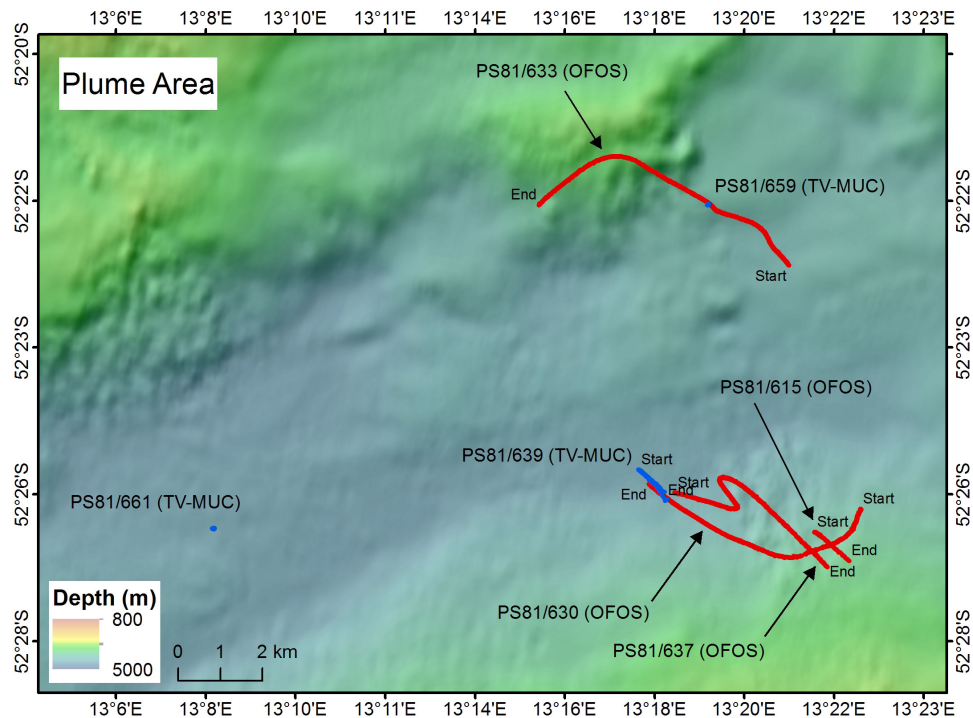
Preliminary results

OFOS and TV-MUC dives were conducted both along the ridge, and off axis (Fig. 7.1.1). Generally, seafloor observations revealed a great variety of terrains, including flat areas with very soft sediments (mostly diatom ooze), slopes of hardened sediments, rocky fields and large escarpments of both magmatic and mantle rocks. The seafloor topography appeared a lot rougher than previously suggested by the hydroacoustic data. An overview of the terrains encountered is provided for each OFOS dive in Appendix A.5.7.1. The observations also showed that faunal abundance and richness varied greatly between the studied areas (see chapter 7.4). Reference stations off axis (PS81/606) and outside the ridge (PS81/626, and PS81/680) showed that the faunal abundance is generally higher in the vicinity of the ridge than away.

Plume Area (Fig. 7.1.2)

This area corresponds to the zone where previous plume mapping detected the highest turbidity anomalies in the water column (Bach *et al.*, 2002). Results from the Plume Area (13°E basin) include visual observations of both flanks of the ridge, as well as of the in-between flat central area. Most observations focused on the southern flank of the ridge, due to the presence of strong turbidity plumes in the area. Observations (PS81/615, PS81/630, PS81/637, and PS81/639) in this area showed that the deepest part of the ridge is filled with very soft and fluffy sediments (diatom ooze). These sediments generated clouds when disturbed by the OFOS frame, which cleared up slowly. The particles looked very differently from the water column-hosted turbidity recorded e.g. at Station PS81/630, which shifted eastward during later dives in the same zone (PS81/637 and PS81/639). The benthic faunal density in this central area was generally lower than towards the slopes, where sediments were denser. As we moved towards the slopes, the sediment cover gradually became thinner, with an increasing occurrence of tephra.

Fig. 7.1.2:
Overview of the
plume area and
of the OFOS
and TV-MUC
deployments



Faunal abundance also increased. Further up the slope, the sediment area gave place to a series of large escarpments (several meters in height) of talus, black and brown brecciated rock, massive basalts, as well as of light-coloured blocks of consolidated sediments, possibly of sepiolite. Towards the top of the mount, soft sediments occurred again. Interestingly, observations (PS81/633, PS81/659) in the northern mount showed a similar sequence with, however, a seemingly lower faunal abundance, than on the southern mount. The exploration of the northern mount also revealed the presence of patches of black reduced sediment as well as a few small tubes (possibly Pogonophora).

Clam Area (Fig. 7.1.3)

A vesicomyid clam was found during the recovery of an Ocean Bottom Seismometer (OBS) in this area. Vesicomyid clams are generally observed at hydrothermal vent and cold seep systems. Hence, the discovery of a vesicomyid clam on the OBS motivated the deployment of OFOS in this area.

From the deepest (-4,300 m) to the shallowest (-3,300 m) point of the dive (PS81/627), we successively observed areas of soft sediments with numerous traces of benthic life (sea cucumber, trails, etc.), of sediment-covered pillow lavas, of soft white sediments scattered with patches of black reduced sediments, abrupt escarpments of peridotite-like rock populated with particle-filtering fauna (crinoids, soft-corals), and finally flatter areas with a hardened sediment cover. A TV-MUC was also deployed to sample the sediments in the area where the clam was recovered.

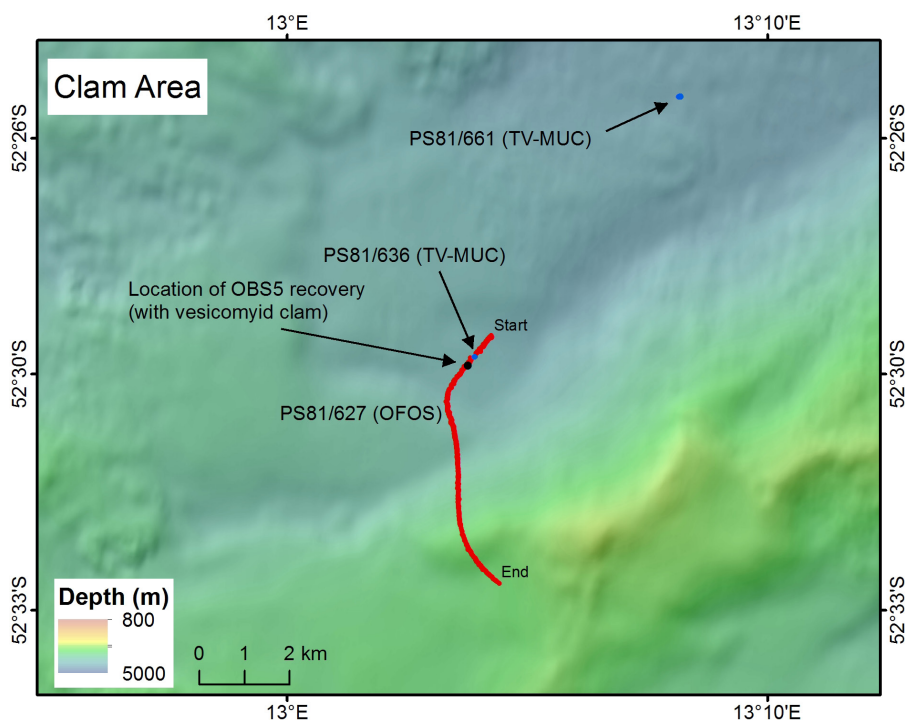


Fig. 7.1.3: Overview of the clam area and of the OFOS and TV-MUC deployments

No further clam was observed during the dives.

7.1 Geobiological observations

"Hot Mound" Area (Fig. 7.1.4)

The "Hot Mound" Area is an area where elevated heat flow values up to 1,000 mW/m² were measured during the cruise, and where sediments recovered were as warm as 8°C on deck. Two OFOS and one TV-MUC stations were conducted. PS81/647 crossed the locations where the highest heat flow values were measured. It revealed areas of soft sediments exclusively. However, blackish sediments, increased turbidity, presence of tubes (possibly Pogonophora) and of siphon-like features (indicating the possible presence of bivalves in the sediments) were observed in the vicinity of the heat flow points. These observations concurred with slight increases in bottom water temperature and H₂S concentrations and with a slight decrease of redox potential (see chapter 7.2). No hard rocks were observed during this dive. Following these observations, stations PS81/649 (TV-MUC) and PS81/650 (OFOS) focused on the same area. Both stations encountered highly turbid bottom waters, in which the seafloor was hardly visible, but at slightly different locations. Indeed, PS81/650 found the densest turbidity about 700 m to the east of the location of the TV-MUC deployment, and about 7 hours later.

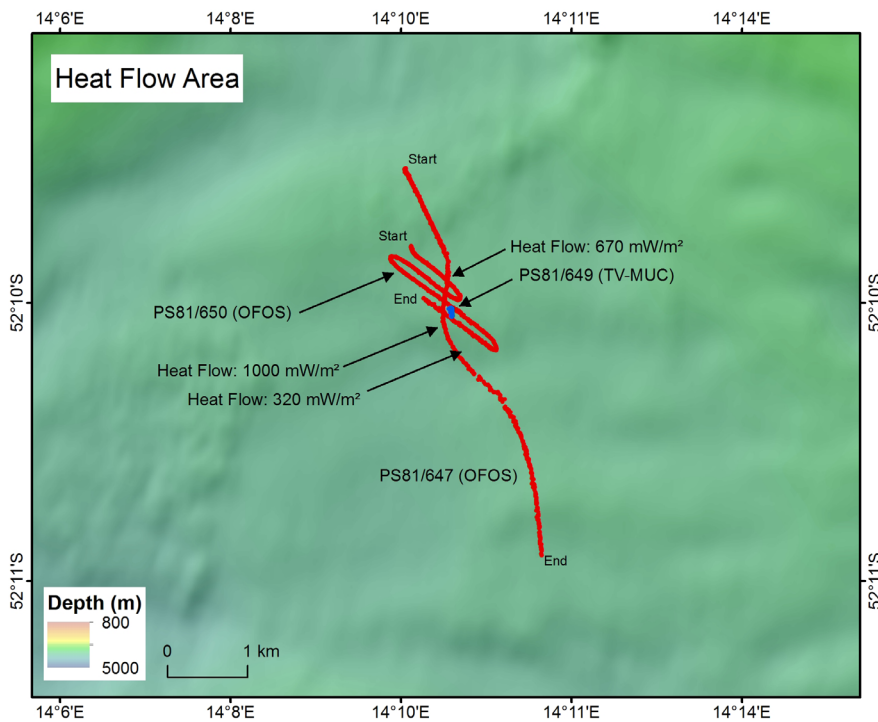


Fig. 7.1.4: Overview of the heat flow area and of the OFOS and TV-MUC deployments

Crater Area (Fig. 7.1.5)

The crater area lies on the northern side of the SWIR, in an area where the bathymetry data show numerous 1 - 2 km-wide crater-like structures, possibly related to volcanic activity. The OFOS station PS81/666 visited the rim between two of these craters. The videos showed mainly sediment-covered areas (diatoms) with patches of tephra. Dark ash-like sediments occurred higher up in the slope, as well as a few large basaltic blocks near the top of the crater's rim, shortly before the end of the dive. Sea cucumbers and a few tubes were also observed.

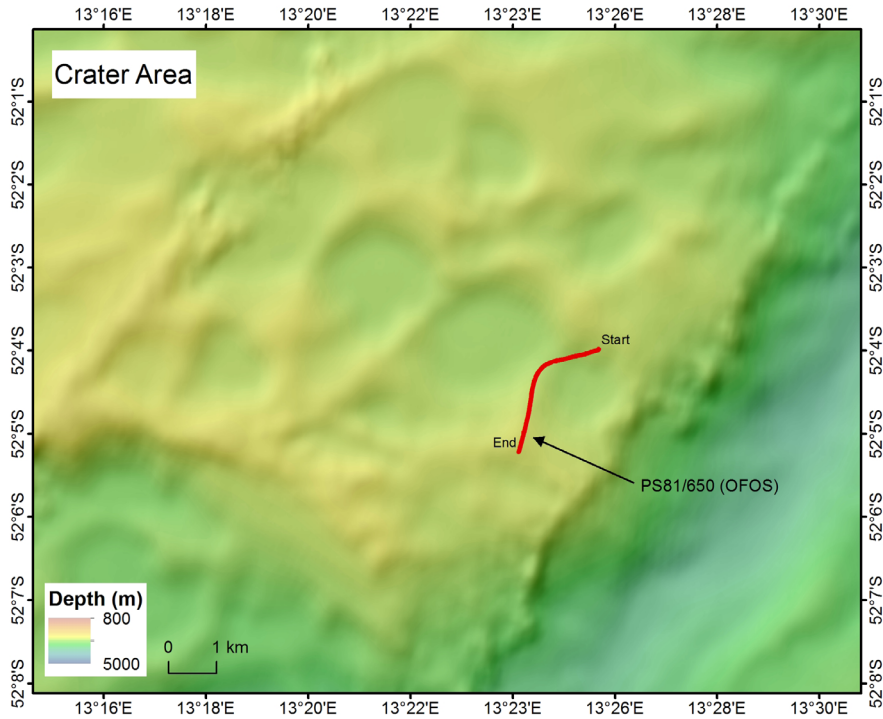


Fig. 7.1.5: Overview of the upper crater area and of the OFOS deployment

Rift flank close to Narrowgate (Fig. 7.1.6)

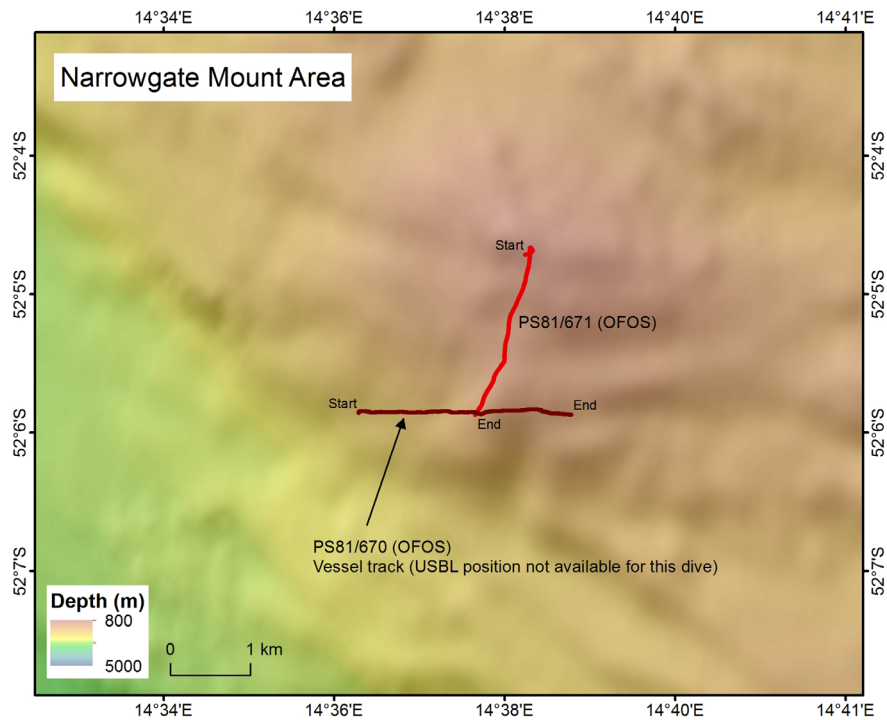


Fig. 7.1.6: Overview of the rift flank close to the Narrowgate area

Two OFOS dives (PS81/670 and PS81/671) were conducted near the summit of the rift flank, close to the Narrowgate volcanic area, between 2,000 and 950 m water

7.1 Geobiological observations

depth. Observations showed mainly steep rocky slopes, with abundant talus-like material, possible pyroclastic rocks, pillow lavas, and a few sedimented terraces. Hydrothermal slabs and dark brown rocks were also observed at about 1,000 m water depth. Results also revealed a richer and more abundant fauna than in the other areas, likely related to the shallower depth. Observed fauna includes Brachiopods (mostly shells), cold water corals (*Lophelia*), soft corals, sponges, sea feather, shrimps and red sea spiders. Embarked sensors measured numerous local decreases in O₂ and redox potential and increases in temperatures during the dives.

Data management

Tracks of video and photography surveys will be stored in PANGAEA Data Publisher for Earth & Environmental Science archive. The photographic material will be made available to taxonomists and further image analysis via BIIGLE.

References

Bach W, Banerjee NR, Dick HJB, Baker ET (2002) Discovery of ancient and active hydrothermal deposits along the ultraslow spreading Southwest Indian Ridge 10°-16°E. *Geochemistry, Geophysics, Geosystems*, 3 (7), pp 1-14, doi: 10.1029/2001GC000279.

7.2 Water column biogeochemistry

Dirk de Beer, Axel Nordhausen, Fabian Schramm

MPI

Objectives

We aimed at linking seawater chemistry to observations on biological diversity and density, and to assess how biology is controlled by fluid flow from hydrothermal venting. The water chemistry was measured by a sensor package combined with a towed underwater video camera system (OFOS) that can focus on the seafloor. OFOS was lowered to the seafloor by a winch and trawled at approximately 3-5 m height above seafloor, due to the wave swell. The sensor unit carried microsensors for O₂, H₂S, pH, ORP, N₂O, H₂ (de Beer *et al.*, 2013; Kühl & Revsbech, 2000) and temperature, all parameters that are directly or indirectly linked to fluid venting, and that may control the biology of the seafloor. The advantage of microsensors over macrosensors is their fast response. This is essential as vents maybe local and be passed in a short time by the towed instrument. The TV MUC (a multicorer equipped with an online video camera) was used on 5 deployments equipped with a MAPR, which measures pressure, temperature, redox potential and turbidity (see chapter 6).

Work at sea

OFOS: A set of micro-sensors, miniaturized temperature loggers (MTL) and a MAPR (Baker & Milburn, 1997) were mounted on the system's frame to record and monitor various physical and chemical parameters (temperature, pressure, turbidity, redox potential, pH, and concentrations in O₂, NO₂ and H₂S). Both the

camera and the sensor unit are available online via the ship's telemetry (see chapter 7.2 below). High-resolution photographs of objects of interest can be taken, and are provided with metadata on position, height above seafloor and time. Especially the concurrent dynamics of the sensor signals are of interest. The choice of the OFOS tracks was determined in close coordination with Oceanography, Marine Geology, and Geophysics (Heat flow) and based on their observations. We aimed specifically at sites where promising heat flow and methane and turbidity plumes were observed in the water column. The camera images and sensor data were further integrated into maps (See Appendix A.5.7.2).

TV MUC: The camera is online via the ship's telemetry, the MAPR data are downloaded upon retrieval. The MAPR data are archived and calibrated and analysed after the dive. The deployments end by sampling sediment cores, after which the MUC is recovered on deck (see 7.4).

Preliminary results

Hydrothermal vents eject hot water laden with reduced substances into the water column, for example reduced metals, hydrogen and sulphide. Many types of hydrothermal vents have a low pH, but those hosted in ultramafic bearing rocks can be alkaline (Edmonds, 2010). We have deployed OFOS 9 times with the sensor modules online (Table 7.2.1). The most sensitive sensors for anomalies indicative of fluid venting were redox and sulfide. Where these anomalies were found also temperature was often slightly elevated. No hydrogen was detected, and oxygen did not show a trend with anomalies in redox or sulfide. In one occasion (OFOS 615) the N_2O signal increased, here it should be noted that N_2O sensors are highly sensitive to some organic sulfur compounds. Preliminary results are that fluid venting in the area is most likely diffusive.

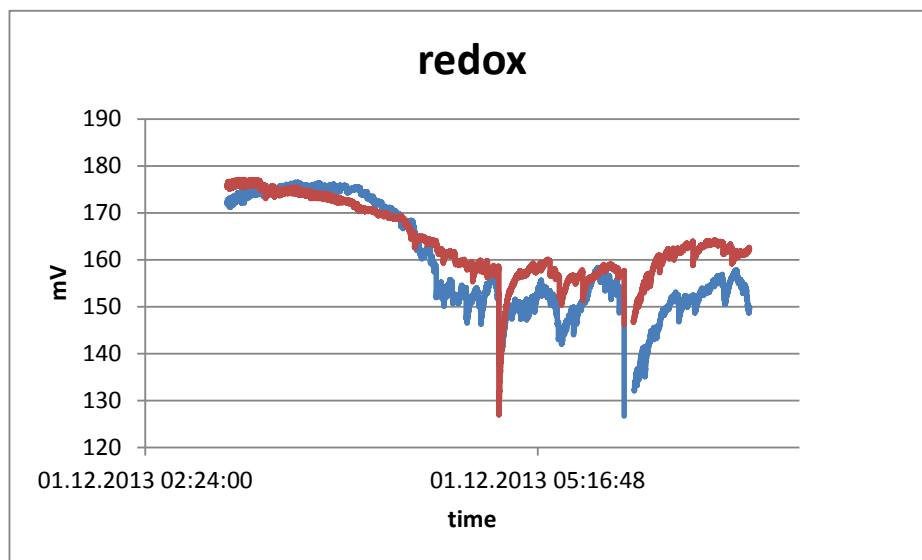


Fig. 7.2.1: The time course of the 2 redox signals. The two very large spikes are caused by bottom contacts of OFOS, the other smaller spikes often occurred simultaneously in both channels and are not noise, but indicative for flares with reducing chemistry.

7.2 Water column biogeochemistry

Areas such as the flanks of the steep ridges were identified with anomalies, but no clear features were observed in the seafloor, except for blackish sediment patches. Remarkable in this respect is that the redox signals showed often spikes in both channels, indicating distinct, small flares of reducing substances (Fig. 7.2.1). Yet, these were not reflected at the seafloor by structures such as holes or cracks, as often observed in cold seep settings with fluid venting. At sites where redox and sulfide showed anomalies, the pH sensors showed only slight variations, but in both directions. This may indicate that several processes with different effects on pH occur in parallel, or that there are different sources of fluids.

The most exciting OFOS dives were No. 630 and 647. Dive 650 was on the same location as 647, but unfortunately the most sensors broke early in the dive due to a winch failure. Dive 630 was downslope into the valley, where at the foot of the slope the redox potential decreased and turbidity increased massively. The oceanography group had recorded a methane and turbidity plume in this area, which had shifted eastwards within the next two days. Thus we concluded that the turbidity plumes were a result of sediment avalanches rather than venting. Such turbid areas detected by the oceanography surveys were crossed during several OFOS and TV-MUC dives (PS81/630, PS81/649, and PS81/650). Interestingly, the bottom of the ridge valley is covered by a thick layer of flocculent sediment, in which redox and pH are reduced. Dive 647 was on a sediment mound where the heat-flow team (Chapter 4) found a high heat flux. Here a reduced redox (Fig. 7.2.1) and 10-20 μM H_2S was detected. Turbidity and temperature were increased. These signals are most likely of hydrothermal origin. No distinct vents were observed, thus the fluid transport may be diffuse. The site showed numerous black sediment patches, and a specific faunal composition with numerous worm tubes and siphons.

Data management

The signals of the sensors were calibrated and T was converted to potential T. Of each dive, the measured parameters are integrated with the images and Posidonia positions (see example in Appendix A.5.7.1 and 2). The archived data will be further quality controlled and archived in the PANGAEA Data Publisher for Earth & Environmental Science along with the dive tracks and station data.

Tab. 7.2.1: OFOS-Observations (for positions and date see station list Appendix A.4; for maps see Appendix A.5.7.1 and 2)

OFOS dive	Remarks
615	Up south- flank canyon (13°E); anomalies in pH, ORP, N ₂ O, T at foot of the hill. Seafloor was mostly sedimented.
627	Up south- flank canyon (13°E); sulfide at top of hill. Seafloor was sedimented in the valley and rocky at the upper flank.
630	Followed south ridge then down slope (13°E), in valley high turbidity, low redox. Massive turbidity. Seafloor was rocky at the flank and sedimented in the valley.
633	Uphill terraces on the northern slope (13°E), no clear anomalies. Seafloor was rocky at the northern flank and sedimented in the valley.
637	Zig-zag uphill the southern flank (13°E), no clear anomalies. Seafloor was sedimented in the valley and rocky on the flanks.
647	Track across mound with high heat flow (14°E), clear anomalies in redox and sulfide. Seafloor was sedimented.
650	Same mound as 647 but now zig-zag (14°E), clear anomalies in redox and sulfide. Sensor pack crashed in bottom, after that only sulfide. Seafloor was sedimented.
666	Crater area (13°E), No anomalies, Seafloor was sedimented.
670	Rift flank area (14°E). Bare rock with diverse fauna. On one location a clear temperature increase of 0.1C was registered by 3 independent sensors. No anomalies in other parameters.
671	Rift flank area (14°E) Track crossed the previous at the anomaly. Now no anomalies were registered. The pH and redox sensors were not working.
680	Track north of the Ridge (16°E), no sensors deployed

References

- de Beer, D, Haeckel, M, Neumann, J, Wegener, G, Inagaki, F, Boetius, A, (2013) Saturated CO₂ inhibits microbial processes in CO₂-vented deep-sea sediments. *Biogeochem.*, accepted.
- Edmonds, H N, (2010) Chemical signatures from hydrothermal venting on slow spreading ridges, in: Rona, P.A., Devey, C.W., Dymont, J., Murton, B.J. (Eds.), *Diversity of Hydrothermal Systems on Slow Spreading Ocean Ridges*. AGU, Washington DC, 27-42.
- Kühl, M, Revsbech, N P, (2000) Biogeochemical microsensors for boundary layer studies., in: Boudreau, B., Jørgensen, B.B. (Eds.), *The benthic boundary layer*. Oxford University Press, 180-210.

7.3 Biological observations

Sergei Galkin¹, Antje Boetius²

¹IORAS

²AWI

Objectives

The benthic fauna of the SWIR is so far poorly explored due to geographically remoteness and bad weather for most of the year. The main objective of this work was to investigate biodiversity and abundance of megafauna and to test whether the SWIR actually represent the connection link between Atlantic and Indian Ocean vents or, together with ESR, it would belong to a distinct Southern Ocean province of vent biogeography (Van Dover *et al.*, 2002). Although vent ecosystems were the main objectives of the cruise, the composition of non-vent bottom communities in this region is of undoubted interest. Generally, the biogeographical status of SWIR at a global scale remains rather uncertain till now. Most traditional schemes attribute this region to the Antarctic deep-sea province, because of the flow of Antarctic bottom water into and along the Ridge system, but it has been concluded previously that it is less endemic than that of the Atlantic and Pacific (Vinogradova *et al.*, 1953; Watling *et al.*, 2013). We combined OFOS observations, with TV-Multicorer, Agassiz trawl and TV-grab samples to fill this gap and to contribute to a better understanding of the identity, migration and dispersal patterns of deep-sea fauna.

Work at sea

Data on megafauna were retrieved from all OFOS stations (11 deployments). During each dive ongoing biological observations were carried out, most significant features and objects were recorded, dominating animals were counted in order to get first qualitative results. Photographs were taken automatically every 20 seconds to conduct photographic transects, additional photos were made to document further observations. For fauna sampling Agassiz trawl was used (4 deployments, 1 failing). Because of bad weather trawl catches were insufficient to estimate total faunal richness and community structure, however they will support taxonomic identification of animals. Additional material was recovered from the colonization of the OBS platforms, which were recovered after a year of deployment (44 samples from 5 stations), as well as from the TV-MUC (1 sample) and TV-Grab (2 samples). Fauna samples were preserved in 96 % ethanol or 4 % formaldehyde for taxonomic identifications. Samples for molecular phylogeny, transmission electron microscopy, and chemical analyses were also taken (see list of samples in the attachment).

Preliminary results

Based on OFOS observations, we can deduce some apparently substrate and depth-controlled changes in bottom fauna. The benthic community in those areas deeper than 3,000 m presented a typical upper abyssal soft-bottom biocoenosis, characterized by the predominance of echinoderms, primarily holothurians. This group displayed high diversity at SWIR. At least 9 species of sea cucumbers have been recorded by OFOS observations and trawl samples. It is worth to note that the same big animals were abundant and caught by trawl (e.g. Molpadid holothurians *Molpadia* sp.), but they were not observed by OFOS because their burrowing mode of life. The most conspicuous animals were two species of the families Psychropotidae (*Psychropotes longicaudata*) and Synallactidae (Fig. 7.3.1A). Their traces together

with traces of sea urchins were remarkable features of the bottom landscape. Sea urchins (Echinoidea, Regularia) were rather numerous as well as Ophiuroidea (at least 3 species), whose precise abundance is likely to be underestimated because of their small size and burrowing behavior. The most common taxa in the deeper part of the observed area were actinarians (several species), starfishes *Hyphalaster* sp. (Fam. Porcellanasteridae) (Fig. 7.3.1C), Cucumariid holothurians (*Abyssocucumis* sp.; Fig. 7.3.1G). But also a large type of Enteropneust was regularly observed on the sediments, including its conspicuous spiral feces. Swimming sea cucumbers *Enipniastes eximia* (Fam. Pelagothuriidae) were regularly observed, as well as a large diversity of deep-sea jelly, and three types of octopus. Hard substrate fauna (Hexactinellid sponges, Actinaria, Gorgonaria (aff. *Lepedisis*), Pennatularia) also played a significant role on the rocky slopes and outcrops of the ridge system. However, except from a few sites, the hard substrate fauna was in total not as abundant as the soft bottom fauna, which partially also invaded the rocky flanks (some of the holothurians and seaurchins). Because of the obvious deficit of hard substrate within the sedimented plains of the ridge valley, small stones expelled by volcanism and debris-flow were intensively exploited by sessile suspension feeders including sea anemones, crinoids, corals and polychaetes. In respect of trophic specialization, the most dominating animals of SWIR are collecting deposit feeders. Besides, carnivorous filter feeders (sea anemones, sea feathers, brisingid starfishes) were well presented. The trophic structure of the benthic community corresponds to relatively productive surface waters, high particle accumulation rates especially around the flanks of the ridges, and weak near-bottom hydrodynamics. The described community was representative of all investigated basins (13-16°E), but showed some local variations, and small scale aggregations (especially Stations 615, 627, 630, 633, 637, 647, 650).

The community observed during the dive at St. 666 (depth range 2,550-2,860 m) was associated with soft, light beige sediment. The degree of bioturbation seemed somewhat higher as compared with deeper sites. The community was partially overlapping with the deep-water stations, but had its own characteristics. The predominance of large holothurians Psychropotidae and Synallactidae was not so pronounced. Most numerous holothurians in observed area were small *Peniagone crozeti*, and whitish-transparent *Oneirophanta mutabilis*. Dominating holothurians showed coherent behavior: all of them were identically oriented. Aside from sea cucumbers, sessile Cnidaria (Actinaria and Ceriantharia) and sea urchins were abundant members of the community. Sea anemones were rather diverse: at least 5 species have been recorded. Unlike at deeper stations, among the sea urchins Echinoidea Irregularia (fam. Pourtalesiidae) were most abundant. Worth sharing was the relative high abundance of Enteropneusta (Fig. 7.3.1B): 17 living individuals have been recorded exposed at the surface during the dive. Four species of starfishes (incl. Pterasteridae, Porcellanasteridae and Brisingidae) were occasionally observed. Sea feathers (at least 2 spp.), polychaetes, stalked crinoids and galatheid crabs occurred more rarely.

During the dives to more shallow sites at the rift flanks of the Narrowgate Mount (670 and 671), the community was dominated by regular sea urchins associated with soft sediment (other species than at deeper stations), and stalked crinoids attached to rocks. Actinaria, Octocorallia, Hexactinellid sponges and sea feathers were common. In the most shallow part of St.671 (1,100 - 1,300 m) lots of small sea feathers and sea anemones have been observed. Highly mobile red crabs were abundant. Hard substrate rocks were occupied by Octocorallia, soft corals (Antipatharia) and crinoids, as well as crustaceans, brittle stars and hydroids

7.2 Water column biogeochemistry

associated with these. At the depth range of 900 - 1,050 m an extensive field of brownish hydrothermal rocks covered with Brachiopod shells (Fig. 7.3.2) were observed and identified as a potentially "extinct vent", giving evidence of recent hydrothermal activity in the region. Similar cemeteries of dead shells marking recently extinguished vents were frequently observed in many hydrothermal sites worldwide.

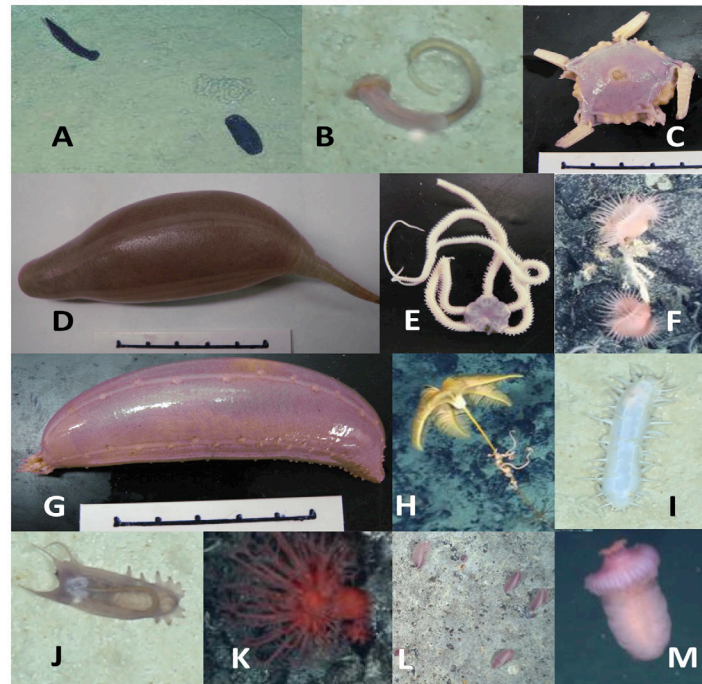


Fig. 7.3.1: Common representatives of the SWIR. A, holothurians *Psychropotes longicauda* (left) and *Synallactidae* (right); B, *Enteropneusta*; C, starfish *Hyphalaster* sp.; D, burrowing holothurian *Molpadia* sp.; E, *Ophiuroidea* (brittle star); F, *Actiniaria* (sea anemones); G, holothurian *Abyssocucumis* sp.; H, *Crinoidea* with symbiont (*Ophiuroidea*) on its stalk; I, holothurian *Oneirophanta mutabilis*; J, holothurian *Peniagone crozetj*; K, *Alcyonaria* (soft coral); L, *Pennatularia* (sea feathers) on the periphery of extinct vent, M., *Enipniastes eximia* (swimming holothurian).



Fig. 7.3.2: *Brachiopoda* field: 52°04.830', 014°38.275'; 1020.8m

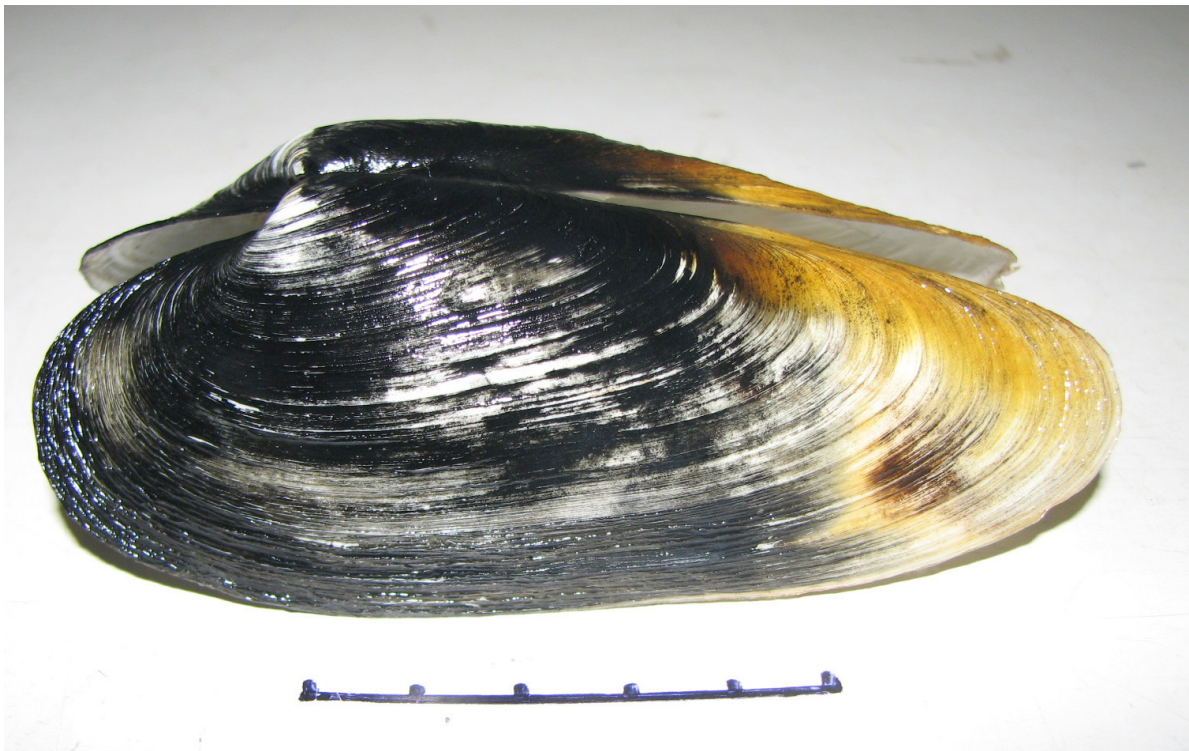


Fig. 7.3.3: *Bivalvia*: fam. *Vesicomiidae*: *Christineconcha* sp.. The line indicates 10 cm

7.2 Water column biogeochemistry

Additional biological samples were obtained from OBS, TV-MUC and TV-Grab. The most remarkable finding was bivalve of the Fam. Vesicomidae *Cristineconcha* sp. from OBS 5 (Fig. 7.3.3). This monotypic genus was previously described from the seeps of Eastern Atlantic (pockmarks Regab and Astrid) and from the Bay of Biscay. This finding along with that of a few thin tubeworms, which resembled pogonophorans, represents direct evidence of existing of reducing habitats and symbiotic macrofauna in the investigated region. Taking into consideration geographical range of the bivalve genus we can suppose an influence of Atlantic seep fauna on chemosynthetic environments in the investigated SWIR region. Other interesting finding was a sea leech (Hirudinea: *Moorebdellina* sp.) at 4 stations. This is the only free-living genus of morabdellin leeches (other genes usually inhabit sharks and ray-fishes).

We thank cordially all specialists from the Laboratory of Ocean Bottom Fauna (IORAS) for the on-the-fly identification of animals and needful consultations, and the OFOS support team for the excellent work at sea.

Data management

Specimens for morphological and phylogenetic analyses will be sent to the corresponding taxonomic experts, in collaboration with the Shirshov Institute and Senckenberg Research Institute and Museum. For molecular analyses, we use multi locus sequencing in the home laboratory for examining the taxonomy and phylogeny of vent biota and their symbiotic microorganisms. All biogeochemical data will be quality checked, stored and made available through PANGAEA Data Publisher for Earth & Environmental Science. Biological data will be submitted to the OBIS database. Tracks of video and photography surveys will be stored in PANGAEA; the photographic material will be made available to taxonomists and further image analysis via BIIGLE. Microbiological sequence data will be archived in GenBank.

References

- Van Dover, C.L., German, C.R., Speer, K.G., Parson, L.M., Vrijenhoek, R.C., 2002. Evolution and biogeography of deep-sea vent and seep invertebrates, *Science*, 295, 1253–1257.
- Vinogradova, N.G., 1953. The zoogeographical distribution of the deep-water bottom fauna in the abyssal zone of the ocean, *Deep Sea Res.*, 5(2-4), 205-206.
- Watling L., Guinotte J., Clark M., Smith C. A proposed biogeography of deep ocean floor. *Progress in Oceanography*, 2013 www.elsevier.com/locate/pocean

7.4 Biogeochemical and microbiological sampling

Massiliano Molari¹, Rafael Stiens¹, Wiebke Stiens¹, Antje Boetius^{1,2}

¹MPI
²AWI

Objectives

The major objectives of the biogeochemical and microbiological work were to compare benthic bacterial diversity and functions (e.g. biomass, dark CO₂ fixation, enzymatic hydrolysis, remineralization rates) in different areas of the SWIR system and in the adjacent abyssal plains north and south of the ridge. Furthermore, we

aimed at obtaining samples from the water column and sediments, to compare bacterial communities and their functions to those of other global deep-sea areas, to better understand the microbial biogeography of the SWIR region. Thirdly, we wanted to assess whether hydrothermal venting would provide energy resources in form of inorganic reduced compounds (i.e. H_2S , CH_4 , H_2 , Fe^{2+} , Mn^{3+}), potentially supporting dense and diverse populations of microorganisms (Orcutt *et al.*, 2011). The principal sampling strategy was to investigate the diversity and the activities of bacterial and archaeal communities inside and outside of potential vent plumes, as well as in the sediments of the ridge valleys and flanks. In addition, two reference areas outside the valley (north and south to the investigated ridge) were sampled in order to compare prokaryotic diversity and activity in areas not directly affected by vent emissions.

Work at sea

Sediment samples for microbiological and biogeochemical analyses were retrieved at all CTD (Tab. 7.4.1), TV-Multicorer (Tab. 7.4.2) and gravity core stations (Tab. 7.4.3). Water from the CTD casts was sampled at different depths. The samples for dark CO_2 fixation (DCF) and DNA were sampled in triplicate with syringes (50 ml) and plastic bottles (1.5 L), respectively. For oxygen the water was sampled with Winkler glass bottles and measured immediately after sampling. Multicorer cores were subsampled in three depth layers (0-1 cm, 1 - 5 cm, 5-10 cm) and further processed in the refrigerated container at 0°C. The porewater was sampled from whole cores (every 1 cm from the top to the bottom) by using Rhizons (19.21.21F, mean pore size 0.15 μm ; Rhizosphere Research Products, Wageningen, Netherlands). Sediment samples were fixed for several microbiological and geochemical analyses that will be conducted in the home laboratory. Measurements of extracellular enzyme activities (EEA) and dark CO_2 fixation (DCF) were conducted directly on board. In addition the DCF was measured after the injection of different reduced compounds (e-donor experiments). All substrate or tracer incubations were carried out in the dark and under *in-situ* temperature. Methods to be carried out in the further analysis of samples include: DOC: dissolved organic carbon; POC: particulate organic carbon; DCF: dark CO_2 fixation; Chl-a: chlorophyll a; EEA: extracellular enzymatic activity; AODC: acridine orange direct counts; TOC: total organic carbon; FISH: fluorescence *in-situ* hybridization.

Tab. 7.4.1: Biogeochemical and microbiological water sampling (CTD rosette, for further informations see chapter 6).

Station n.	Investigations
PS81/605-1	Oxygen concentrations, DNA for prokaryotic diversity, DCF
PS81/614-1	Oxygen concentrations, DOC, DNA for prokaryotic diversity, DCF
PS81/628-1	Oxygen concentrations, DNA for prokaryotic diversity, DCF
PS81/629-1	Oxygen and sulfide concentrations, DOC, DNA for prokaryotic diversity, DCF
PS81/631-1	Oxygen and sulfide concentrations, DOC, DNA for prokaryotic diversity, DCF
PS81/638-1	Oxygen and sulfide concentrations
PS81/642-1	Oxygen and sulfide concentrations, DOC

7.4 Biogeochemical and microbiological sampling

Station n.	Investigations
PS81/645-1	Oxygen and sulfide concentrations, DOC, DNA for prokaryotic diversity, DCF, methane, POC
PS81/648-1	Oxygen and sulfide concentrations
PS81/651-1	DNA based prokaryotic diversity, DCF, POC
PS81/660-1	Oxygen concentrations
PS81/663-1	DNA for prokaryotic diversity, DCF

Tab. 7.4.2: Biogeochemical and microbiological TV MUC sampling

Station n.	Observations	Investigations
PS81/606-1	Fluffy material, diatom ooze	DNA/RNA based prokaryotic diversity, phospholipids, porosity, TOC, Chal-a, EEA, DCF, Porewater, AODC, FISH
PS81/626-1	Beige sediments, compact diatom ooze	DNA/RNA based prokaryotic diversity, phospholipids, porosity, TOC, Chal-a, EEA, DCF, Porewater, AODC, FISH
PS81/636-1	Fluffy material, diatom ooze	DNA/RNA based prokaryotic diversity, phospholipids, porosity, TOC, Chal-a, EEA, DCF, Porewater, AODC, FISH
PS81/639-1	Fluffy material, diatom ooze	DNA/RNA based prokaryotic diversity, phospholipids, porosity, TOC, Chal-a, EEA, DCF, Porewater, AODC, FISH
PS81/646-1	Fluffy material, diatom ooze with thick black layer under the surface, overlying beige sediments	DNA/RNA based prokaryotic diversity, phospholipids, porosity, TOC, Chal-a, EEA, DCF, Porewater, AODC, FISH
PS81/649-1	Fluffy material, diatom ooze	DNA/RNA based prokaryotic diversity, phospholipids, porosity, TOC, Chal-a, EEA, DCF, Porewater, AODC, FISH
PS81/659-1	Fluffy material, diatom ooze with thick black layer under the surface, overlying beige sediments	DNA/RNA based prokaryotic diversity, phospholipids, porosity, TOC, Chal-a, EEA, DCF, Porewater, AODC, FISH
PS81/661-1	Fluffy material, diatom ooze	DNA/RNA based prokaryotic diversity, phospholipids, porosity, TOC, Chal-a, EEA, DCF, Porewater, AODC, FISH
PS81/681-1	Beige, pelagic sediments, compact diatom ooze	DNA/RNA based prokaryotic diversity, phospholipids, porosity, TOC, Chal-a, EEA, DCF, Porewater, AODC, FISH

Tab.7.4.3: Biogeochemical and Microbiological gravity core sampling

Station n.	Site description	Investigations
PS81/652	Whitish-greenish sediments, diatom ooze	Methane, AODC, DNA, DCF, e-donor experiments, alive samples, Chl-a
PS81/653	Whitish-greenish sediments, diatom ooze	Methane, AODC, DNA, alive samples, Chl-a
PS81/656	Whitish-greenish sediments, diatom ooze	Methane, AODC, DNA, alive samples, Chl-a
PS81/657	Whitish-greenish sediments, diatom ooze, with black layers and strong smell of sulphur	Methane, AODC, DNA, DCF, e-donor experiments, alive samples, Chl-a

Preliminary results

In almost all water and sediment samples microbial inorganic carbon fixation was measured. The DCF ranged from 0 to 5.8 $\mu\text{mol C m}^{-3} \text{d}^{-1}$ in the water, with lower value in intermediate depths (2,500 m) and higher in deeper waters and close to the bottom. These incorporation rates are higher than those reported for other water masses at the same depths (Reinthal *et al.*, 2010). Furthermore, the injection of methane at concentrations similar to those measured in plumes (see chapter 6) showed an increase of DCF in deep picoplankton, suggesting the presence of active methanotrophic populations. However, no clear spatial or depth-related gradient in inorganic carbon fixation was observed. In the sediments the DCF ranged from 0.21 to 2.5 $\text{ng C ml}^{-1} \text{h}^{-1}$ at the surface, and decreased to not detectable values in the deeper layers. We did not observe significant differences between the stations situated in the valley to those located outside of the ridge system. Furthermore, our preliminary data are comparable with those reported for detritus-fuelled deep sediments not affected by vent emissions (Molari *et al.*, 2013). In contrast to water samples, the experiments with the injection of different reduced compounds (thiosulfate, sulfide, methane, hydrogen, ferrous iron and ammonia) into sediments, did not confirm a presence of active chemosynthetic communities. According with DCF results, also the enzymatic activities in the sediments did not show any trend with spatial location within the ridge system, nor a significant difference between the valley and reference stations.

Although these on board preliminary results have to be confirmed by further analysis of porewater gradients, microbial community density and composition, they suggest that in the area investigated there are some diffuse fluid transport events causing methane elevation and responsive pelagic communities, but these apparently did not affect the microbial communities of the sedimented ridge valleys.

Data management

The station list and all metadata from sampling and observations will be stored in the WDC MARE data base PANGAEA Data Publisher for Earth & Environmental Science (<http://www.pangaea.de>). This includes also biogeochemical and some microbiological data which are already defined in PANGAEA. Molecular data will be deposited in globally accessible databases such as GenBank. Reference microbiological and sedimentological samples will be stored deep frozen or fixed at the MPI in Bremen.

References

- Molari M, Manini E, Dell'Anno A (2013) Dark inorganic carbon fixation sustains the functioning of benthic deep-sea ecosystems. *Global Biogeochemical Cycles*, pp 212-221, doi:10.1002/gbc.20030.
- Orcutt B, Sylvan JB, Knab NJ and Edwards K (2011) Microbial Ecology of the Dark Ocean: above, at, and below the Seafloor. *Microbiol. Mol. Biol. Rev.* 2011, 75(2):361. doi: J.10.1128/MMBR.00039-10.
- Reinthalder T, van Aken HM, Herndl GJ (2010) Major contribution of autotrophy to microbial carbon cycling in the deep North Atlantic's interior. *Deep-Sea Research Part II*, 57(16), 1572–1580.

7.5 Biological experiments

Amandine Nunes, Christian Borowski, MPI
Nicole Dubilier (not on board)

Objectives

The Symbiosis group at the Max Planck Institute for Microbiology (MPI-MM) in Bremen is investigating the diversity and biogeography of bacteria-animal symbioses in chemosynthetic habitats and sunken wood on the deep-sea floor. For this purpose we deploy colonization substrates to the deep-sea floor. During RV *Polarstern* cruise ANT-XXIX/2 in December 2012 ten colonization experiments attached to Ocean Bottom Seismometers (OBS) were deployed on the Southwest Indian Ridge (SWIR) between 52°1.14'S – 52°17.7'S and 12°50.07'E – 13°45.82'E. Our aim in cruise ANT-XXIX/8 was to recover the experiments after one year on the seafloor and process the colonization substrates for molecular analyses in the home laboratory at MPI-MM. The colonizers consisted of two compartments. One compartment was holding microscopic glass slides serving as substrates for free-living bacteria from bottom-near water. We regularly deploy such slides next to chemosynthetic environments in the deep sea to analyze bacterial films for free-living close relatives of chemosynthetic symbionts. The other compartment was holding a wood block designed to attract wood-colonizing invertebrates (Fig. 7.5.1). Our particular interest was to attract wood-boring bivalves (family: Pholadidae, sub-family: Xylophaginae), which occur worldwide in the deep sea and degrade sunken wood with the help of their cellulolytic symbionts. We planned to analyze the biogeography of the hosts and the diversity and biogeography of the symbionts.

Work at sea

Nine of the ten OBS were retrieved (OBS2–10, see section 3), and the attached nine colonization experiments were processed immediately upon recovery. Some of the glass slides were missing but the recovered glass slides were removed carefully from the colonizers and preserved for DNA analyses and Fluorescence In Situ Hybridizations (FISH). Wood blocks were removed from the colonizers, carefully examined for attached fauna and then opened with hammer and chisel to extract organisms sitting inside. Small pieces of uncolonized wood were preserved separately for the analysis of microbial DNA. For a detailed list of samples, see table Appendix A.5.7.5.

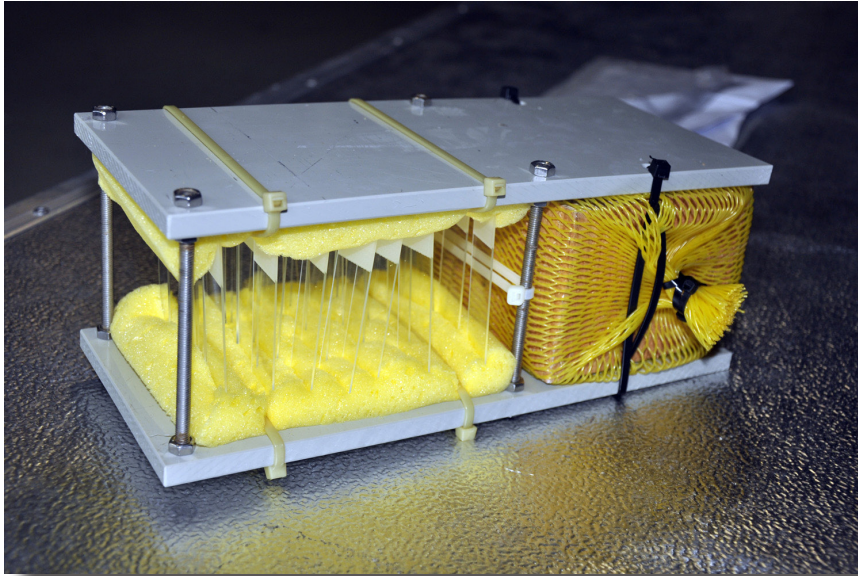


Fig. 7.5.1: Colonization device before deployment holding glass slides (around 30 units) on the left and a 10x10x10 cm wood block wrapped in a plastic net bag on the right side.

Preliminary results

The molecular analyses of the microscopic slides will be conducted at the home laboratory (MPI-MM, Bremen) and will provide us with first insights on diversity and relative abundances of the free-living microbial diversity at the SWIR.

Visual examination of the wood block surfaces revealed that there was no fauna and no traces of wood degradation by invertebrate fauna or microbes (Fig. 7.5.2.a). The opened blocks confirmed that none of them was colonized by wood-associated fauna (Fig. 7.2.5.b). This noticeable lack of wood degradation is in accordance with observations on wood that was deposited for one year on the continental shelf of the West Antarctic Peninsula (Glover *et al.*, 2003). These woods were also recovered in an intact condition without any sign of degradation. Our colonization experiment showed the same absence of degradation in a more central region of the Southern Ocean.

Generally, wood-boring bivalves are opportunistic species with high reproductive and dispersal rates, which can rapidly colonize wood in any kind of deep-sea environment (Turner, 1973; Turner, 2002; Voight, 2007). Therefore their absence in this region is intriguing. This could be linked to the absence of naturally occurring wood in this area of the world. As these organisms must use wood as food and shelter, they probably do not disperse in an area that does not usually harbour such resources. Their absence in the Antarctic region could also be due to the Antarctic Circumpolar Current (ACC) and its deep-sea representatives: the Polar Front and the Sub-Antarctic Front (Barker & Thomas, 2004). These powerful currents could prevent the intrusion of wood-boring bivalve larvae in this region of the world. However, observations of the distribution of other types of fauna north and south of the SWIR do not support the hypothesis of such a dispersal barrier (see section 7.4).

7.5 Biological experiments

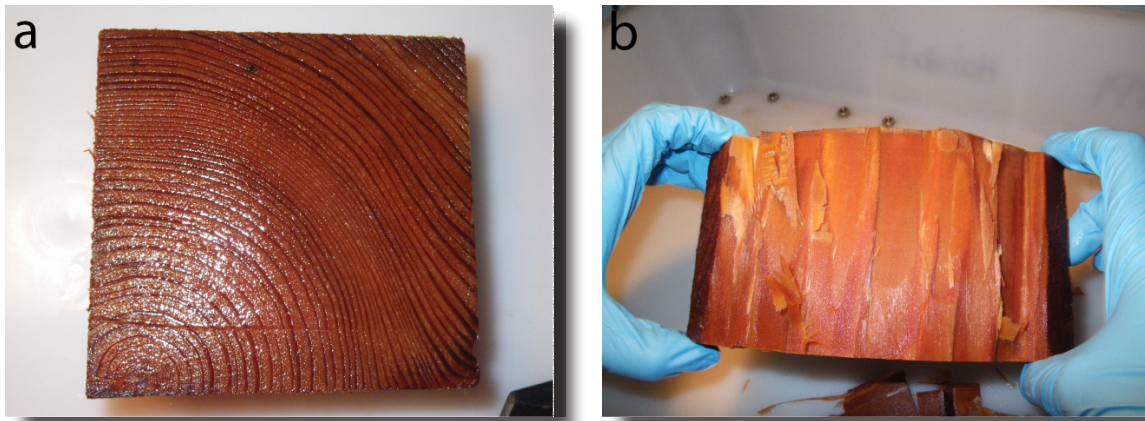


Fig. 7.5.2: Wood block from colonization device attached to OBS 10 after one year of deployment. a: external view of wood showing its intact state, b: internal view of wood showing no trace of colonization by wood-associated fauna.

Data management

Samples will be stored in the Max Planck Institute of Marine Microbiology in Bremen until further analysis (MPI, Bremen). All molecular data will be stored in international data bases (GenBank).

References

- Barker PF, Thomas E (2004) Origin , signature and palaeoclimatic influence of the Antarctic Circumpolar Current. *Earth-Science Reviews*, 66, 143-162.
- Glover AG, Wiklund H, Taboada S, Avila C, Cristobo J, Smith CR, Kemp KM, Jamieson AJ, Dahlgren TG (2013) Bone-eating worms from the Antarctic: the contrasting fate of whale and wood remains on the Southern Ocean seafloor Bone-eating worms from the Antarctic : the contrasting fate of whale and wood remains on the Southern Ocean seafloor. *Proceedings of the royal society B*, 280, doi: 2013.1390.
- Turner R (1973) Wood-Boring Bivalves , Opportunistic Species in the Deep Sea. *Science*, 180, 1377-1379.
- Turner R (2002) On the subfamily xylophagainae (Family Pholadidae, Bivalvia, Mollusca). *Bulletin Museum of Comparative zoology*, 157(4), 223-307.
- Voight JR (2007) Experimental deep-sea deployments reveal diverse northeast Pacific wood-boring bivalves of Xylophagainae (Myoida: Pholadidae). *Journal of Moluscan studies*, 73, 377-391.

8. HYDROACOUSTICS

8.1 Bathymetry

Jan Erik Arndt, Ines Egelkraut, Karolin Gersberg

AWI

Objectives

In most areas of the world ocean, knowledge about the seafloor topography is sparse. However, detailed knowledge of the bathymetry is essential to identify appropriate locations for spot observations and to relate these to its surrounding environment. For the survey area of the Southwest Indian Ridge between 12°E and 16°E swath bathymetry data sets were available from multiple cruises of RV *Knorr* and RV *Melville*. These were acquired more than 10 years ago in the time period 1996-2003. This data, however, shows some gaps, artefacts and inaccuracies in the survey area that could lead to inadequate decisions about sampling locations or track planning. Up to date surveyed bathymetry with *Polarstern's* fix-mounted *ATLAS Hydrosweep DS3*, therefore, supports the scientific work on board. In addition, the areas south and north of the ridge area, as well as the transit area from and to Cape Town, are so far nearly unmapped. In addition to bathymetry, water column data are acquired to examine the water body of the surveyed area.

Work at sea

Bathymetric surveying took place during the entire cruise. The settings of the *ATLAS Hydrosweep DS3* multibeam echosounding system were set using *ATLAS Hydromap Control*. The multibeam data were processed using the *Hypack* program suite. For beam and depth correction, up to date sound velocity profiles, calculated from CTD stations or directly measured with a *Valeport* velocity profiler, have been applied to the multibeam data. Data processing then was performed in *CARIS Hips and Sips*. Afterwards the data was gridded with the *Generic Mapping Tools* and imported to *ArcGIS* projects.

Preliminary (expected) results

In the survey area, the surrounding bathymetry of all scientific sampling sites has been surveyed. The in-between transit surveys led to a complete coverage of the central rift valley (Fig. 8.1). At times of rough sea, impeding other scientific operations, bathymetric surveys have been undertaken in the adjacent areas, including an escape to calmer weather conditions to the south at about 55° S.

8.1 Bathymetry

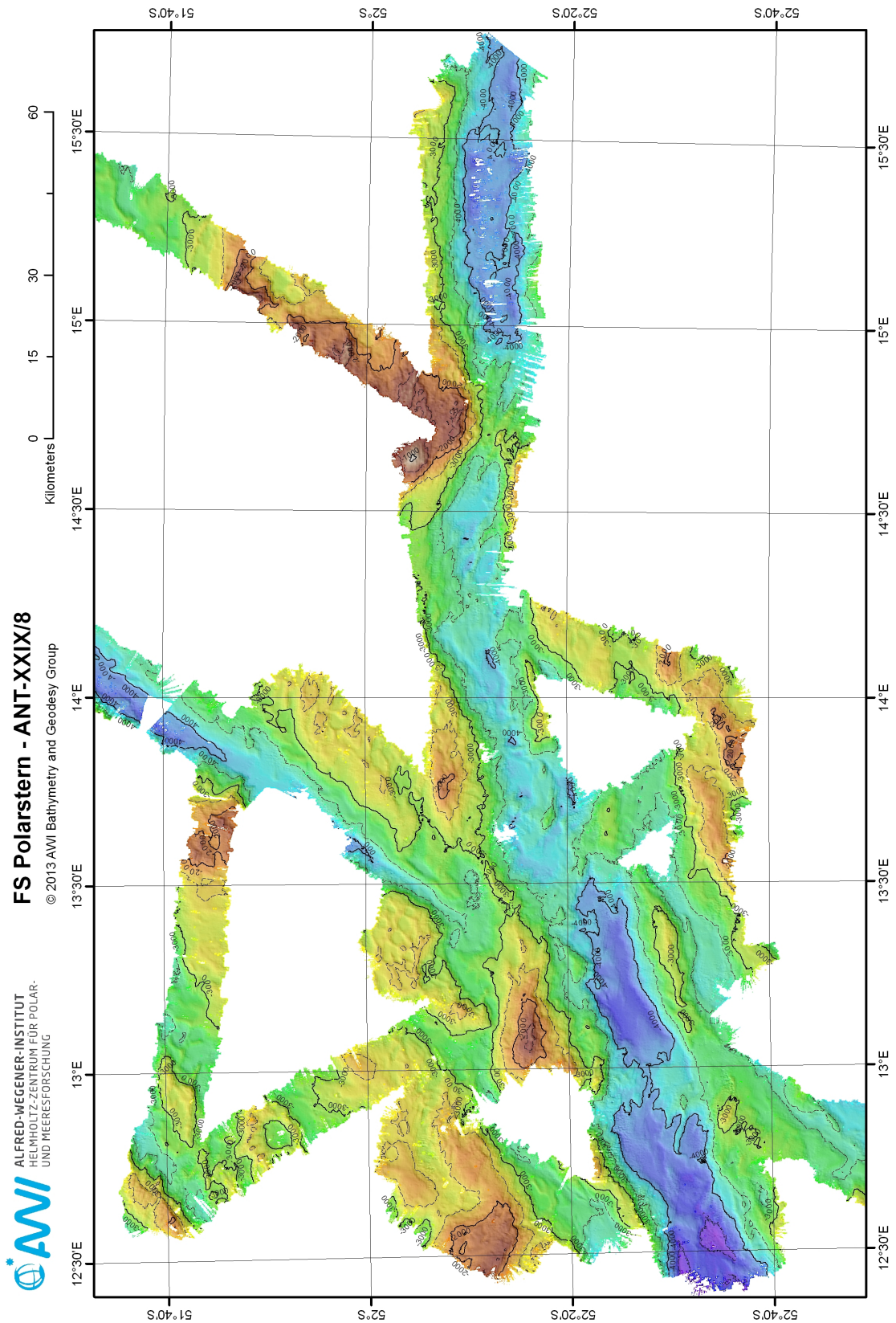


Fig. 8.1: Bathymetric overview map of the survey area at the South-West Indian Ridge

On transit from back a so far unknown elevation has been discovered (Fig. 8.2). The IHO/IOC Bathymetric Publication No. 6 on the 'Standardization of Undersea Feature Names' defines a seamount as a large isolated elevation greater than 1,000 m in relief above the seafloor. The discovered elevation is located in the Agulhas Basin and rises from about 5,400 m depth to about 3,460 m depth, resulting in an relative height of about 1,940 m. Thus, it fulfils the definition of a seamount. We will propose to name the seamount "Madiba Seamount" to honour the life of Nelson 'Madiba' Mandela, former president of South Africa, who passed away during this expedition.

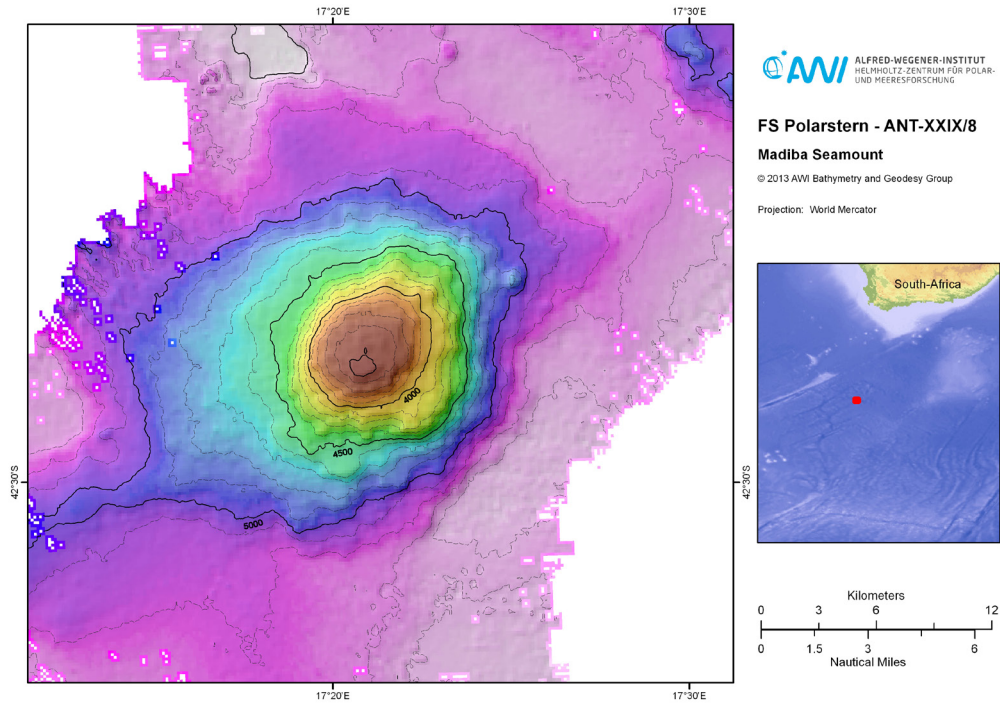


Fig. 8.2: Discovered Seamount in the Agulhas Basin (proposed name "Madiba Seamount")

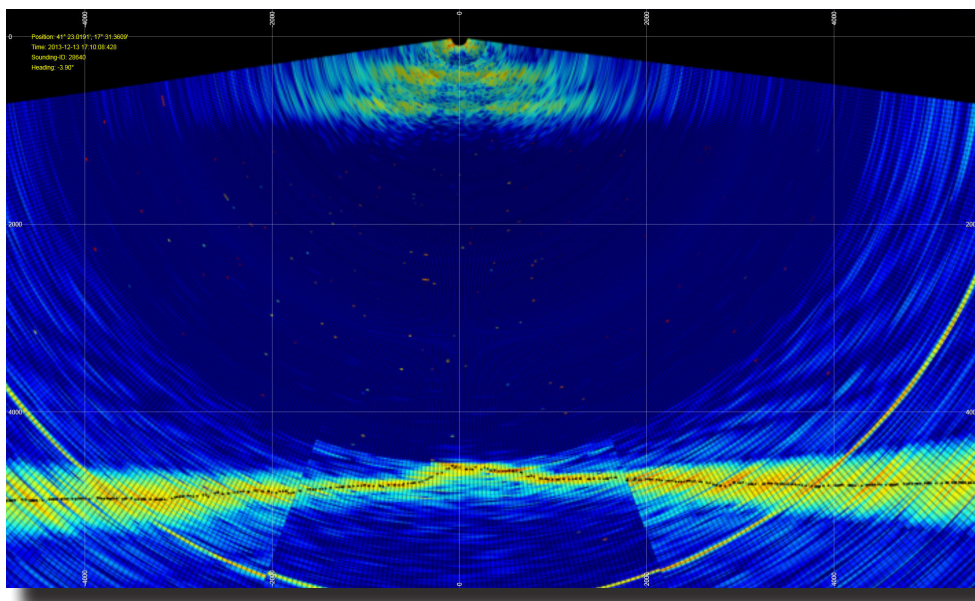


Fig. 8.3: Snapshot of the water column data

Water column data have been acquired in the survey area. On-the-fly observation of these data did not show irregular patterns that could indicate any kind of water disturbance. However, these data clearly shows the water layers in the upper 1,000 m of the water column (Fig. 8.3).

Data management

All acquired bathymetric data will be stored in the PANGAEA Data Publisher for Earth & Environmental Science.

8.2 Parasound

Sebastian Albrecht

FIELAX

Objectives

The *Atlas Parasound P-70* is a hull-mounted sub-bottom profiling echo sounder on board *Polarstern*. It is used to detect the internal structures of sedimentary cover along the ship's track. To penetrate the sedimentary layers at the sea floor, a low frequency signal is required. Since a combination of a reasonably small transducer and a very narrow beam is desired the system takes advantage of the parametric effect, which results from the non-linear hydro-acoustic behaviour of water for high energy signals. The transmission of 2 high energy wave-form signals of slightly different frequencies (18 kHz and 22 kHz) creates harmonics at the difference frequency (i. e. 4 kHz) and at the frequency sum (e. g. 40 kHz). With an opening angle of $4 \times 4.5^\circ$ the system provides high resolution information of the sedimentary layers down to a depth of 200 m below sea floor. The system automatically compensates ship's movements by applying roll, pitch and heave values from the motion platform *MINS*. Navigation data is added by a *Trimble* GPS receiver.

Main objective of the *Parasound* operations was the detection of seafloor characteristics and sediment structures along the cruise track which supports geological analyses of the surveyed ridge system. The success rate of stations with sediment penetrating instruments (e.g. gravity corer, heat flow probe) can be highly increased by previous *Parasound* surveys and analyses of the seabed.

For the water column work/plume-hunting another objective was to find out if the *Parasound* could help in finding anomalies in the water column. This has been already done successfully at methane gas seeps and gas flares in 1,200 m depth by carefully interpreting *Parasound's* high frequency channels. In case plumes are found by other instruments it is considered to check the sounding data for related echoes or acoustic anomalies. This would improve the future plume-hunts by being able to survey larger areas for those anomalies.

Work at sea

The *Parasound* was in operation 24 hours per day. The echo sounder's parameters were set to 18.8 kHz desired primary high frequency (PHF) and 4 kHz secondary low frequency (SLF). The acoustic pulse type was set to a frequency modulated chirp signal within 1 kHz range. The pulse length was adjusted between 0.5 to 1.0 ms. The system was configured to alternately ping with the multibeam echo sounder

Hydrosweep. This helps to reduce interferences but also results in a reduced along track resolution for both systems. Data of high and low frequency were recorded in the formats ASD, PS3 and SGY. For direct visual analyses both frequencies were displayed continuously in different scales. The received amplitude ranges have been regularly adjusted to optimize the data monitoring.

During station time and low-speed transects with towed instruments the ship's bow thruster highly disturbed the low frequency signal. Especially the low-speed transects were very interesting to receive a high-resolution image of the seabed. One solution therefore was the increase of the systems pulse length to values between 10 and 25 ms. This results in a decrease of the vertical resolution and 'blurring' of the signal but also in more interpretable data.

As for the plume-hunt, significant indications for hydro-acoustic anomalies due to plumes, active vents or gas flares were not found.

All data have been post-processed at sea. Data files have been organised to daily subsets and data of both frequencies have been plotted in 4 hour segments using the software *SeNT* (Se suite for Windows NT) and saved as PNG image files.

Preliminary results

The collected data cover two long transects from South Africa through the *Agulhas Basin* down to the main research area at the *South West Indian Ridge* and back. Inside the research area data was continuously logged as well.

A data example is shown in Fig. 8.2.1. The so called *Pillow Mound* has been crossed during CTD tow-yo transect PS81/0660-1 with an average speed of 1 knot. The mound consists of at least 150 m deep visible sediment layers which may have been accumulated due to the location in a water flow related lee of a mountain structure west of the mound with an approx. height of 800 m above the surrounding terrain. Perpendicular fractions indicate seismic activities in the area.

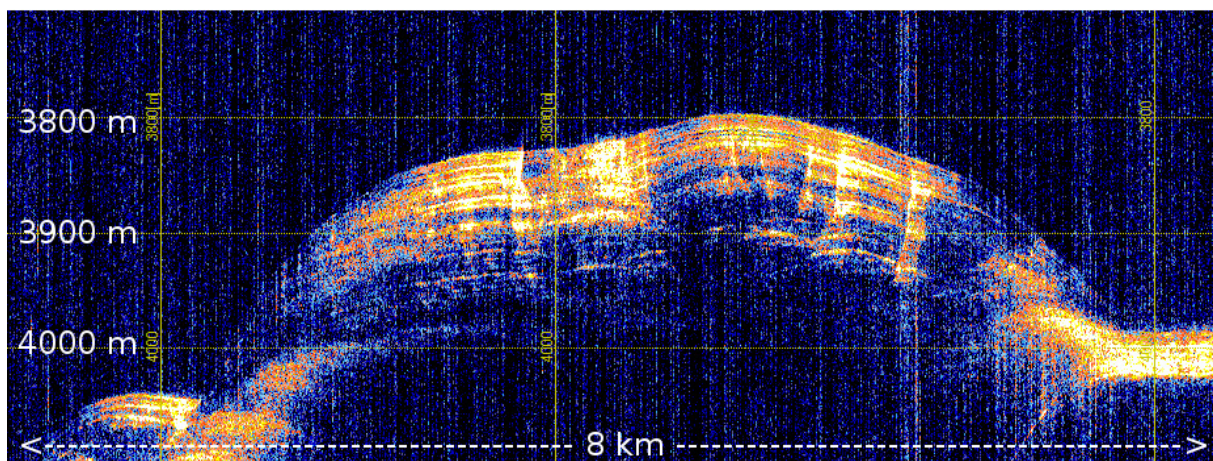


Fig. 8.4: Example of Parasound low frequency data recorded during a low-speed towing station above the Pillow Mound showing sediment layers down to 150 m below seafloor and perpendicular fractions.

Overall the *Parasound's* system performance was stable and reliable with no reportable problems. The data quality was perfect during ideal survey conditions.

8.3 Underwater positioning with Posidonia

Otherwise it was influenced by station work (bow thrusters), irregular topography in the ridge system with steep slopes and unfavourable vessel speeds.

Data management

The data will be transferred to the AWI Geology department and be made available in the PANGAEA Data Publisher for Earth & Environmental Science.

8.3 Underwater positioning with Posidonia

Sebastian Albrecht¹, Yann Marcon²

¹FIELAX

²MARUM

Objectives

The *IXSEA Posidonia* is an acoustic underwater positioning system used to determine and track positions of underwater vehicles and instruments. The system is composed of two ultra-short baselines (USBL) consisting of four hydrophones and one main transducer. A *Posidonia* transponder beacon has to be mounted on the instrument to be tracked before the launch. Once the gear is lowered into the water, the system's main transducer transmits an acoustic signal in shape of a 60° wide cone and a frequency of 10.5 kHz to the water. The transponder on the instrument receives this signal and replies with a 9.5 kHz acknowledge signal. This is being received by the four hydrophones of the vessel with small differences in travel time and phase from which a relative angle and distance to the transponder can be calculated. An absolute geographic transponder position and depth is then calculated by the system by applying the ship's current GPS position, the current motion state (roll, pitch and heading) and a sound velocity profile to compensate the refraction of the signal in the water column. The data are continuously acquired and distributed to the ship's network to data visualization and mapping programs.

A main objective of the cruise was the plume-hunting during which instruments like CTDs or video sleds are slowly towed by the ship. This results in an offset between the ship's and instrument's position of up to 2 km (at 4 km water depth). Also towed instruments react very slowly to course changes of the ship. In case plume signals or interesting spots are found in CTD or imagery data it would be mandatory to be able to relocate these positions for further sampling. Therefore every towed instrument has to be equipped with a *Posidonia* transponder beacon.

Work at sea

The following instruments were permanently equipped with transponders: CTD/Rosette water sampler, Ocean Floor Observation System (OFOS), TV-Multicorer (TV-Multicorer) and TV-Grabber. There are two hydrophone arrays and two different processing units available on board. During this cruise the mobile array has been used mounted in the moon pool of the ship and the IXBLUE USBL-BOX processing unit. The recurrence interval of the system has been set to 10 seconds. Acquired position data have been locally logged on a PC as raw NMEA telegram data. Positions of ship and transponder were displayed in real-time in the software PosiView (Ralf Krockner, AWI) and the mapping software GlobalMapper. GlobalMapper was used to display current positions and tracks from *Posidonia* with other geographical datasets such as bathymetry grid layers, station waypoints or points of interest

(Fig. 8.5). This highly contributed to the station work for keeping an overview of the instrument's track related to the local bathymetry and other features. Current bathymetry datasets were kindly provided by the Bathymetry group on board.

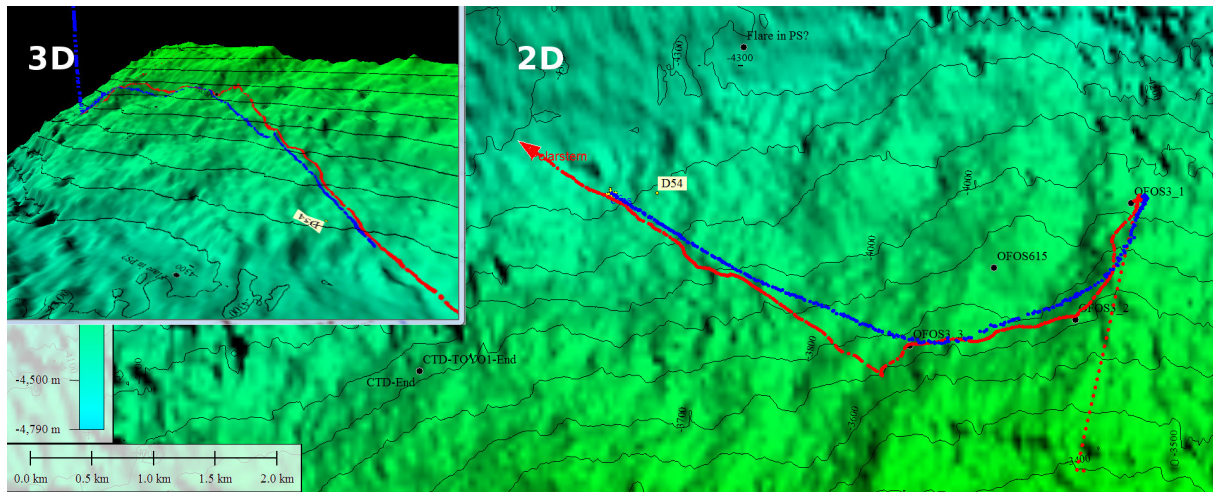


Fig. 8.5: A screenshot of the Global Mapper software during an OFOS transect showing the ship's track (red) and the OFOS' track (blue) above a bathymetry layer and waypoints / points of interest which is essential for track planning and adjustments during a station.

Data management

All position data have been post-processed on board by using a filtering and interpolation tool by Yann Marcon (MARUM). The program filters outliers by applying a speed filter. Afterwards data are interpolated to create a continuous dataset in 1 second intervals. The data can then be easily referenced by time to datasets such as photo imagery, MAPR and micro profiler data acquired during a station.

The station positions of the final cruise station list have been modified accordingly so that for tracked instruments the much more accurate USBL position has been inserted instead of the default (ship's) position.

The post-processed USBL navigation data for CTD-TOYO, OFOS, TV-MUC and TV-GRAB transects will be made available in the PANGAEA Data Publisher for Earth & Environmental Science.

APPENDIX

A.1 PARTICIPATING INSTITUTIONS

A.2 CRUISE PARTICIPANTS

A.3 SHIP'S CREW

A.4 STATION LIST

A.5 SCIENTIFIC APPENDIX

A.5.1 Sample lists

A.5.2 Summary of OFOS Dives

A.1 TEILNEHMENDE INSTITUTE / PARTICIPATING INSTITUTIONS

	Address
AWI	Alfred-Wegener-Institut Helmholtz-Zentrum für Polar- und Meeresforschung Postfach 120161 27515 Bremerhaven Germany
DWD	Deutscher Wetterdienst Geschäftsbereich Wettervorhersage Seeschiffahrtsberatung Bernhard Nocht Str. 76 20359 Hamburg Germany
FB5, Uni Bremen	Fachbereich 5 Geowissenschaften der Universität Bremen GEO Gebäude Klagenfurter Straße 28359 Bremen Germany
FIELAX	FIELAX Gesellschaft für wissenschaftliche Datenverarbeitung mbH Schleusenstr. 14 D-27568 Bremerhaven Germany
HGF MPG	HGF MPG Research Group on Deep Sea Ecology and Technology Alfred Wegener Institute Helmholtz Centre for Polar and Marine Research Am Handelshafen 12 27515 Bremerhaven Germany
iSiTEC	iSiTEC GmbH Bussestr. 27 27570 Bremerhaven Germany

	Address
MARUM	MARUM Center for Marine Environmental Research University Bremen Leobener Str. D-28359 Bremen Germany
MPI	Max-Planck-Institut für Marine Mikrobiologie Celsiusstr. 1 28359 Bremen Germany
UHB-IUP	Universität Bremen Institut für Umweltphysik/ Sektion Ozeanographie Otto Hahn Allee 1; Gebäude: NW1 28359 Bremen Germany
Shirshov Institute	P.P. Shirshov Institute of Oceanology Russian Academy of Sciences Nakhimovsky Pr., 36 Moscow 117997 Russia

A.2 FAHRTTEILNEHMER / CRUISE PARTICIPANTS

Name/ Last name	Vorname/ First name	Institut/ Institute	Beruf/ Profession
Albrecht	Sebastian	Fielax	Technician, data management, parasound
Arndt	Jan-Erik	AWI	Group leader, bathymetry
Bach	Wolfgang	MARUM/UHB-GEO	Group leader, rock/ plume water chemistry
Boetius	Antje	HGF MPG Group (AWI)	Group leader, deep-sea ecology
Coers	Susanne	AWI	Student, seismology
De Beer	Dirk	Microsensor Group MPI	Scientist, microsensors
Egelkraut	Ines	AWI	Student, bathymetry
Galkin	Sergey	Shirshov Institute	Scientist, zoology
Gersberg	Karolin	AWI	Student, bathymetry
Hannemann	Tim	UHB-IUP	Student, oceanography
Hans	Kerstin	UHB-IUP	Scientist, oceanography
Hansen	Christian	FB5, Uni Bremen	Scientist, plume water chemistry
Hausen	Robert	DWD	Meteorologist
Heesemann	Bernd	FB5, Uni Bremen	Technician, heat flow
Hempelt	Juliane	DWD	Technician, meteorology
Hochmuth	Katharina	AWI	Scientist, seismology
Jöns	Niels	FB5, Uni Bremen	Scientist, rock/ plume water chemistry
Kaul	Norbert	FB5, Uni Bremen	Group leader, heat flow
Kirk	Henning	AWI	Technician, OBS
Lange	Florian	AWI	Engineer, ship construction
Lensch	Norbert	AWI	Technician, air guns
Marcon	Yann	MARUM	Scientist, videomapping
Molari	Massimiliano	HGF MPG Group (MPI)	Scientist, microbiology
Nordhausen	Axel	HGF MPG Group (MPI)	Technician, TV grab
Nunes-Jorge	Amandine	Symbiosis Group MPI	Student, symbiosis

Name/ Last name	Vorname/ First name	Institut/ Institute	Beruf/ Profession
Rieper	Norbert	IsiTec	Technician, video mapping
Schlindwein	Vera	AWI	Scientist, seismology, Chief scientist
Schmid	Florian	AWI	Student, seismology
Scholz	John-Robert	AWI	Student, seismology
Schramm	Fabian	HGF MPG Group (MPI)	Technician, TV grab
Stiens	Rafael	HGF MPG Group (MPI)	Technician, biogeochemistry
Stiens	Wiebke	HGF MPG Group (MPI)	Technician, biogeochemistry
Thiel	Daniel	FB5, Uni Bremen	Student, heat flow
Vogt	Martin	MARUM/UHB-IUP	Group leader, oceanography

A.3 SCHIFFSBESATZUNG / SHIP'S CREW

No.	Name	Rank
1	Wunderlich, Thomas	Master
2	Spielke, Steffen	1. Offc.
3	Ziemann, Olaf	Ch. Eng.
4	Hering, Igor	2. Offc.
5	Kentges, Felix	2. Offc.
6	Lauber, Felix	3. Offc.
7	Spilok, Norbert	Doctor
8	Koch, Georg	R. Offc.
9	Kotnik, Herbert	2. Eng.
10	Schnürch, Helmut	2. Eng.
11	Westphal, Henning	2. Eng.
12	Brehme, Andreas	Elec. Eng.
13	Dimmler, Werner	ELO
14	Feiertag, Thomas	ELO
15	Ganter, Armin	ELO
16	Winter, Andreas	ELO
17	Schröter, René	Boatsw.
18	Neisner, Winfried	Carpenter
19	Burzan, Gerd-Ekkeh.	A.B.
20	Clasen, Nils	A.B.
21	Gladow, Lothar	A.B.
22	Hartwig-Lab.,Andreas	A.B.
23	Kreis, Reinhard	A.B.
24	Kretzschmar, Uwe	A.B.
25	Moser, Siegfried	A.B.
26	Schröder, Norbert	A.B.
27	Sedlak, Andreas	A.B.
28	Beth, Detlef	Storek.
29	Dinse, Horst	Mot-man
30	Fritz, Günter	Mot-man
31	Krösche, Eckard	Mot-man

No.	Name	Rank
32	Plehn, Markus	Mot-man
33	Watzel, Bernhard	Mot-man
34	Fischer, Matthias	Cook
35	Tupy, Mario	Cooksmate
36	Völske, Thomas	Cooksmate
37	Dinse, Petra	1. Stwdess
38	Schwitzky-Schwarz,C.	Stwdess/N.
39	Chen, Quan Lun	2. Steward
40	Dibenau, Torsten	2. Steward
41	Hischke, Peggy	2. Stwdess
42	Hu, Guo Yong	2. Steward
43	Wartenberg, Irina	2. Stwdess
44	Ruan, Hui Guang	Laundrym.

A.4 STATIONSLISTE / STATION LIST PS 81

Gear abbreviations:

AGT	Agassiz Trawl
CTD	CTD
HF	Heat Flow Lance
GC	Gravity Corer
MUC	Multi Corer
OBS	Ocean Bottom Seismometer
OFOS	Ocean Floor Observation System
RO	Rosette water sampler
SEISREFR	Refraction Seismic Profiles
SVP	Sound Velocity Profiler
TVG	TV-Grab
TVMUC	TV-Multicorer

In the following list all position and depth information marked from position sensor SHIP are based on GPS positions and multibeam echosounder's center beam depth. Position and depth information from position sensor USBL are based on the acoustic underwater positioning system Posidonia. The depth then is the gear's/transponder depth.

Station	Date	Time	Gear	Action	Position Lat	Position Lon	Depth [m]	Pos. -Sens.
PS81/0603-1	15.11.2013	02:08	HF	on ground/ max depth	48°51.500'S	17°23.400'E	4783	SHIP
PS81/0603-2	15.11.2013	02:54	HF	on ground/ max depth	48°51.710'S	17°23.150'E	4794	SHIP
PS81/0604-1	16.11.2013	07:40	HF	on ground/ max depth	51°26.000'S	14°13.630'E	4478	SHIP
PS81/0604-2	16.11.2013	08:41	HF	on ground/ max depth	51°26.190'S	14°13.460'E	4430	SHIP
PS81/0604-3	16.11.2013	09:30	HF	on ground/ max depth	51°26.350'S	14°13.190'E	4394	SHIP
PS81/0605-1	16.11.2013	13:08	CTD/RO	on ground/ max depth	51°26.920'S	14°12.630'E	4344	SHIP
PS81/0606-1	16.11.2013	17:51	TVMUC	profile start	51°25.417'S	14°13.310'E	4367	USBL
PS81/0606-1	16.11.2013	18:49	TVMUC	profile end	51°25.980'S	14°13.427'E	4466	USBL
PS81/0606-2	16.11.2013	18:49	TVMUC	on ground/ max depth	51°25.980'S	14°13.427'E	4466	USBL
PS81/0607-1	17.11.2013	00:21	HF	on ground/ max depth	51°39.200'S	13°59.280'E	4146	SHIP
PS81/0607-2	17.11.2013	01:09	HF	on ground/ max depth	51°39.420'S	13°59.030'E	4164	SHIP
PS81/0608-1	17.11.2013	06:03	HF	on ground/ max depth	51°50.680'S	13°45.720'E	3984	SHIP
PS81/0609-1	17.11.2013	09:17	SEISREFR	profile start	51°51.230'S	13°56.440'E	3072	SHIP

Station	Date	Time	Gear	Action	Position Lat	Position Lon	Depth [m]	Pos. -Sens.
PS81/0609-1	17.11.2013	23:36	SEISREFR	profile end	52°38.770'S	12°33.410'E	3340	SHIP
PS81/0610-1	18.11.2013	01:06	SEISREFR	profile start	52°32.900'S	12°27.500'E	4542	SHIP
PS81/0610-1	18.11.2013	13:54	SEISREFR	profile end	52°12.190'S	14°11.090'E	3798	SHIP
PS81/0611-1	18.11.2013	18:12	SEISREFR	profile start	52°35.950'S	13°59.790'E	2765	SHIP
PS81/0611-1	19.11.2013	04:07	SEISREFR	profile end	52°27.120'S	12°40.200'E	3753	SHIP
PS81/0612-1	19.11.2013	07:00	SEISREFR	profile start	52°34.810'S	13°3.410'E	3488	SHIP
PS81/0612-1	19.11.2013	10:46	SEISREFR	profile end	52°16.280'S	13°4.000'E	1501	SHIP
PS81/0613-1	19.11.2013	12:52	SEISREFR	profile start	52°9.530'S	13°19.020'E	3388	SHIP
PS81/0613-1	19.11.2013	18:25	SEISREFR	profile end	52°37.010'S	13°19.010'E	3020	SHIP
PS81/0614-1	19.11.2013	21:51	CTD/RO	profile start	52°25.610'S	13°28.760'E	3881	SHIP
PS81/0614-1	20.11.2013	03:17	CTD/RO	profile end	52°26.540'S	13°21.480'E	3920	SHIP
PS81/0615-1	20.11.2013	06:29	OFOS	profile start	52°26.519'S	13°21.581'E	3891	USBL
PS81/0615-1	20.11.2013	07:30	OFOS	profile end	52°26.917'S	13°22.354'E	3589	USBL
PS81/0616-1	20.11.2013	11:05	OBS	on deck	52°23.850'S	13°16.410'E	4353	SHIP
PS81/0617-1	20.11.2013	13:26	OBS	on deck	52°14.600'S	13°18.810'E	2975	SHIP
PS81/0618-1	20.11.2013	16:54	OBS	on deck	52°1.940'S	13°38.960'E	3333	SHIP
PS81/0619-1	20.11.2013	20:24	OBS	on deck	52°18.320'S	13°46.550'E	3796	SHIP
PS81/0620-1	20.11.2013	23:30	HF	on ground/ max depth	52°15.960'S	13°37.970'E	3854	SHIP
PS81/0620-2	21.11.2013	00:27	HF	on ground/ max depth	52°16.080'S	13°37.560'E	3858	SHIP
PS81/0620-3	21.11.2013	01:07	HF	on ground/ max depth	52°16.200'S	13°37.180'E	3859	SHIP
PS81/0621-1	21.11.2013	04:52	OBS	on deck	52°18.880'S	13°33.350'E	3991	SHIP
PS81/0622-1	21.11.2013	07:52	OBS	on deck	52°34.890'S	13°50.870'E	2688	SHIP
PS81/0623-1	21.11.2013	11:30	OBS	on deck	52°33.240'S	13°22.220'E	3695	SHIP
PS81/0624-1	21.11.2013	14:20	OBS	on deck	52°29.770'S	13°4.070'E	4242	SHIP
PS81/0625-1	21.11.2013	18:28	OBS	on deck	52°28.720'S	12°50.250'E	4366	SHIP
PS81/0626-1	22.11.2013	13:08	TVMUC	profile start	54°55.977'S	12°27.276'E	4864	USBL
PS81/0626-1	22.11.2013	15:58	TVMUC	profile end	54°57.547'S	12°28.748'E	4869	USBL
PS81/0626-2	22.11.2013	15:58	TVMUC	on ground/ max depth	54°57.547'S	12°28.748'E	4869	USBL
PS81/0627-1	23.11.2013	12:27	OFOS	profile start	52°29.528'S	13°4.273'E	4276	USBL
PS81/0627-1	23.11.2013	16:22	OFOS	profile end	52°32.656'S	13°4.424'E	3348	USBL
PS81/0628-1	23.11.2013	20:43	CTD/RO	profile start	52°26.410'S	13°22.560'E	3811	SHIP
PS81/0628-1	24.11.2013	02:34	CTD/RO	profile end	52°26.230'S	13°13.860'E	4546	SHIP
PS81/0629-1	25.11.2013	09:11	CTD/RO	profile start	52°20.960'S	13°17.260'E	3260	SHIP
PS81/0629-1	25.11.2013	16:08	CTD/RO	profile end	52°27.470'S	13°22.090'E	3434	SHIP
PS81/0630-1	25.11.2013	19:09	OFOS	profile start	52°26.208'S	13°22.602'E	3932	USBL
PS81/0630-1	26.11.2013	00:50	OFOS	profile end	52°25.870'S	13°17.905'E	4387	USBL
PS81/0631-1	26.11.2013	02:57	CTD/RO	profile start	52°25.440'S	13°22.170'E	4303	SHIP
PS81/0631-1	26.11.2013	08:32	CTD/RO	profile end	52°26.250'S	13°16.730'E	4341	SHIP
PS81/0632-1	26.11.2013	11:03	OBS	on deck	52°21.880'S	13°4.770'E	3233	SHIP
PS81/0633-1	26.11.2013	13:21	OFOS	profile start	52°22.928'S	13°21.056'E	3045	USBL
PS81/0633-1	26.11.2013	19:38	OFOS	profile end	52°22.005'S	13°15.514'E	3609	USBL

A.4 Stationsliste / Station List PS 81

Station	Date	Time	Gear	Action	Position Lat	Position Lon	Depth [m]	Pos. -Sens.
PS81/0634-1	26.11.2013	23:59	HF	on ground/ max depth	52°11.480'S	13°22.750'E	3465	SHIP
PS81/0634-2	27.11.2013	00:54	HF	on ground/ max depth	52°11.710'S	13°22.490'E	3502	SHIP
PS81/0634-3	27.11.2013	01:45	HF	on ground/ max depth	52°11.910'S	13°22.210'E	3512	SHIP
PS81/0635-1	27.11.2013	06:48	HF	on ground/ max depth	52°26.460'S	13°8.160'E	4434	SHIP
PS81/0635-2	27.11.2013	07:46	HF	on ground/ max depth	52°26.590'S	13°7.770'E	4438	SHIP
PS81/0636-1	27.11.2013	14:50	TVMUC	on ground/ max depth	52°29.790'S	13°3.870'E	4199	SHIP
PS81/0637-1	27.11.2013	21:04	OFOS	profile start	52°25.985'S	13°18.466'E	4391	USBL
PS81/0637-1	28.11.2013	02:19	OFOS	profile end	52°27.018'S	13°21.883'E	3534	USBL
PS81/0638-1	28.11.2013	04:34	CTD/RO	profile start	52°23.860'S	13°23.760'E	4214	SHIP
PS81/0638-1	28.11.2013	11:27	CTD/RO	profile end	52°27.980'S	13°21.460'E	3310	SHIP
PS81/0639-1	28.11.2013	13:50	TVMUC	profile start	52°25.669'S	13°17.664'E	4379	USBL
PS81/0639-1	28.11.2013	14:55	TVMUC	profile end	52°26.063'S	13°18.287'E	4375	USBL
PS81/0639-2	28.11.2013	14:55	TVMUC	on ground/ max depth	52°26.063'S	13°18.287'E	4375	USBL
PS81/0640-1	28.11.2013	22:01	HF	on ground/ max depth	52°9.980'S	14°10.300'E	3685	SHIP
PS81/0640-2	28.11.2013	22:59	HF	on ground/ max depth	52°10.150'S	14°10.550'E	3718	SHIP
PS81/0640-3	28.11.2013	23:44	HF	on ground/ max depth	52°10.310'S	14°10.810'E	3745	SHIP
PS81/0641-1	29.11.2013	05:00	HF	on ground/ max depth	52°12.370'S	14°41.690'E	3212	SHIP
PS81/0641-2	29.11.2013	05:46	HF	on ground/ max depth	52°12.420'S	14°41.310'E	3206	SHIP
PS81/0641-3	29.11.2013	06:19	HF	on ground/ max depth	52°12.490'S	14°40.830'E	3205	SHIP
PS81/0642-1	29.11.2013	09:26	CTD/RO	on ground/ max depth	52°14.980'S	14°46.720'E	3444	SHIP
PS81/0643-1	29.11.2013	15:22	HF	on ground/ max depth	52°10.550'S	14°29.700'E	3888	SHIP
PS81/0643-2	29.11.2013	16:16	HF	on ground/ max depth	52°10.760'S	14°30.150'E	3901	SHIP
PS81/0643-3	29.11.2013	16:59	HF	on ground/ max depth	52°10.920'S	14°30.570'E	3886	SHIP
PS81/0644-1	29.11.2013	22:08	HF	on ground/ max depth	52°14.520'S	14°59.790'E	4199	SHIP
PS81/0644-2	29.11.2013	23:01	HF	on ground/ max depth	52°14.470'S	15°0.130'E	4215	SHIP
PS81/0644-3	29.11.2013	23:44	HF	on ground/ max depth	52°14.420'S	15°0.620'E	4216	SHIP
PS81/0645-1	30.11.2013	04:25	CTD/RO	profile start	52°12.030'S	15°38.010'E	4170	SHIP
PS81/0645-1	30.11.2013	10:18	CTD/RO	profile end	52°13.960'S	15°44.290'E	4176	SHIP
PS81/0646-1	30.11.2013	13:02	TVMUC	profile start	52°11.834'S	15°38.707'E	4068	USBL
PS81/0646-1	30.11.2013	14:06	TVMUC	profile end	52°12.168'S	15°39.825'E	4145	USBL
PS81/0646-2	30.11.2013	14:06	TVMUC	on ground/ max depth	52°12.168'S	15°39.825'E	4145	USBL

Station	Date	Time	Gear	Action	Position Lat	Position Lon	Depth [m]	Pos. -Sens.
PS81/0647-1	01.12.2013	03:01	OFOS	profile start	52°9.031'S	14°10.059'E	3648	USBL
PS81/0647-1	01.12.2013	06:51	OFOS	profile end	52°11.819'S	14°11.661'E	3728	USBL
PS81/0648-1	01.12.2013	09:34	CTD/RO	profile start	52°8.390'S	14°10.560'E	3773	SHIP
PS81/0648-1	01.12.2013	15:23	CTD/RO	profile end	52°10.810'S	14°10.570'E	3775	SHIP
PS81/0649-1	01.12.2013	17:45	TVMUC	profile start	52°10.048'S	14°10.570'E	3650	USBL
PS81/0649-1	01.12.2013	18:15	TVMUC	profile end	52°10.095'S	14°10.602'E	3655	USBL
PS81/0649-2	01.12.2013	18:15	TVMUC	on ground/ max depth	52°10.095'S	14°10.602'E	3655	USBL
PS81/0650-1	01.12.2013	21:34	OFOS	profile start	52°9.584'S	14°10.144'E	3555	USBL
PS81/0650-1	02.12.2013	02:46	OFOS	profile end	52°9.967'S	14°10.273'E	3674	USBL
PS81/0651-1	02.12.2013	05:13	CTD/RO	profile start	52°7.450'S	14°15.050'E	3280	SHIP
PS81/0651-1	02.12.2013	12:56	CTD/RO	profile end	52°10.350'S	14°10.990'E	3744	SHIP
PS81/0652-1	02.12.2013	15:03	GC	on ground/ max depth	52°10.140'S	14°10.540'E	3703	SHIP
PS81/0653-1	02.12.2013	17:32	GC	on ground/ max depth	52°10.220'S	14°10.830'E	3709	SHIP
PS81/0654-1	02.12.2013	21:49	AGT	profile start	52°10.190'S	14°10.700'E	3693	SHIP
PS81/0654-1	02.12.2013	22:54	AGT	profile end	52°10.060'S	14°10.240'E	3705	SHIP
PS81/0655-1	03.12.2013	05:51	HF	on ground/ max depth	52°14.480'S	13°52.420'E	4028	SHIP
PS81/0656-1	04.12.2013	12:46	GC	on ground/ max depth	52°21.970'S	13°19.040'E	3968	SHIP
PS81/0657-1	04.12.2013	17:06	GC	on ground/ max depth	52°26.450'S	13°8.110'E	4448	SHIP
PS81/0658-1	04.12.2013	22:42	AGT	profile start	52°22.010'S	13°19.290'E	3954	SHIP
PS81/0658-1	05.12.2013	00:17	AGT	profile end	52°21.700'S	13°18.490'E	3921	SHIP
PS81/0659-1	05.12.2013	04:34	TVMUC	on ground/ max depth	52°22.051'S	13°19.215'E	3941	USBL
PS81/0660-1	05.12.2013	08:21	CTD	profile start	52°25.980'S	13°0.730'E	4192	SHIP
PS81/0660-1	05.12.2013	16:19	CTD	profile end	52°32.000'S	12°58.600'E	3914	SHIP
PS81/0661-1	05.12.2013	19:12	TVMUC	profile start	52°26.475'S	13°8.197'E	4415	USBL
PS81/0661-1	05.12.2013	19:29	TVMUC	profile end	52°26.462'S	13°8.195'E	4415	USBL
PS81/0661-2	05.12.2013	19:30	TVMUC	on ground/ max depth	52°26.462'S	13°8.196'E	4415	USBL
PS81/0662-1	06.12.2013	02:05	OBS	on ground/ max depth	52°28.470'S	12°50.620'E	4420	SHIP
PS81/0663-1	06.12.2013	06:35	CTD/RO	on ground/ max depth	52°38.730'S	12°31.570'E	3700	SHIP
PS81/0664-1	06.12.2013	14:42	AGT	profile start	52°29.810'S	13°3.770'E	4181	SHIP
PS81/0664-1	06.12.2013	15:41	AGT	profile end	52°29.790'S	13°2.800'E	4128	SHIP
PS81/0665-1	06.12.2013	22:16	HF	on ground/ max depth	52°21.990'S	13°18.950'E	3971	SHIP
PS81/0665-2	07.12.2013	00:06	HF	on ground/ max depth	52°21.940'S	13°19.830'E	3926	SHIP
PS81/0665-3	07.12.2013	00:56	HF	on ground/ max depth	52°21.970'S	13°20.750'E	3980	SHIP
PS81/0665-4	07.12.2013	02:02	HF	on ground/ max depth	52°21.990'S	13°21.720'E	4097	SHIP

A.4 Stationsliste / Station List PS 81

Station	Date	Time	Gear	Action	Position Lat	Position Lon	Depth [m]	Pos. -Sens.
PS81/0665-5	07.12.2013	02:57	HF	on ground/ max depth	52°22.010'S	13°22.490'E	4056	SHIP
PS81/0666-1	07.12.2013	10:30	OFOS	profile start	52°3.973'S	13°25.676'E	2462	USBL
PS81/0666-1	07.12.2013	13:12	OFOS	profile end	52°5.221'S	13°24.127'E	2594	USBL
PS81/0667-1	07.12.2013	16:20	TVG	profile start	52°3.648'S	13°24.877'E	2624	USBL
PS81/0667-1	07.12.2013	17:26	TVG	profile end	52°3.740'S	13°25.079'E	2608	USBL
PS81/0667-2	07.12.2013	17:26	TVG	on ground/ max depth	52°3.740'S	13°25.079'E	2608	USBL
PS81/0668-1	07.12.2013	22:25	TVG	profile start	52°6.705'S	13°17.264'E	2913	USBL
PS81/0668-1	07.12.2013	23:06	TVG	profile end	52°6.772'S	13°17.111'E	2976	USBL
PS81/0668-2	07.12.2013	23:10	TVG	on ground/ max depth	52°6.779'S	13°17.109'E	2984	USBL
PS81/0669-1	08.12.2013	07:55	AGT	profile start	52°10.170'S	14°10.990'E	3709	SHIP
PS81/0669-1	08.12.2013	09:18	AGT	profile end	52°9.740'S	14°9.380'E	3676	SHIP
PS81/0670-1	08.12.2013	14:16	OFOS	profile start	52°5.850'S	14°36.300'E	1992	SHIP
PS81/0670-1	08.12.2013	17:15	OFOS	profile end	52°5.870'S	14°38.790'E	1366	SHIP
PS81/0671-1	08.12.2013	18:46	OFOS	profile start	52°4.704'S	14°38.306'E	929	USBL
PS81/0671-1	08.12.2013	21:05	OFOS	profile end	52°5.871'S	14°37.663'E	1399	USBL
PS81/0672-1	08.12.2013	22:40	TVG	profile start	52°4.703'S	14°38.439'E	870	USBL
PS81/0672-1	08.12.2013	23:36	TVG	profile end	52°4.766'S	14°38.312'E	923	USBL
PS81/0672-2	08.12.2013	23:40	TVG	on ground/ max depth	52°4.768'S	14°38.309'E	923	USBL
PS81/0673-1	09.12.2013	01:54	CTD/RO	on ground/ max depth	52°6.660'S	14°36.600'E	2248	SHIP
PS81/0674-1	09.12.2013	04:51	CTD/RO	on ground/ max depth	52°12.350'S	14°41.800'E	3154	SHIP
PS81/0675-1	09.12.2013	09:29	HF	on ground/ max depth	52°1.880'S	14°52.320'E	1959	SHIP
PS81/0675-2	09.12.2013	10:29	HF	on ground/ max depth	52°2.240'S	14°51.960'E	1925	SHIP
PS81/0676-1	09.12.2013	15:38	HF	on ground/ max depth	51°54.190'S	15°1.440'E	2285	SHIP
PS81/0676-2	09.12.2013	16:30	HF	on ground/ max depth	51°54.360'S	15°1.240'E	2274	SHIP
PS81/0677-1	09.12.2013	21:18	HF	on ground/ max depth	51°36.460'S	15°19.450'E	3419	SHIP
PS81/0677-2	09.12.2013	22:11	HF	on ground/ max depth	51°36.630'S	15°19.690'E	3368	SHIP
PS81/0677-3	09.12.2013	22:52	HF	on ground/ max depth	51°36.790'S	15°19.940'E	3310	SHIP
PS81/0678-1	10.12.2013	03:48	HF	on ground/ max depth	51°17.390'S	15°31.280'E	3190	SHIP
PS81/0678-2	10.12.2013	04:50	HF	on ground/ max depth	51°17.300'S	15°30.840'E	3236	SHIP
PS81/0678-3	10.12.2013	05:43	HF	on ground/ max depth	51°17.290'S	15°30.350'E	3246	SHIP
PS81/0679-1	10.12.2013	15:53	HF	on ground/ max depth	50°47.920'S	16°4.510'E	4337	SHIP
PS81/0679-2	10.12.2013	16:17	HF	on ground/ max depth	50°47.930'S	16°4.560'E	4204	SHIP

ANT-XXIX/8

Station	Date	Time	Gear	Action	Position Lat	Position Lon	Depth [m]	Pos. -Sens.
PS81/0679-3	10.12.2013	17:18	HF	on ground/ max depth	50°48.190'S	16°4.520'E	4256	SHIP
PS81/0680-1	11.12.2013	10:34	OFOS	profile start	48°46.240'S	15°44.143'E	4244	USBL
PS81/0680-1	11.12.2013	13:00	OFOS	profile end	48°45.336'S	15°42.209'E	4339	USBL
PS81/0681-1	11.12.2013	16:41	TVMUC	on ground/ max depth	48°43.838'S	15°40.717'E	4351	USBL

A.5 SCIENTIFIC APPENDIX

The scientific appendix contains additional information to individual chapters. The contents are numbered by the chapter number they refer to.

A.5.1 Sample lists

Tab. A.5.7.5: List of samples collected from the colonization devices (see chapter 7.5).

Station Number	OBS Number	Type of sample	Fixation	Storage	Purpose
616	OBS 4	Slides (15)	Frozen	-20°C	DNA characterization
616	OBS 4	Slides (12)	PFA4% transfer in ethanol	-20°C	FISH
616	OBS 4	wood	Frozen	-20°C	DNA characterization
616	OBS 4	wood	Ethanol 96%	-20°C	DNA characterization
616	OBS 4	yellow foam	Frozen	-20°C	DNA characterization
616	OBS 4	yellow foam	PFA4% transfer in ethanol	-20°C	FISH
617	OBS 3	Slides (15)	Frozen	-20°C	DNA characterization
617	OBS 3	Slides (14)	PFA4% transfer in ethanol	-20°C	FISH
617	OBS 3	wood	Frozen	-20°C	DNA characterization
617	OBS 3	wood	Ethanol 96%	-20°C	DNA characterization
617	OBS 3	yellow foam	Frozen	-20°C	DNA characterization
617	OBS 3	yellow foam	PFA4% transfer in ethanol	-20°C	FISH
618	OBS 10	Slides (14)	Frozen	-20°C	DNA characterization
618	OBS 10	Slides (14)	PFA4% transfer in ethanol	-20°C	FISH
618	OBS 10	wood	Frozen	-20°C	DNA characterization

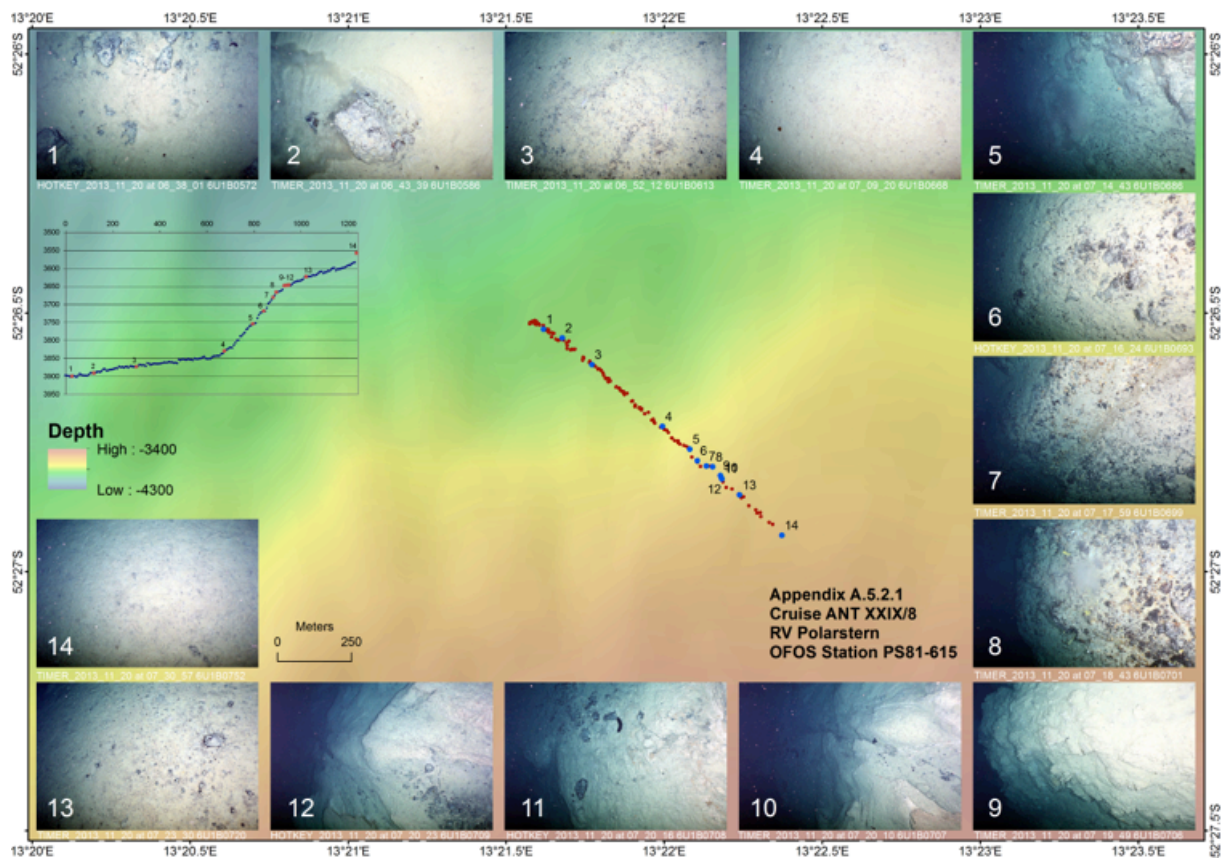
Station Number	OBS Number	Type of sample	Fixation	Storage	Purpose
618	OBS 10	wood	Ethanol 96%	-20°C	DNA characterization
618	OBS 10	yellow foam	Frozen	-20°C	DNA characterization
618	OBS 10	yellow foam	PFA4% transfer in ethanol	-20°C	FISH
619	OBS 9	Slides (1)	PFA4% transfer in ethanol	-20°C	FISH
619	OBS 9	wood	Frozen	-20°C	DNA characterization
619	OBS 9	wood	Ethanol 96%	-20°C	DNA characterization
619	OBS 9	yellow foam	Frozen	-20°C	DNA characterization
619	OBS 9	yellow foam	PFA4% transfer in ethanol	-20°C	FISH
620	OBS 8	Slides (14)	Frozen	-20°C	DNA characterization
620	OBS 8	Slides (14)	PFA4% transfer in ethanol	-20°C	FISH
620	OBS 8	wood	Frozen	-20°C	DNA characterization
620	OBS 8	wood	Ethanol 96%	-20°C	DNA characterization
620	OBS 8	yellow foam	Frozen	-20°C	DNA characterization
620	OBS 8	yellow foam	PFA4% transfer in ethanol	-20°C	FISH
621	OBS 7	Slides (14)	Frozen	-20°C	DNA characterization
621	OBS 7	Slides (14)	PFA4% transfer in ethanol	-20°C	FISH
621	OBS 7	wood	Frozen	-20°C	DNA characterization
621	OBS 7	wood	Ethanol 96%	-20°C	DNA characterization
621	OBS 7	yellow foam	Frozen	-20°C	DNA characterization
621	OBS 7	yellow foam	PFA4% transfer in ethanol	-20°C	FISH
622	OBS 6	Slides (14)	Frozen	-20°C	DNA characterization

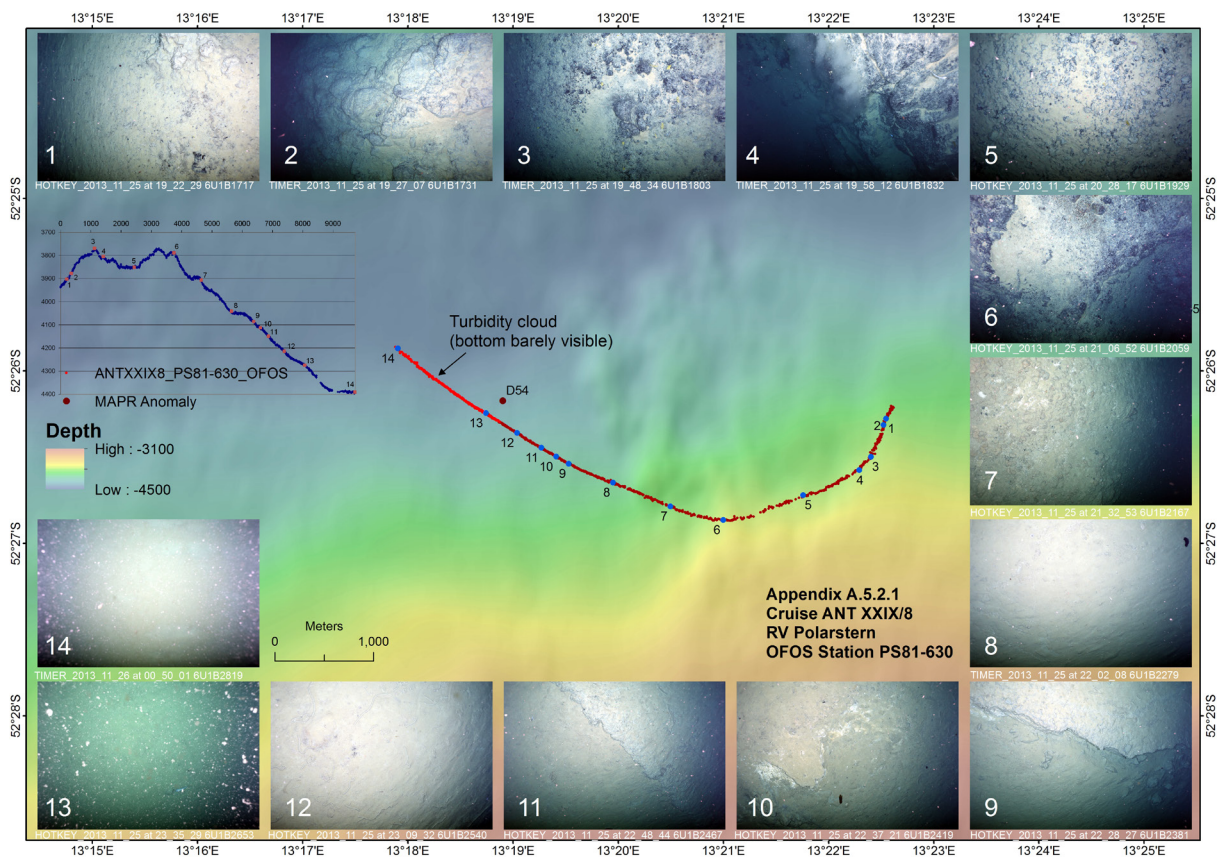
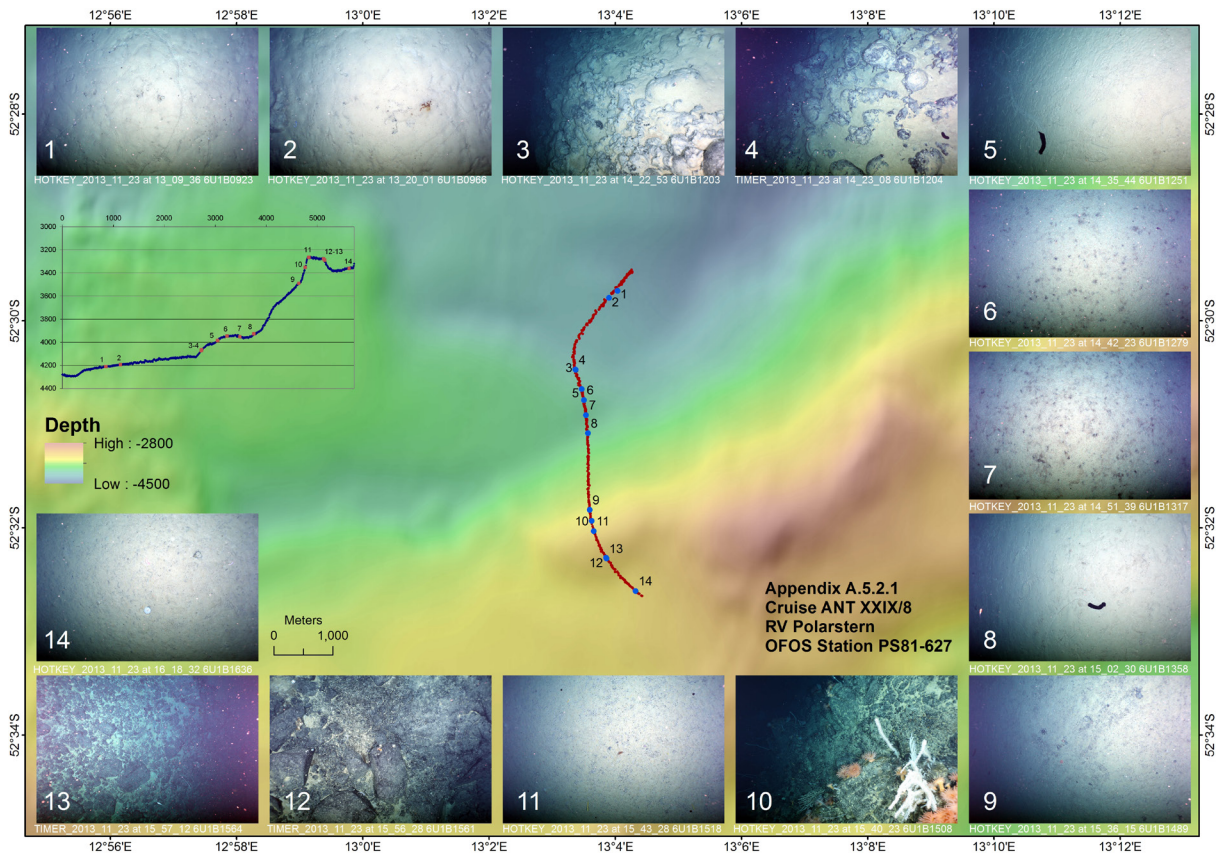
A.5 Scientific Appendix

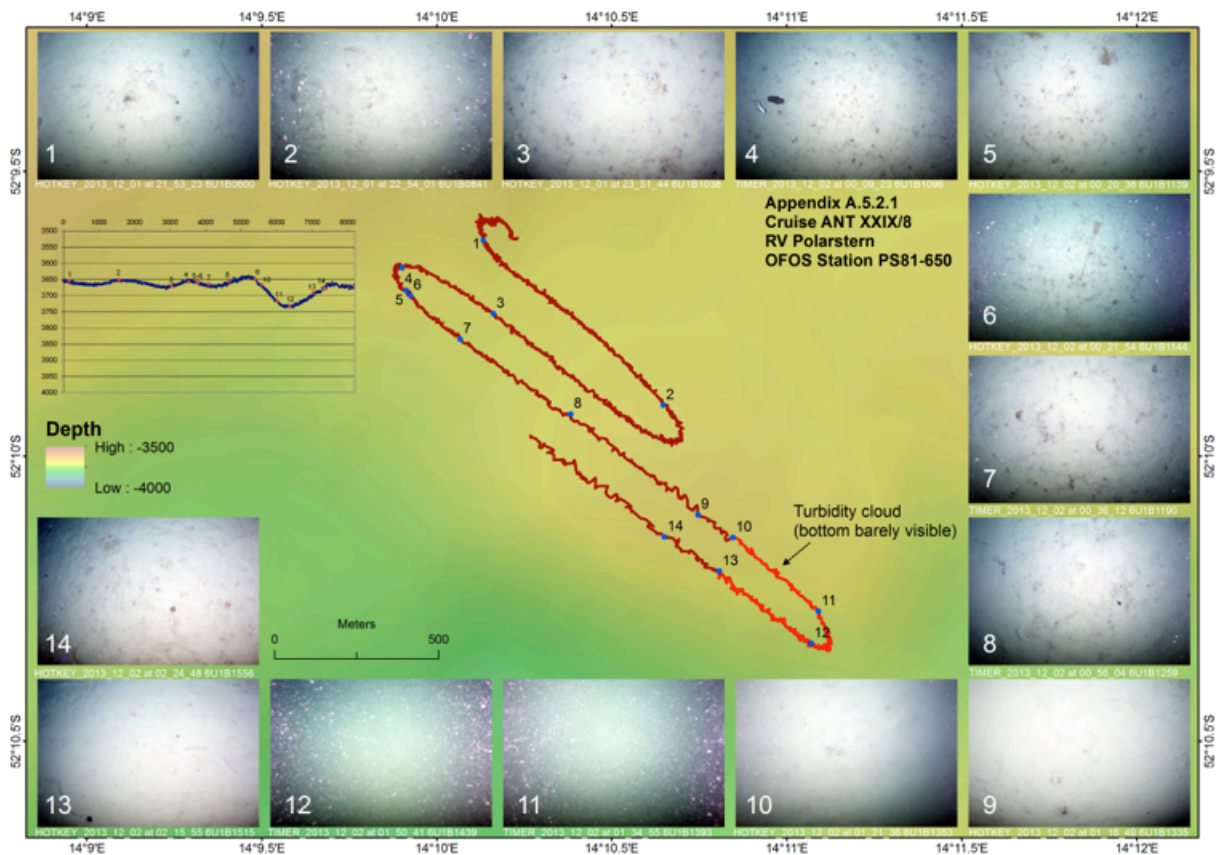
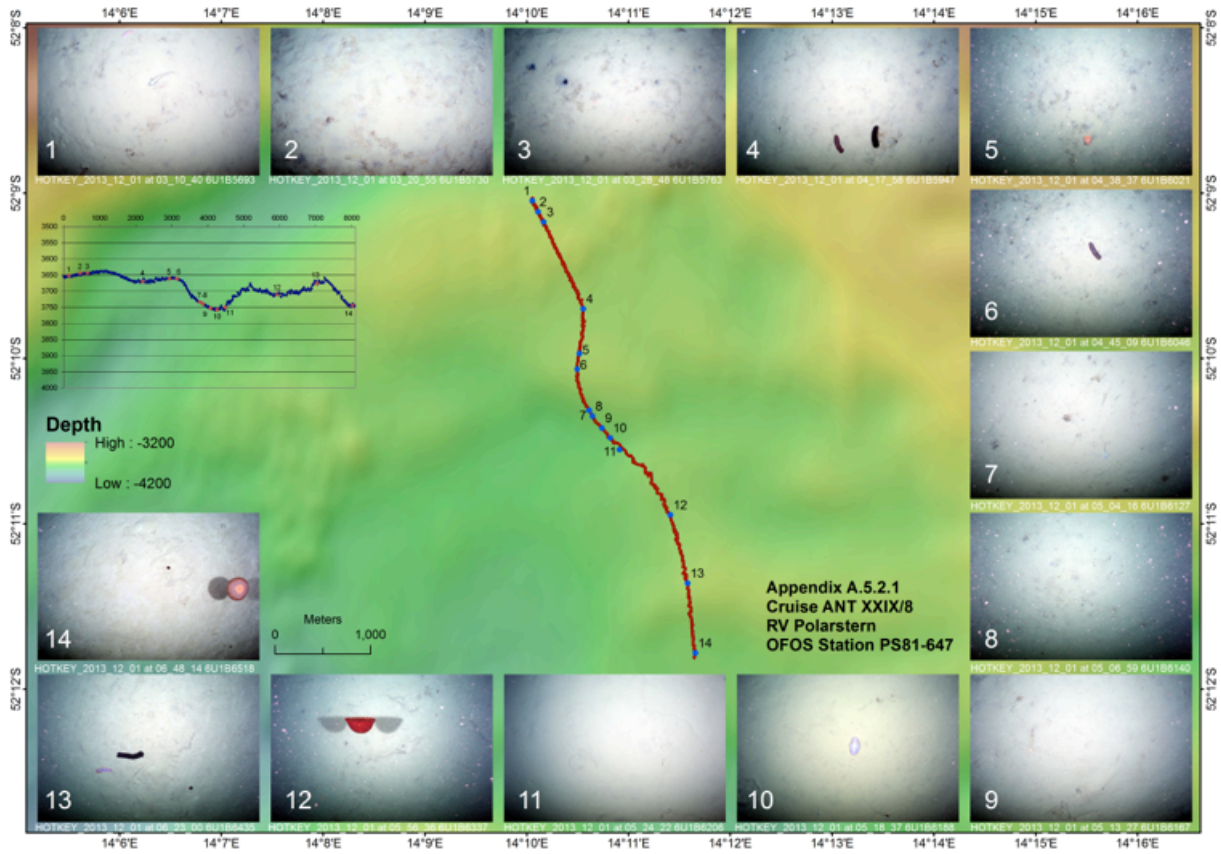
Station Number	OBS Number	Type of sample	Fixation	Storage	Purpose
622	OBS 6	Slides (14)	PFA4% transfer in ethanol	-20°C	FISH
622	OBS 6	wood	Frozen	-20°C	DNA characterization
622	OBS 6	wood	Ethanol 96%	-20°C	DNA characterization
622	OBS 6	yellow foam	Frozen	-20°C	DNA characterization
622	OBS 6	yellow foam	PFA4% transfer in ethanol	-20°C	FISH
623	OBS 5	Slides (14)	Frozen	-20°C	DNA characterization
623	OBS 5	Slides (14)	PFA4% transfer in ethanol	-20°C	FISH
623	OBS 5	wood	Frozen	-20°C	DNA characterization
623	OBS 5	wood	Ethanol 96%	-20°C	DNA characterization
623	OBS 5	yellow foam	Frozen	-20°C	DNA characterization
623	OBS 5	yellow foam	PFA4% transfer in ethanol	-20°C	FISH
632	OBS 2	Slides (15)	Frozen	-20°C	DNA characterization
632	OBS 2	Slides (17)	PFA4% transfer in ethanol	-20°C	FISH
632	OBS 2	wood	Frozen	-20°C	DNA characterization
632	OBS 2	wood	Ethanol 96%	-20°C	DNA characterization
632	OBS 2	yellow foam	Frozen	-20°C	DNA characterization
632	OBS 2	yellow foam	PFA4% transfer in ethanol	-20°C	FISH

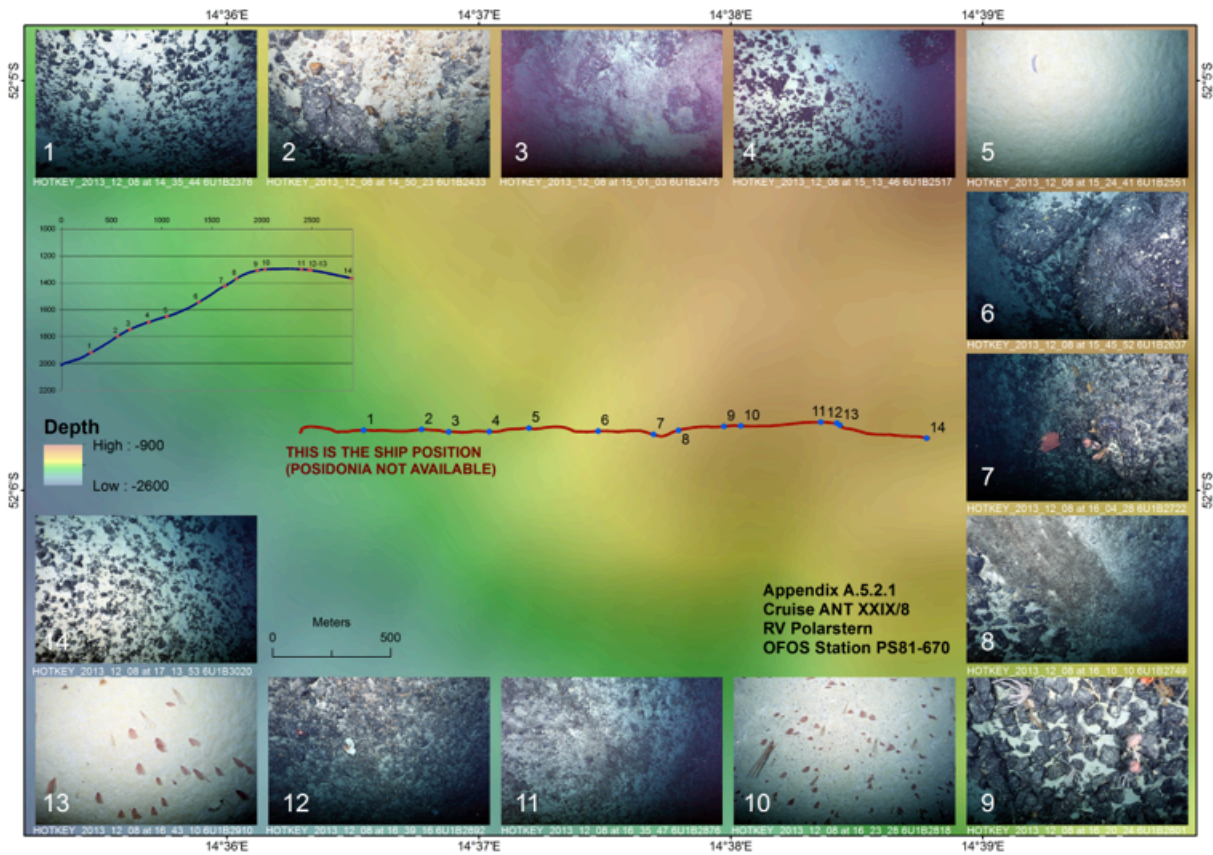
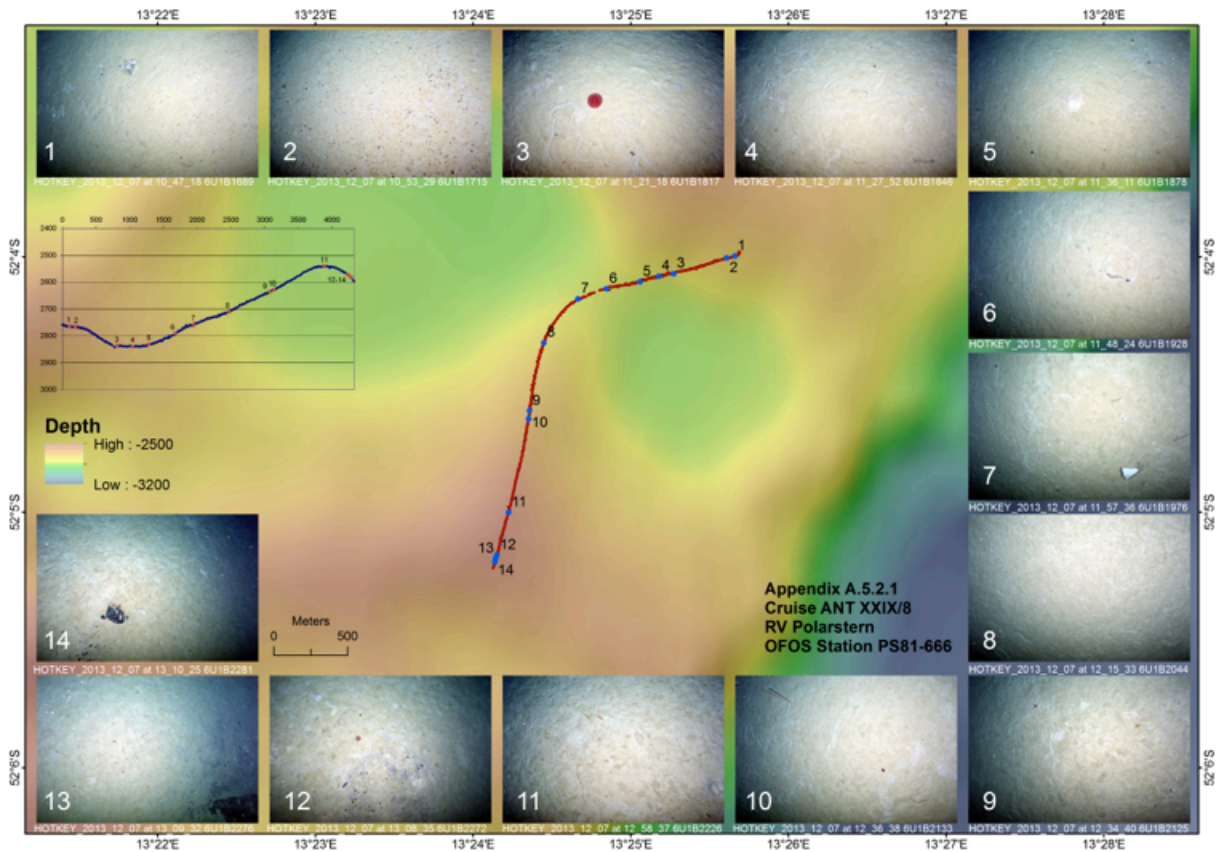
A.5.2 Summary of OFOS dives

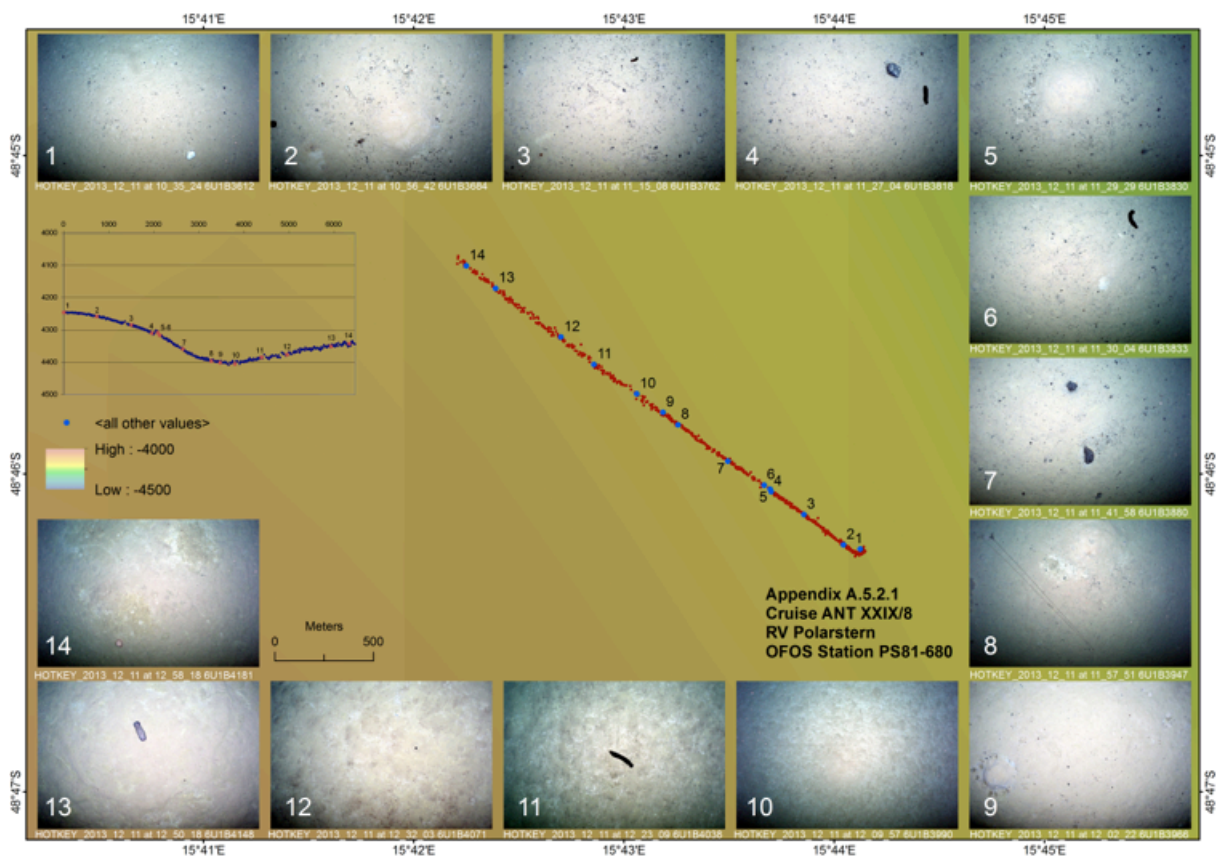
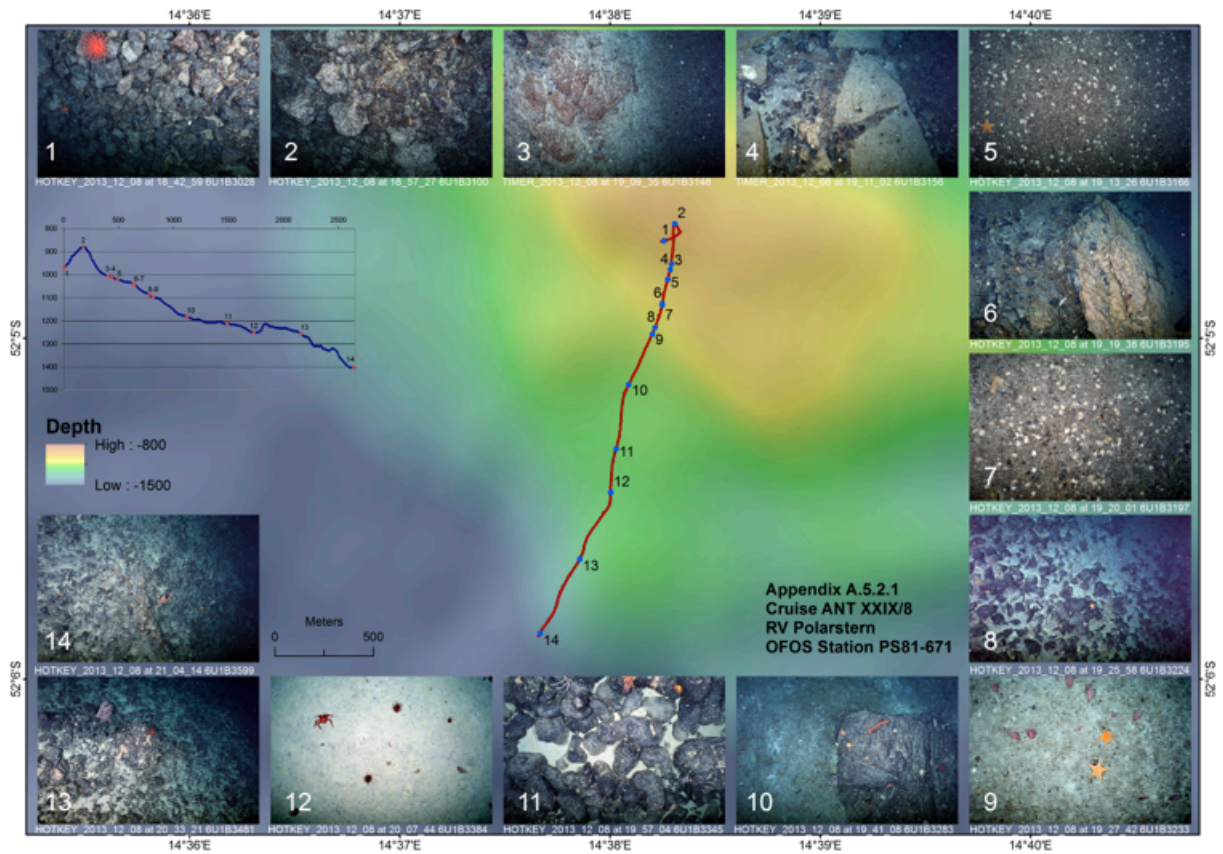
The figures shown in A.5.2.1 are a series of summary maps for each OFOS dive. Station number as indicated. The respective map shows the OFOS track using Posidonia locations. Numbered photos were taken from locations marked in blue along the track and the ones in red on the cross-section (inset).



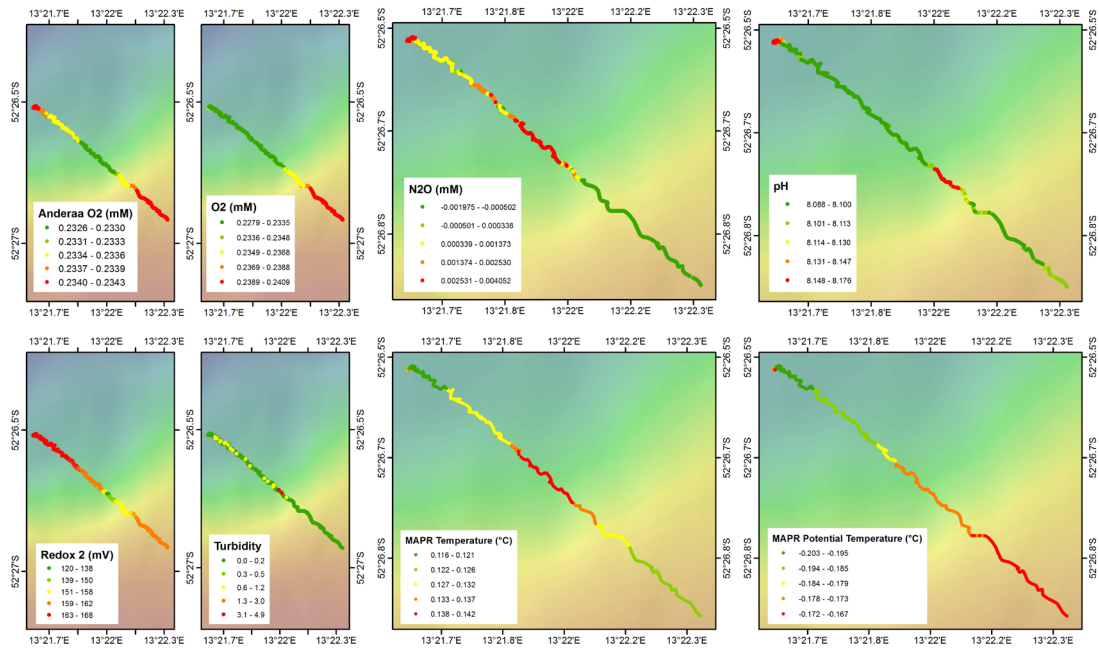




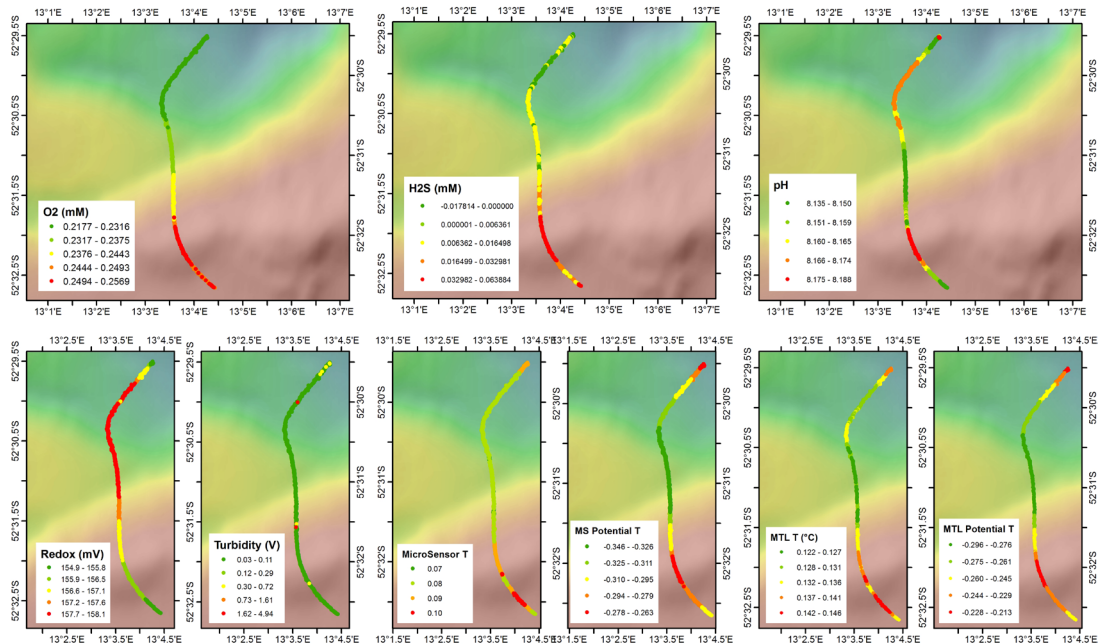
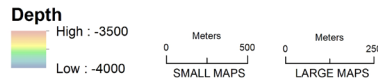




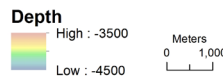
Figures A.5.2.2 show series of summary figures for each OFOS dive. Station number as indicated. The maps show chemical and physical parameters colour-coded along the track lines.

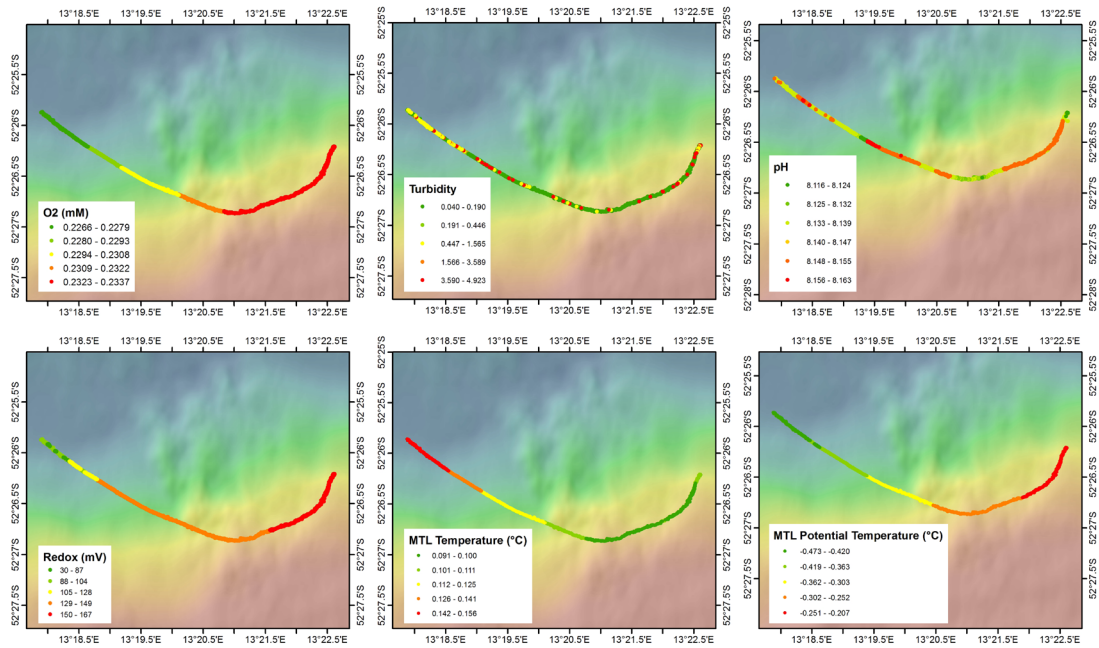


Appendix A.5.2.2
Cruise ANT XXIX/8
RV Polarstern
Station PS81/615 - OFOS Dive 1

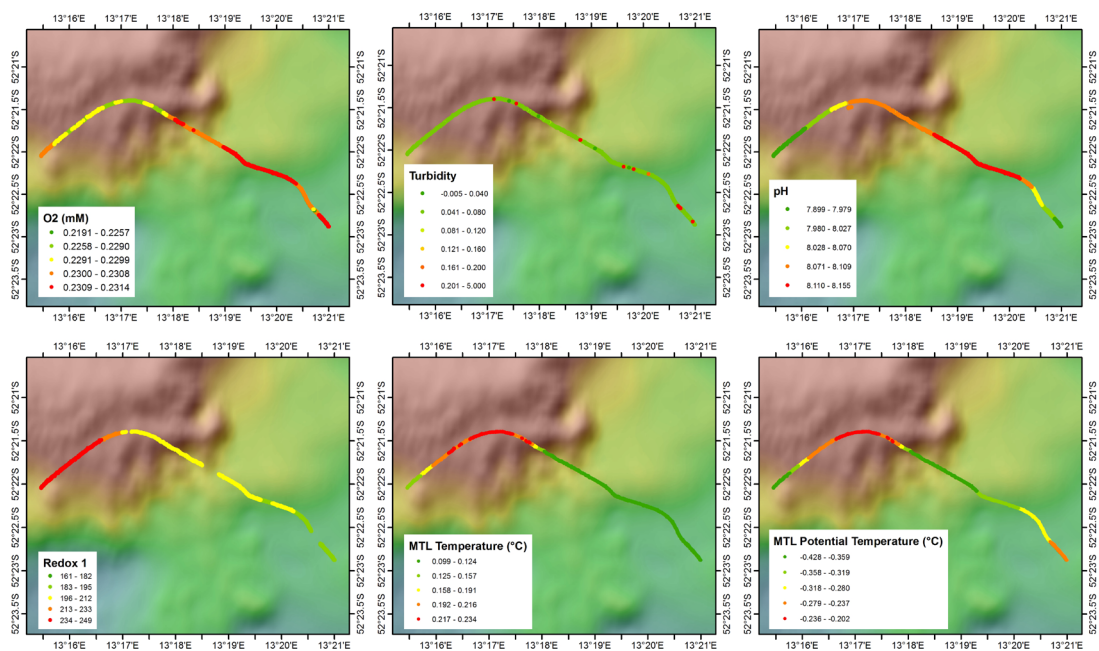
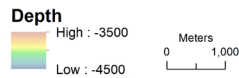


Appendix A.5.2.2
Cruise ANT XXIX/8
RV Polarstern
Station PS81/627 - OFOS Dive 2



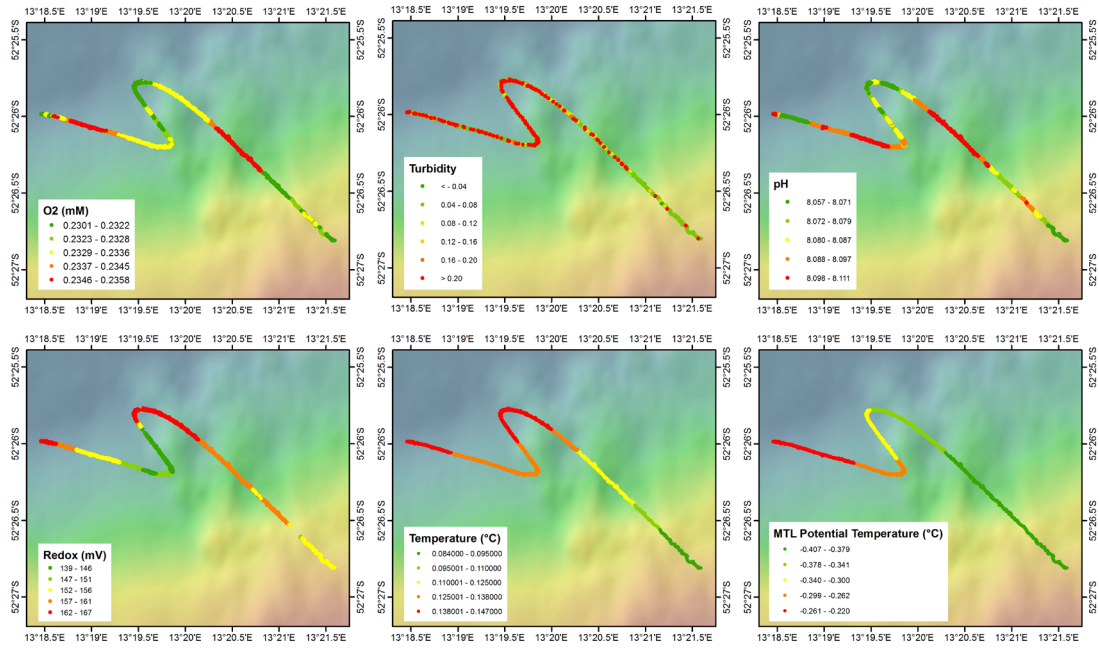


Appendix A.5.2.2
Cruise ANT XXIX/8
RV Polarstern
Station PS81/630 - OFOS Dive 3

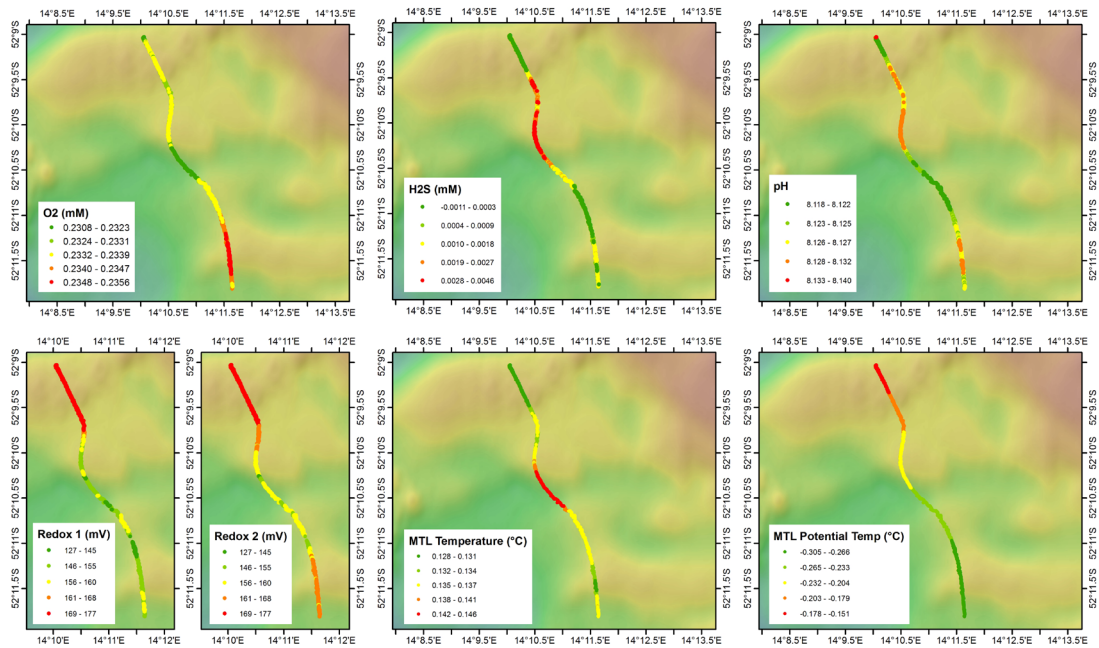
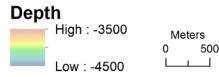


Appendix A.5.2.2
Cruise ANT XXIX/8
RV Polarstern
Station PS81/633 - OFOS Dive 4

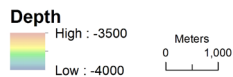


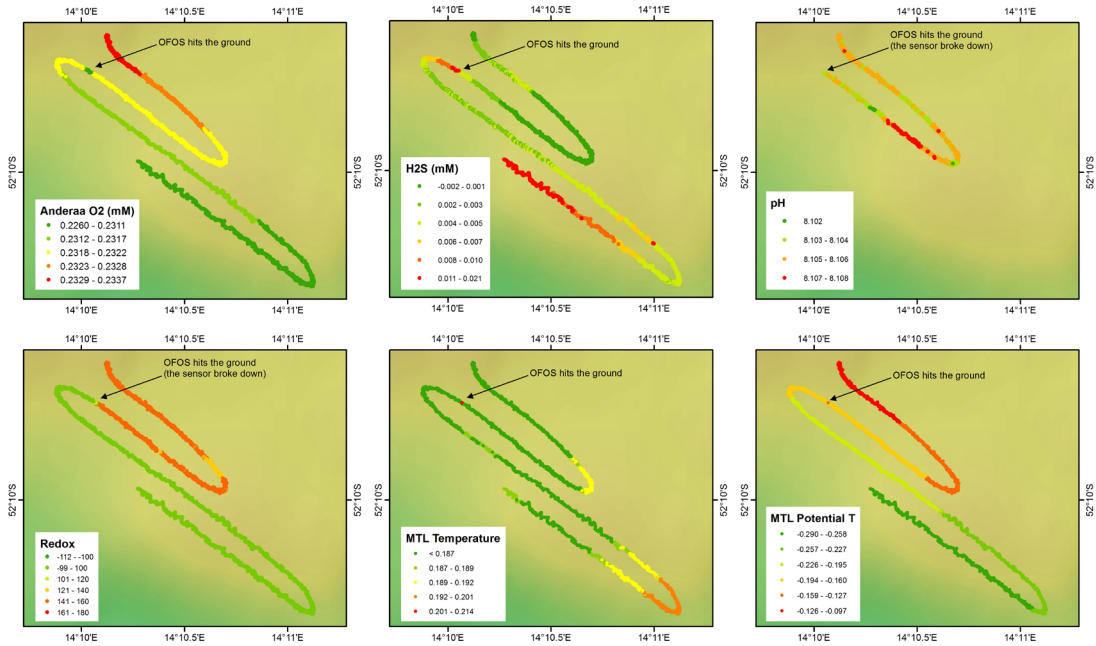


Appendix A.5.2.2
Cruise ANT XXIX/8
RV Polarstern
Station PS81/637 - OFOS Dive 5

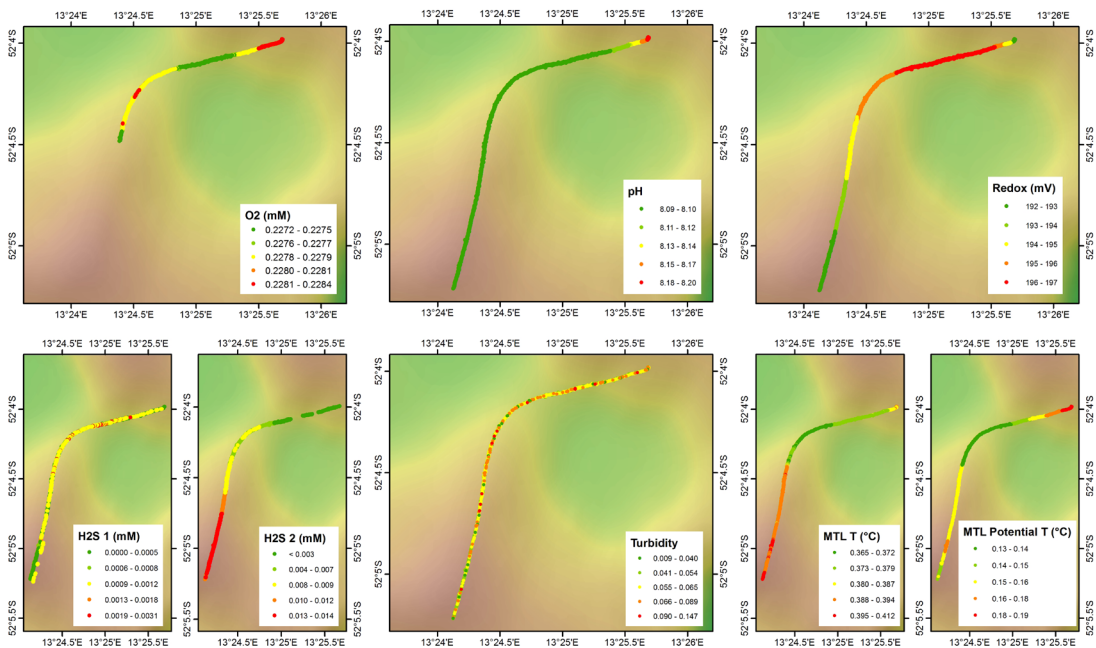
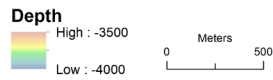


Appendix A.5.2.2
Cruise ANT XXIX/8
RV Polarstern
Station PS81/647 - OFOS Dive 6

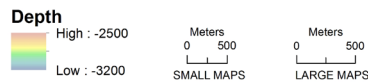


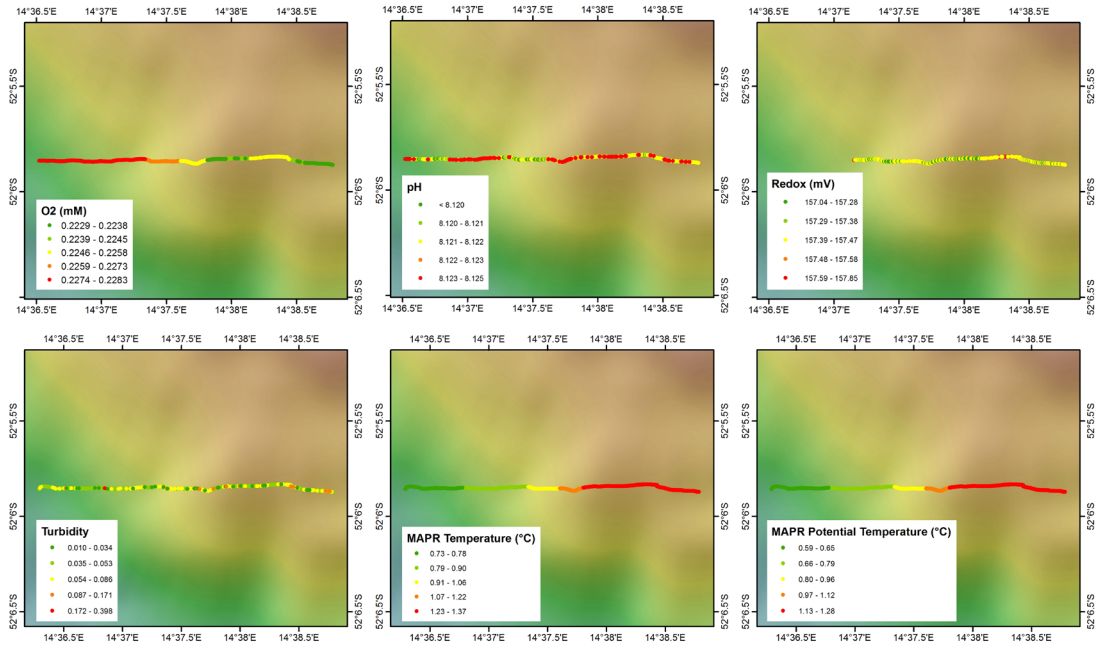


Appendix A.5.2.2
Cruise ANT XXIX/8
RV Polarstern
Station PS81/650 - OFOS Dive 7

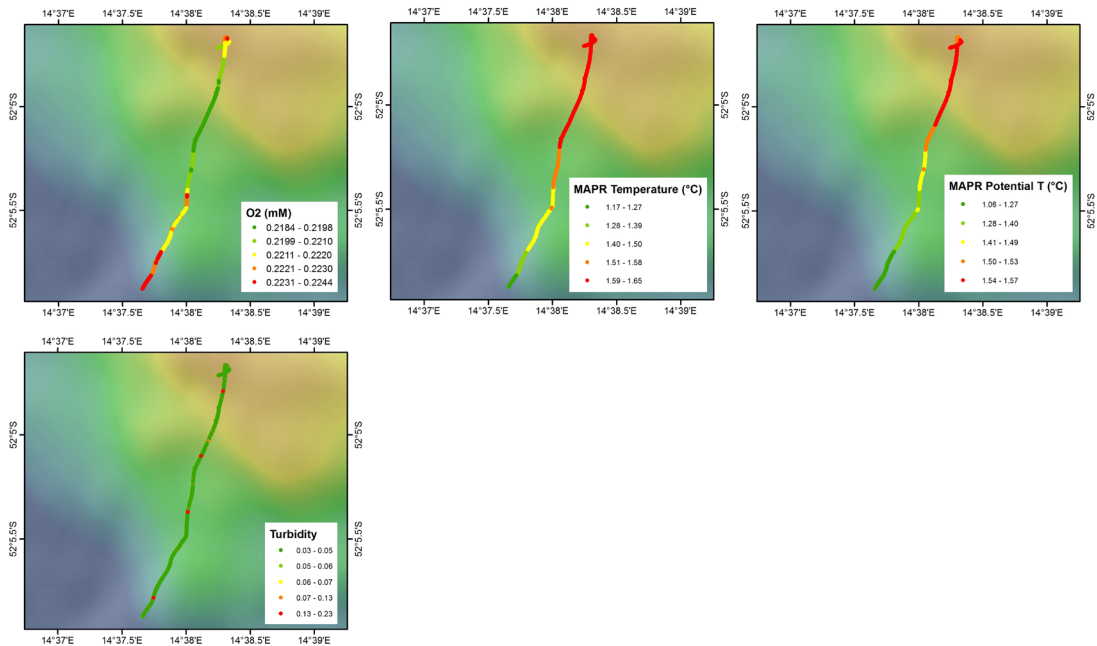


Appendix A.5.2.2
Cruise ANT XXIX/8
RV Polarstern
Station PS81/666 - OFOS Dive 8

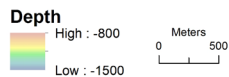


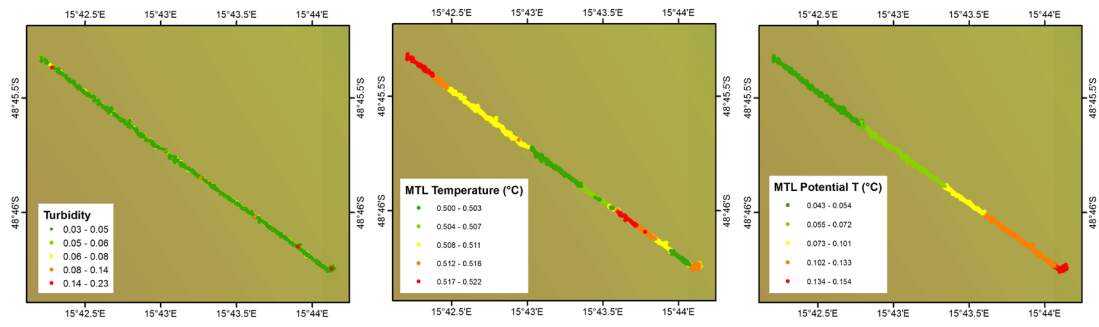


Appendix A.5.2.2
Cruise ANT XXIX/8
RV Polarstern
Station PS81/670 - OFOS Dive 9

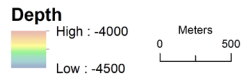


Appendix A.5.2.2
Cruise ANT XXIX/8
RV Polarstern
Station PS81/671 - OFOS Dive 10





Appendix A.5.2.2
 Cruise ANT XXIX/8
 RV Polarstern
 Station PS81/680 - OFOS Dive 11



Die "**Berichte zur Polar- und Meeresforschung**" (ISSN 1866-3192) werden beginnend mit dem Heft Nr. 569 (2008) als Open-Access-Publikation herausgegeben. Ein Verzeichnis aller Hefte einschließlich der Druckausgaben (Heft 377-568) sowie der früheren "**Berichte zur Polarforschung**" (Heft 1-376, von 1981 bis 2000) befindet sich im open access institutional repository for publications and presentations (**ePIC**) des AWI unter der URL <http://epic.awi.de>. Durch Auswahl "Reports on Polar- and Marine Research" (via "browse"/"type") wird eine Liste der Publikationen sortiert nach Heftnummer innerhalb der absteigenden chronologischen Reihenfolge der Jahrgänge erzeugt.

To generate a list of all Reports past issues, use the following URL: <http://epic.awi.de> and select "browse"/"type" to browse "Reports on Polar and Marine Research". A chronological list in declining order, issues chronological, will be produced, and pdf-icons shown for open access download.

Verzeichnis der zuletzt erschienenen Hefte:

Heft-Nr. 660/2013 — "The Expedition of the Research Vessel 'Polarstern' to the Arctic in 2012 (ARK-XXVII/1)", edited by Agnieszka Beszczyńska-Möller

Heft-Nr. 661/2013 — "The Expedition of the Research Vessel 'Polarstern' to the Antarctic in 2012 (ANT-XXVIII/3)", edited by Dieter Wolf-Gladrow

Heft-Nr. 662/2013 — "Climate Change in the Marine Realm: An international summer school in the framework of the European Campus of Excellence", edited by Angelika Dummermuth and Klaus Grosfeld

Heft-Nr. 663/2013 — "The Expedition of the Research Vessel 'Polarstern' to the Arctic in 2012 (ARK-XXVII/3)", edited by Antje Boetius

Heft-Nr. 664/2013 — "Russian-German Cooperation SYSTEM LAPTEV SEA: The Expeditions Laptev Sea - Mamontov Klyk 2011 & Buor Khaya 2012", edited by Frank Günther, Pier Paul Overduin, Aleksandr S. Makarov, and Mikhail N. Grigoriev

Heft-Nr. 665/2013 — "The Expedition of the Research Vessel 'Polarstern' to the Antarctic in 2013 (ANT-XXIX/3)", edited by Julian Gutt

Heft-Nr. 666/2013 — "The Expedition of the Research Vessel 'Polarstern' to the Antarctic in 2013 (ANT-XXIX/5)", edited by Wilfried Jokat

Heft-Nr. 667/2013 — "The Sea Ice Thickness in the Atlantic Sector of the Southern Ocean", by Axel Behrendt

Heft-Nr. 668/2013 — "The Expedition of the Research Vessel 'Polarstern' to the Antarctic in 2013 (ANT-XXIX/4)", edited by Gerhard Bohrmann

Heft-Nr. 669/2013 — "Processes in the Southern Ocean carbon cycle: Dissolution of carbonate sediments and inter-annual variability of carbon fluxes", by Judith Hauck

Heft-Nr. 670/2013 — "The Expedition of the Research Vessel 'Polarstern' to the Antarctic in 2012 (ANT-XXIX/1)", edited by Holger Auel

Heft-Nr. 671/2013 — "The Expedition of the Research Vessel 'Polarstern' to the Antarctic in 2012/2013 (ANT-XXIX/2)", edited by Olaf Boebel

Heft-Nr. 672/2014 — "The Expedition of the Research Vessel 'Polarstern' to the Antarctic in 2013 (ANT-XXIX/8)", edited by Vera Schlindwein